ANALYSIS AND OPTIMIZATION OF AUTOFRETTAGED AND SHRINK-FITTED COMPOUND CYLINDERS UNDER THERMO-MECHANICAL LOADS

Ossama M. Ramy Y. Abdelsalam

A Thesis

in

The department

of

Mechanical and Industrial Engineering

Presented in Partial Fulfillment of the Requirements

for the Degree of

Doctor of Philosophy at

Concordia University

Montreal, Quebec, Canada

November, 2012

CONCORDIA UNIVERSITY

SCHOOL OF GRADUATE STUDIES

This is to certify that the thesis prepared

By: **Ossama Ramy Abdelsalam**

Entitled: **Analysis and Optimization of Autofrettaged and Shrink-Fitted Compound Cylinders under Thermo-Mechanical Loads**

and submitted in partial fulfillment of the requirements for the degree of

DOCTOR OF PHILOSOPHY (Mechanical Engineering)

complies with the regulations of the University and meets the accepted standards with respect to originality and quality.

Signed by the final examining committee:

_____ Chair
Dr. L.A. Lopes

_____ External Examiner
Dr. K. Behdinan

_____ External to Program
Dr. A. Aghdam

_____ Examiner
Dr. W. Ahmed

_____ Examiner
Dr. M. Packirisamy

_____ Thesis Supervisor
Dr. R. Sedaghati

Approved by _____
Dr. A. Dolatabadi, Graduate Program Director

November 23, 2012

_____
Dr. Robin A.L. Drew, Dean
Faculty of Engineering and Computer Science

ABSTRACT

ANALYSIS AND OPTIMIZATION OF AUTOFRETTAGED AND SHRINK-FITTED COMPOUND CYLINDERS UNDER THERMO-MECHANICAL LOADS

Ossama Ramy Abdelsalam, Ph.D.

Concordia University, 2012.

Cylindrical shells have large industrial applications ranging from pressure vessels, engine cylinders and hydraulic chambers to chemical and power plants and they are typically subjected to severe mechanical or thermo-mechanical environmental conditions. The fatigue life, pressure and thermal load bearing capacities of thick-walled cylinders can be considerably improved by inducing near the bore compressive residual hoop stresses. Shrink-fit and autofrettage processes have been effectively applied to generate favorable compressive residual stresses. The main goal of this research study is to fundamentally investigate the compound cylinders subjected to autofrettage and shrink-fit processes and develop new design processing technique and practical design optimization strategies to enhance their fatigue life under cyclic thermo-mechanical loads.

First, the residual stresses of compound cylinders subjected to different combinations of shrink-fit and autofrettage processes have been evaluated using the developed finite element model in the ANSYS environment. The stresses due to different cyclic thermo-mechanical loads have also been calculated for the different combinations of compound cylinders considering the fully coupled thermo-elastic finite element model. To validate

the finite element model, an experimental setup has been designed to measure the temperature history at three different locations through the wall thickness and also hoop strain at the outer surface of a two-layer compound cylinder under internal quasi-static and cyclic thermal loads. The experimental results have then been compared with those obtained from the finite element model. Moreover, to compare the performance of compound cylinders under different thermo-mechanical loads, the fatigue life due to cyclic pressure, cyclic thermal pulses and cyclic combined thermo-mechanical pulses has been calculated using ASME code for high pressure vessel.

Next, to enhance the residual stress distribution along the wall thickness of the cylinder, a new double autofrettage process has been introduced. In the proposed double autofrettage process, an outer autofrettage cycle is performed prior to a standard inner autofrettage cycle. This can provide an increase in the beneficial compressive residual stresses at the near bore area of the cylinder while decreasing the detrimental tensile residual stress at the outer part of the cylinder. The proposed process has then been utilized to construct new combinations of autofrettage, shrink-fit and double autofrettage processes. The residual stress distribution through the thickness and fatigue life of these new combinations have been evaluated and compared with those based on conventional combinations of shrink-fit and autofrettage processes.

Finally, a practical design optimization methodology has been developed to identify the optimal configuration of autofrettaged and shrink-fitted cylinders. Optimization problems based on the high-fidelity finite element model is computationally very expensive and may not render accurate optimum results. Considering this in the presented research, design of experiment (DOE) and response surface method (RSM) have been used in

combination with the finite element model to create smooth response surface functions which can accurately describe the behavior of the residual hoop stresses with respect to the change of design variables. The developed response surface functions have been effectively utilized in the design optimization problems to simultaneously maximize the residual compressive hoop stress and minimize the residual tensile hoop stress through the thickness of the compound cylinder. Nonlinear mathematical programming technique based on the powerful sequential quadratic programming (SQP) algorithm has been used in combination with the genetic algorithm (GA) in order to accurately capture the global optimal solutions. At the end, the residual hoop stress distribution and fatigue life of the optimum configurations for each combination of autofrettage and shrink-fit processes have been evaluated and compared.

Dedication

To my ***parents***, my precious jewels ***Malak*** and ***Lojayne*** and special to my beloved wife ***Enas***.

ACKNOWLEDGEMENT

First of all, I would like to give the ultimate thanks to Allah for everything you have given me in my life.

Having written my thesis, I find the writing of acknowledgements by far the most daunting – there are many more aspects than merely the technical that must be narrated. There are so many to thank and little space to do so in. That said; I would like to express the deepest appreciation to my supervisor Professor ***Ramin Sedaghati*** for his guidance, encouragement, and support and for helping me complete my work. His helpful suggestions have meant a lot to me and to my research. His enthusiasm, patience and steadfast support gave me the inspiration to complete this doctoral research.

The contributions and insightful observations of my committee members, Drs. A. K. W. Ahmed, Dr. M. Packirisamy, and Dr. A. Aghdam, are also most appreciated and acknowledged. Also, I would like to thank Dr. I. Hassan for allowing me use his lab facilities during my experimental work, also, special thanks to his student Mr. Othman for his help during the experiments. I would also like to extend my thanks to all of Concordia University's professors and administrative staff with whom I have had the opportunity to take courses or engage in discussions with. I would also like to thank all my lab-mates, and all those who have helped me carryout my work.

Finally, my words stop if I want to thank ***my wife Enas***; she gave me great continuous support, time and encouragement more than I need throughout my years of study.

TABLE OF CONTENTS

LIST OF FIGURES

Figure Page

LIST OF TABLES

Table Page

NOMENCLATURE

Roman symbols

Symbol	Description
a	inner radius [m]
a_c	depth for a semielliptical crack [m]
a_{c_o}	initial depth for a semielliptical crack [m]
A_i	polynomial coefficients
b	outer radius [m]
$[B]$	strain-displacement matrix
C	interference radius [m]
c_p	specific heat [J/m.^{o}C]
$[C^t]$	element specific heat matrix [J/m.^{o}C]
$[C^{tu}]$	element thermo-elastic damping matrix
C_f	crack growth rate factor
$[D]$	elastic stiffness matrix relating stress to strain
DOF	Degree-of-freedom
DOE	Design of experiment
$\{e\}$	Error vector
E	modulus of elasticity [Pa]
$\{F\}$	element pressure vector [Pa]
GA	Genetic Algorithm
G_i	free surface correction factors

H	Tangential modulus of elasticity in the kinematic hardening [Pa]
$[K]$	element stiffness matrix
k^t	thermal conductivity coefficient [W/m.^{o}C]
$[K^{ut}]$	element thermo-elastic stiffness matrix
K_I	Stress Intensity Factor [MPa.m$^{0.5}$]
l_c	major axis of crack flaw [mm]
$[m]$	element mass matrix [kg]
m_f	crack growth rate factor
MCRS	Maximum Compressive Residual Stress
MTRS	Maximum Tensile Residual Stress
N	number of designed cycles
$[N_s]$	element shape function in the domain relating displacement function to the nodal displacement vector
$[N_n]$	element shape function evaluated at the surfaces on the boundary
$\{P\}$	external pressure vector [Pa]
P_{sh}	shrink-fit interference pressure [Pa]
P_{1in}	autofrettage pressure at the inner surface of the inner layer [Pa]
P_{1out}	the autofrettage pressure at the outer surface of the inner layer [Pa]
P_{2in}	autofrettage pressure at the inner surface of the outer layer [Pa]
P_{2out}	autofrettage pressure at the outer surface of the outer layer [Pa]
$\{Q\}$	thermal flux vector
$\{q\}$	heat flux vector
Q_c	crack flaw shape parameter

r	radial position [m]
RSM	Response Surface Method
R2	Coefficient of Determination
RSM	Root Square Mean
SIF	stress intensity factor
SFC	Shrink-Fit Cylinder
SLAC	single layer autofrettage cylinder
SLDAC	Single layer double autofrettaged cylinder
SVC	Single virgin cylinder
SQP	Sequential Quadratic Programming
T	temperature time [^{o}C]
t	time [s]
T_o	initial base temperature [^{o}C]
$\{T\}$	temperature vector [^{o}C]
t_1	thickness of the inner layer [m]
t_2	thickness of the outer layer [m]
$\{u\}$	nodal displacement vector [m]
u_r	radial displacement [m]
$\ddot{u}_r$	radial acceleration at radius r [m/s^2]
V	element volume [m^3]
x	distance through the cylinder wall measured from the inner surface [m]
$[X]$	design matrix
$\{\hat{y}\}$	approximate response vector

$\{y\}$	true response vector

Greek symbols

ν	Poisson's ratio
σ_y	yield stress [Pa]
ρ	density [kg/m^3]
δ	total radial interference [m]
σ_θ	hoop stresses [Pa]
σ_r	radial stresses [Pa]
ε_r	radial strain
ε_θ	tangential strain
α	the coefficient of thermal expansion [1/ ^{o}C]
$\{\alpha\}$	thermal expansion coefficient vector [1/ ^{o}C]
σ_z	axial stress [Pa]
α^*	thermal diffusivity [m^2/s]

CHAPTER 1

INTRODUCTION

1.1 Motivation and Statement of the Problem

Nuclear reactors, gun barrels, chemical plants, particles accelerators, hyper-sonic wind tunnels, food sterilization, water jet cutting, fluid transmitting, and ultra-fast pulsed lasers (used in micromachining) have common severe loading conditions. In these applications, dynamically thermal and mechanical loads are applied in a very short period of time. The cylindrical shell is one of the most widespread components used in these prementioned applications.

As a result of these extreme environmental conditions, mono-block cylinders have shown some limitations and may not be able to resist the applied extreme load. In order to increase the life-time, durability, pressure and thermal capacities of these cylinders or even reduce their weight, researchers have tried to cope with these limitations by designing multilayer shrink-fitted cylinders. They have also attempted to enhance the load carrying capacity of cylinders by autofrettage process in which the cylinder is pressurized internally so that the near bore region in the cylinder goes beyond the elastic regime and a controlled yielded zone is created. The main objective in both shrink-fit and

autofrettage techniques is to induce beneficial residual hoop stresses in the near bore region of the cylindrical shell. Considering this, the following design approaches have been mainly studied to improve the limitations of single monoblock cylinders:

- Shrink-fit of monoblock cylinders with different interface pressures and different materials.
- Autofrettage (partial plastic deformation of the cylinder wall due to internal pressure).
- Combined shrink-fit and autofrettaged technique.

Research in dynamic thermo-mechanical analysis and design optimization of shrink-fitted and autofrettaged multi-layered cylinders has not been received appropriate attention by the research community. The present research dissertation attempts to present fundamental investigation on analysis and design optimization of layered cylinders subjected to combined autofrettage and shrink-fit processes under thermo-mechanical loading conditions.

1.2 State of the Art

Increasing the life-time and the thermal and mechanical capacities are the most important features for cylinders used under thermal and mechanical environments. The use of pre-existing residual stresses in the cylinders before operation is essential to sustain severe conditions. Different approaches are used to acquire these residual stresses, such as

shrink-fit or autofrettage, in order to enhance their life-time, durability and increase their thermo-mechanical capacities.

The analysis of residual stresses in a thick-walled cylinder subjected to shrink-fit, autofrettage, or combined autofrettage and shrink-fit techniques has been discussed by many researchers. These processes improve cylinder behavior against working mechanical and thermal loads. Moreover due to many design parameters involved, design optimization of compound cylinder should be properly addressed in order to increase the load bearing capacities. The relevant reported studies in these subjects are thus systematically reviewed to build essential knowledge and determine the scope of the dissertation research. The reviewed studies, grouped under related subjects, are discussed in the following sections.

1.2.1 Shrink-fit cylinders

Shrink-fit or interference fit is one of the most reliable and economical techniques for co-signing mechanical parts. In addition, it presents residual stresses which are very important in pressure vessels as they enhance their load carrying capacity. For small components, shrink-fitting can be accomplished by press fitting, but in large parts usually the external part is heated and then, after assembling the inner part, the whole assembly is allowed to cool down to room temperature.

The stress and radial displacement distribution in an elastic-plastic shrink-fitted ring-disk based on tresca yield conditions have been investigated in Ref.s. [1-4]. Pedersen [5] investigated a 3-D model for a shrink-fit cylinder to illustrate the influence of the axial

boundary condition. Generally, the distribution of residual hoop and radial stresses through the thickness of shrink-fit cylinder is as shown in Figure 1.1. Also, Figure 1.2 shows the hoop and radial stresses distribution for the same cylinder when subjected to inner pressure.

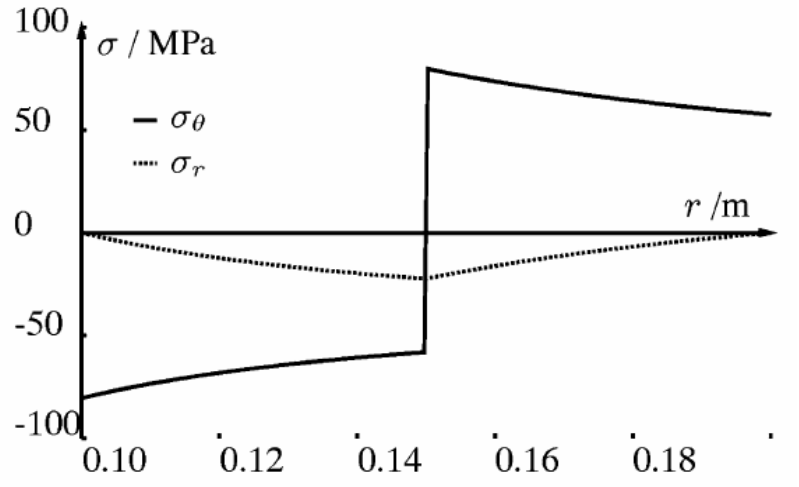

Figure 1.1: Residual hoop and radial stresses distribution through cylinder thickness due to shrink-fit only [5].

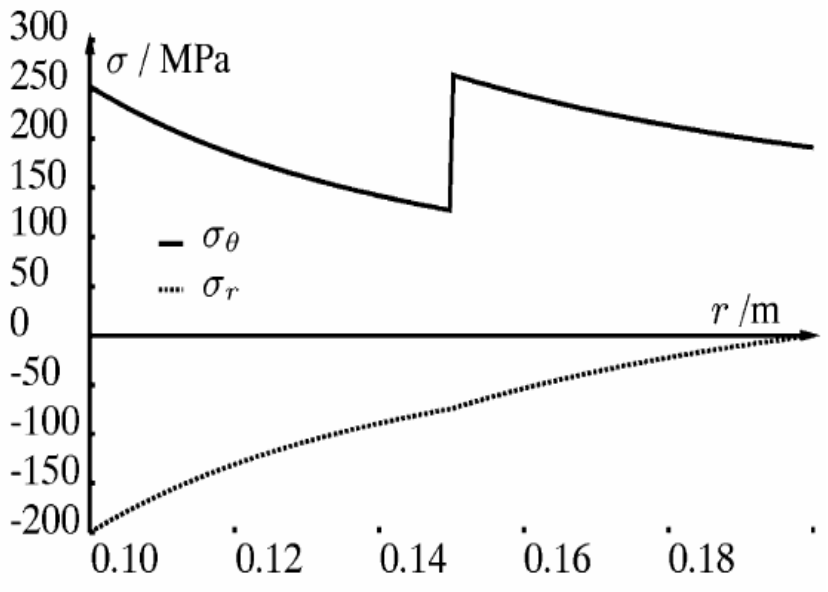

Figure 1.2: Resulting hoop and radial stresses distribution through cylinder thickness due to internal pressure and shrink-fit [5].

It should be noted that the residual hoop stresses as shown in Figure 1.1 switched from compressive to tensile nature immediately after the interference radius which may cause some limitations for optimal design of the shrink-fitted cylinder. Also, Figure 1.2 shows that the limitations take two different positions in the shrink-fit cylinder after applying the internal pressure load at the inner surface of the cylinder and the interference surface between the layers.

1.2.2 Autofrettage cylinders

Autofrettage is a process based on applying an internal pressure sufficient enough to deform the cylinder bore plastically, but not high enough to deform the outer part of the cylinder. The result is that, after the pressure is removed, the elastic recovery of the outer part of the cylinder puts the inner part into compression, providing residual compressive stresses.

However, reduction of the compressive yield strength due to the Bauschinger-effect is considered to reduce the effect of the autofrettage technique. The Bauschinger-effect refers to a property of material's stress/strain characteristic change as a result of the microscopic stress distribution of the material. By applying a tensile or compressive load beyond the elastic limit, the elastic limit for compression or tension, respectively, is reduced considerably and the more the load exceeds the elastic limit, the greater the reduction.

There have been numerous investigations relating the analysis of residual stresses and deformation in a thick-walled cylinder subjected to autofrettage, such as Franklin and

Morrison [6], Chen [7, 8] and Stacey [9]. Few of these investigations reflect the unloading behaviour of the autofrettage process while considering the Bauchinger effect [10, 11]. The most popular models to mimic the stress-strain behaviour during unloading of the autofrettage process have been either bilinear isotropic or kinematic hardening models.

Parker et al. [12-13] started their investigations on autofrettaged mono-block cylinders by reviewing and comparing extensively different unloading models. Then, Parker [14] extended his work on the Bauschinger effect and found that the Bauschinger effect is evident when the ratio of autofrettage radius to bore radius exceeds 1.2, irrespective of the ratio of the outer diameter of a cylinder to its inner diameter. It was shown that, below that ratio (1.2), the results followed the ideal elastic perfectly plastic results without considering the Bauschinger effect.

Livieri and Lazzarin [15] analytically investigated the residual stress distributions for autofrettaged cylindrical vessels considering the Bauschinger effect. Jahed and Ghanbari [16] measured the actual tensile–compressive stress-strain behaviour of alloy steel during the autofrettage process. They found that there is 30% over-estimation of compressive residual stress when compared with the ideal and bilinear isotropic hardening model. Huang [17] proposed a general autofrettage model that integrates the material strain-hardening relationship and the Bauschinger effect, based upon the actual tensile–compressive stress–strain curve. The model incorporates the von Mises yield criterion, an incompressible material, and the plane strain condition to produce the residual stress distribution formula. Huang and Moan [18] proposed an analytical model for autofrettage while considering Young's modulus and the reverse yield stress dependent on the prior

plasticity. This model is based on the actual tensile-compressive curve of the material and the von Mises yield criterion incorporating the Bauschinger effect factor and the unloading modulus variation as a function of prior plastic strain, and hence of the radius. Figure 1.3 shows the distribution of residual hoop and radial stresses in an autofrettage cylinder considering the model in Ref. [18].

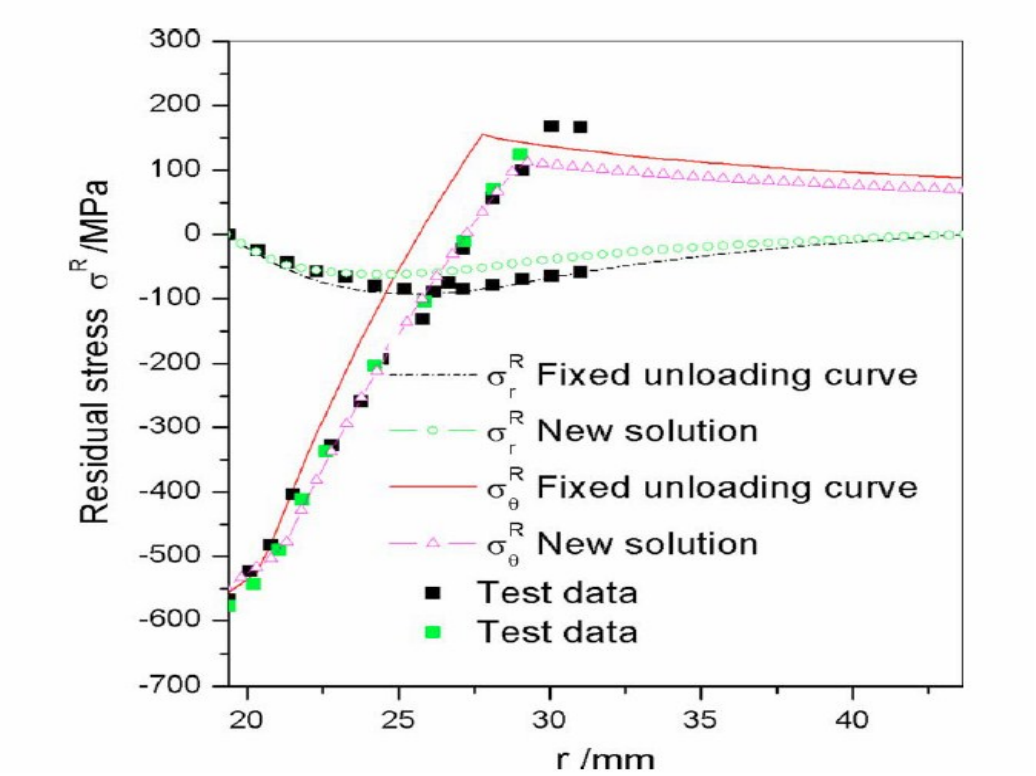

Figure 1.3: Residual stress via radial position for an autofrettage cylinder [18].

1.2.3 Multiple-autofrettage cylinders

Few researchers have attempted to use what they called re-autofrettage. This is a procedure wherein the pressure vessel is autofrettaged once and then, without any

intervening process, is subjected to a second similar autofrettage cycle. This process may enhance the compressive residual stresses in the near bore area of the cylinder.

Parker [19] investigated double and triple autofrettage processes for his thick-wall cylinder to mitigate the Bauschinger effect, as shown in Figure 1.4. It has been found that the fatigue life of the cylinder improved by at least a factor of 2, according to the geometry and the ratio of the autofrettage pressure to the yield strength.

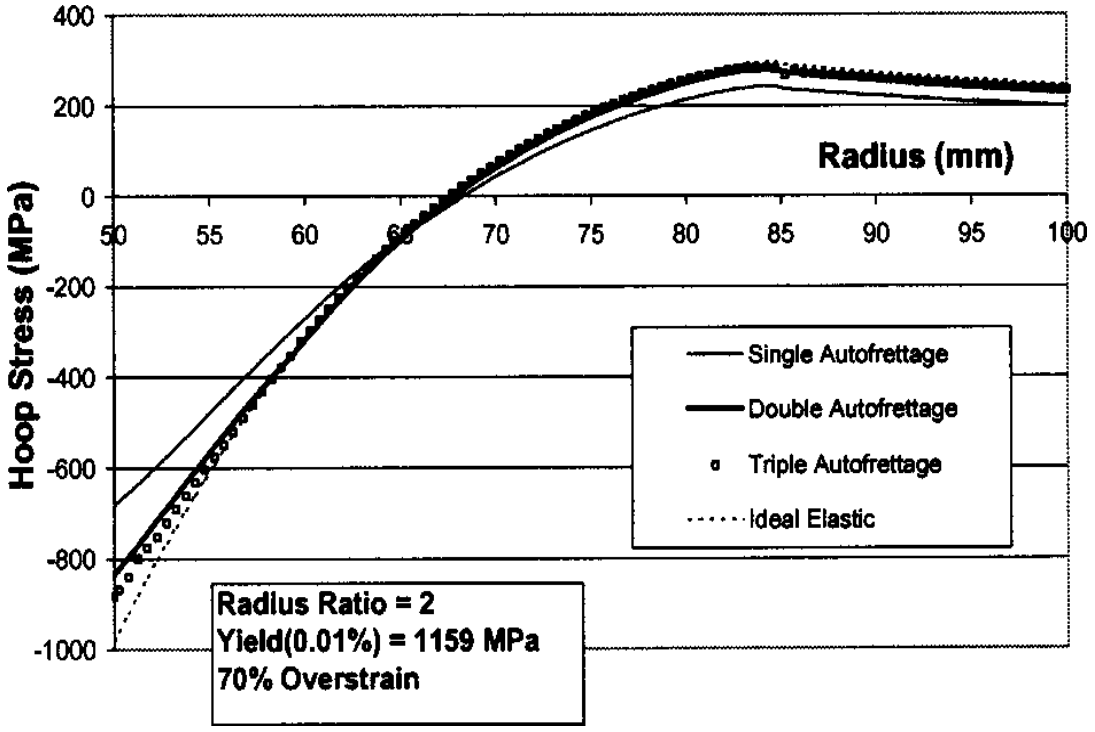

Figure 1.4: Residual hoop stresses for single, double and triple autofrettage [19].

Jahed et al. [20] used the same technique implemented by Parker [19] but the autofrettage pressure was changed for each cycle. They found that there is no benefit in the re-autofrettage of a tube with the same autofrettage pressure, and the real benefit comes from using a low autofrettaged pressure first then a higher one, as shown in Figure 1.5.

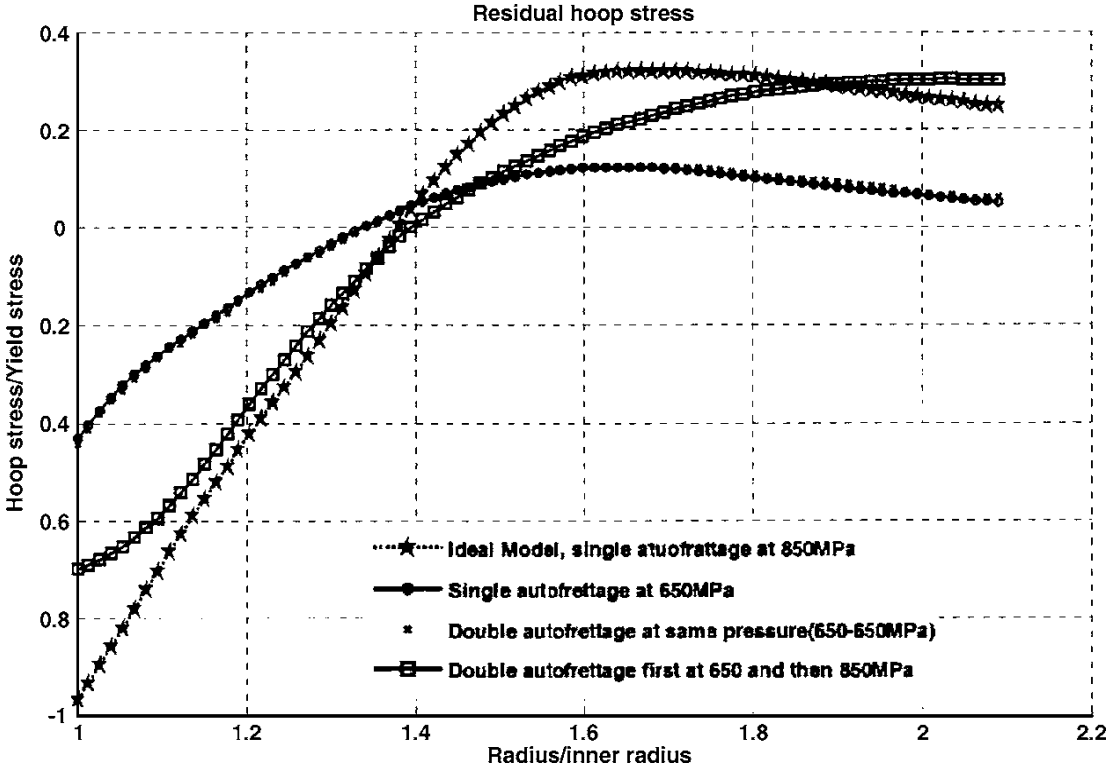

Figure 1.5: Residual hoop stresses for single and double autofrettage with different autofrettage pressures [20].

It should be noted that in all previous works autofrettage applied only on the inner surface. No research has been done on applying autofrettage on the outer surface of the cylinder.

1.2.4 Autofrettaged and shrink-fitted compound cylinders

As mentioned before, there are limitations regarding autofrettage and shrink-fit processes. Both techniques are generally used to introduce beneficial residual stresses into pressure vessels. Regarding the autofrettage process, the Bauschinger effect can considerably reduce this beneficial residual stress near the bore and, also, shrink-fit alone generates

much less compressive residual stress compared with autofrettage in the region near the bore and higher detrimental tensile stress at the outer layer of the cylinder. Considering this, combination of both autofrettage and shrink-fit may provide a more suitable residual stress profile and thus increase the load carrying capacity and fatigue life of multilayer cylinders. Researchers have used different design techniques by combining the autofrettage and shrink-fit to enhance the residual stress distribution and to improve the fatigue life. Regarding the combined autofrettage and shrink-fit, the following sequence may be considered:

(a) Shrink-fitting all the layers of the cylinder first and then performing the autofrettage process to the whole assembly, commonly known as shrink-fit, prior to autofrettage.
(b) Shrink-fitting all autofrettaged cylindrical layers (autofrettage prior to shrink-fit).
(c) Interchanging the shrink-fit and autofrettage techniques and find a suitable combination.

Kapp et al. [21] proposed a multilayer design involving a shrink-fit procedure on a previously autofrettaged monoblock tube to achieve a very long life. Parker [22] enhanced his cylinder by shrink-fitting the autofrettaged cylinder with an inside liner, as shown in Figure 1.6.

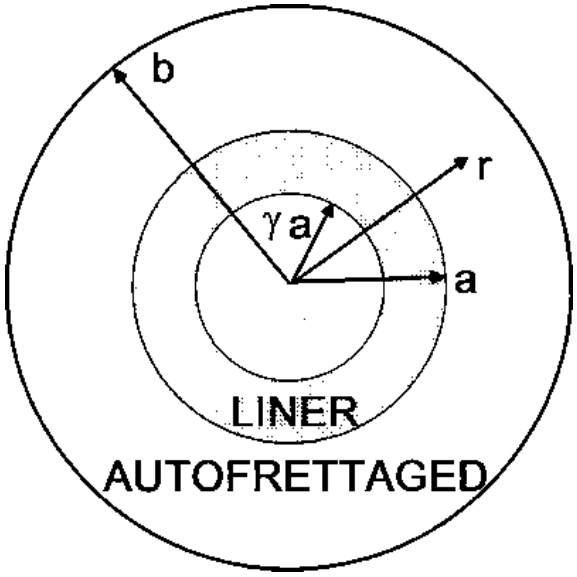

Figure 1.6: Parker's combined tube geometry [22].

Parker and Kendell [23] proposed a different design philosophy for combined cylinders. They investigated a procedure consisting of a sequence involving shrink-fit followed by autofrettage, which might reduce Bauschinger effect losses at important locations and hence enhance residual compressive hoop stresses in the near-bore region. The shrink-fit cylinder consists of an inside cylinder (completely elastic) called liner and an outside cylinder called "jacket". Depending on the magnitude of the initial interface pressure and the autofrettage pressure, it is possible to generate plastic deformation in both liner and jacket (plastic deformation in the liner followed by plastic deformation in the jacket, or vice versa). Thus, there are three possible failure locations: the internal surface of the liner, the outside surface of the liner, (internal surface of the jacket) and the outside surface of the jacket, as shown in Figure 1.7.

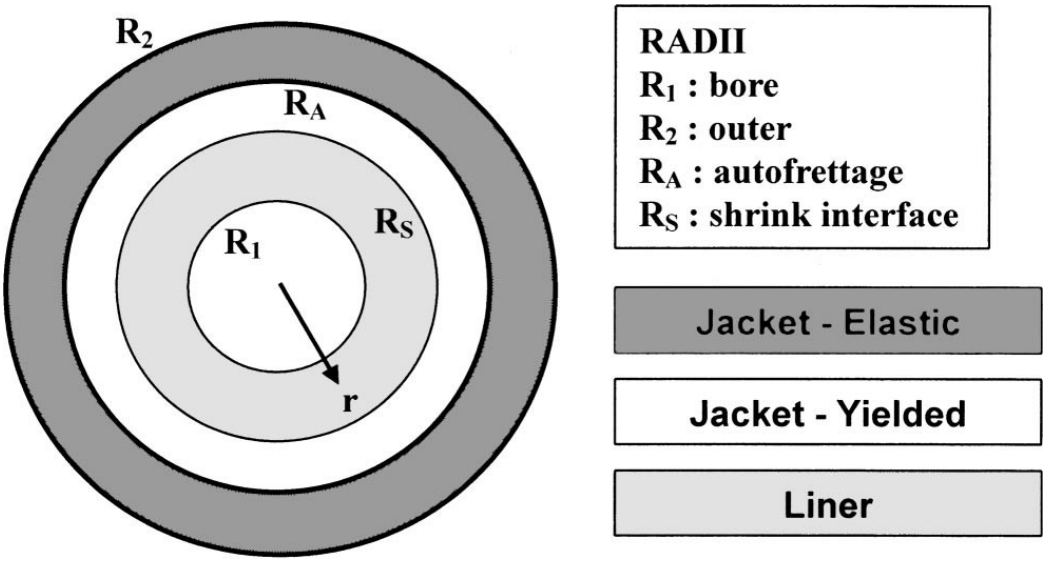

Figure 1.7: Tube geometry before the effect of autofrettage pressure [23].

The residual hoop stress profile has been investigated for the following cases [23]:

a) Ideal autofrettage. Autofrettage of a single cylinder considering perfectly plastic material with equal yield strength in tension and compression (the Bauschinger effect has been ignored).

b) Mono-block autofrettage. Autofrettage of a single cylinder considering the Bauschinger effect. Practically, the unloading is not linear and also tensile and compressive strength after unloading is not equal due to the Bauschinger effect.

c) 60 MPa Shrink-fit. Here, two virgin tubes which are free of residual stresses are shrink-fitted. This shrink-fit process develops the interference pressure of 60 MPa between the outer jacket and inner liner at interference radius of 65 mm with no plastic deformation.

d) 90 MPa Shrink-fit + autofrettage and 120 MPa Shrink-fit+ autofrettage. Here, two virgin tubes are shrink-fitted in a manner to develop shrink-fit pressures of first 90 MPa and then 120MPa. The shrink-fitted compound tubes are then subjected to the autofrettage.

Figure 1.8 shows the results for the above-mentioned combinations [23]. As it can be seen, the compressive residual stresses due to combining autofrettage and shrink-fit, especially in the near bore area have been considerably enhanced.

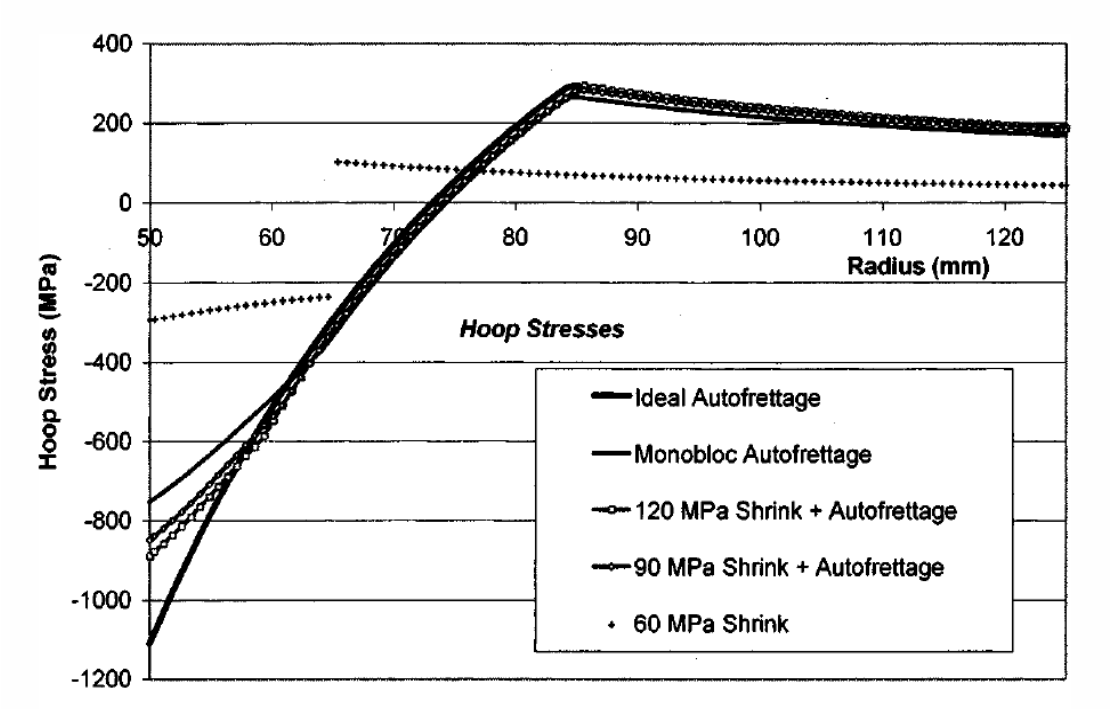

Figure 1.8: Residual hoop stresses profile for different cases in Ref. [23].

Majzoobi et al. [24] simulated aluminum shrink-fit cylinders for different shrink-fit pressures and interference radii to predict the optimum shrink-fit radius when subjected to autofrettaged pressures. The optimum interference diameter was found corresponding

to the situation when the maximum von-Mises stress at the internal radii of both the inner and outer cylinders become equal.

Jahed et al. [25] proposed three different combinations of both shrink-fit and autofrettage processes. The optimum values of the layer thicknesses, shrink-fitting pressures, and autofrettage percentages were then determined to achieve the maximum fatigue life of a three-layer vessel for each combination. Due to its relevant importance, the considered combinations by Jahed et al. [25] have been summarized as: (i) perform autofrettage on each layer separately, and then shrink-fit; (ii) shrink-fit first the two inside layers, followed by the autofrettage of the assembly. Next, perform autofrettage on the third layer and then shrink-fit it to the previous assembly; (iii) shrink-fit all three layers sequentially, and then perform autofrettage on the whole assembly. Figures 1.9-1.11 show the distribution of residual hoop stresses along the radial position for the above combinations presented by Jaded et al. [25].

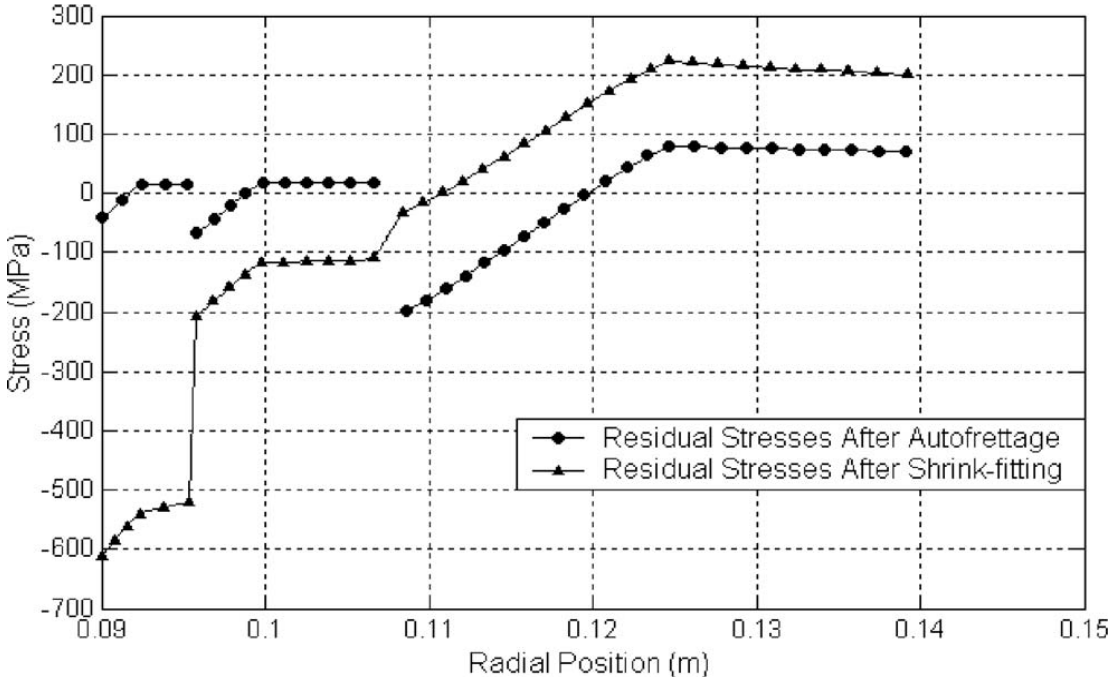

Figure 1.9: Residual hoop stresses during the sequence of the first combination [25].

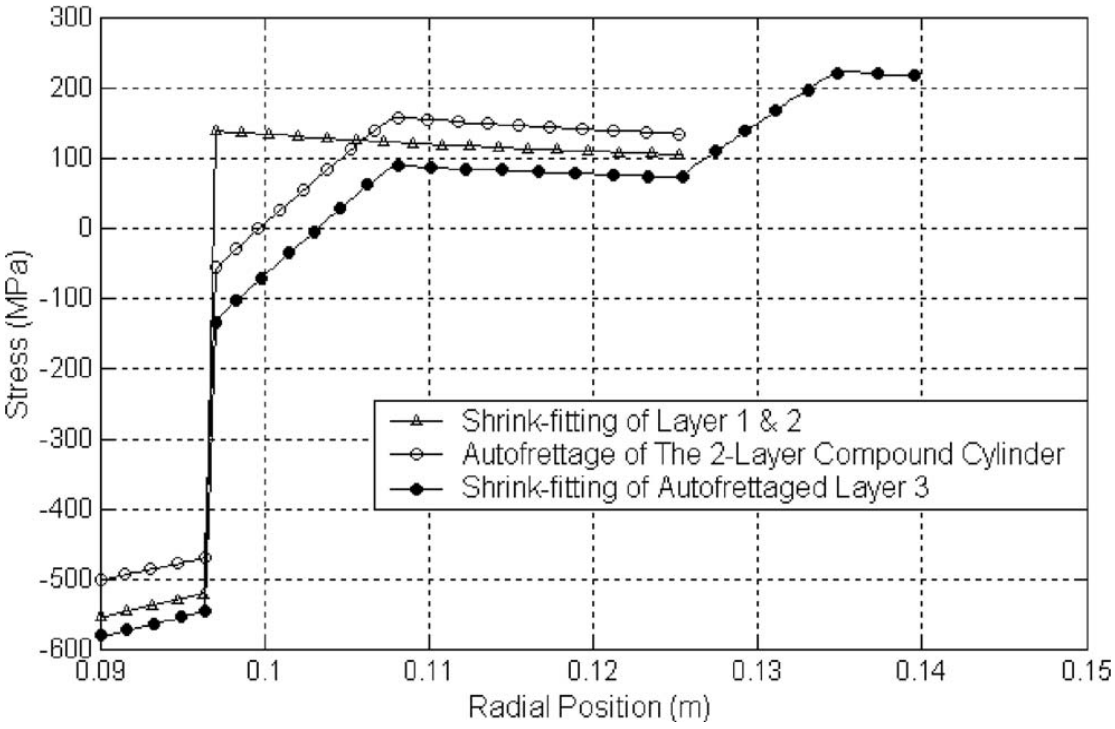

Figure 1.10: Residual hoop stresses during sequences of the second combination [25].

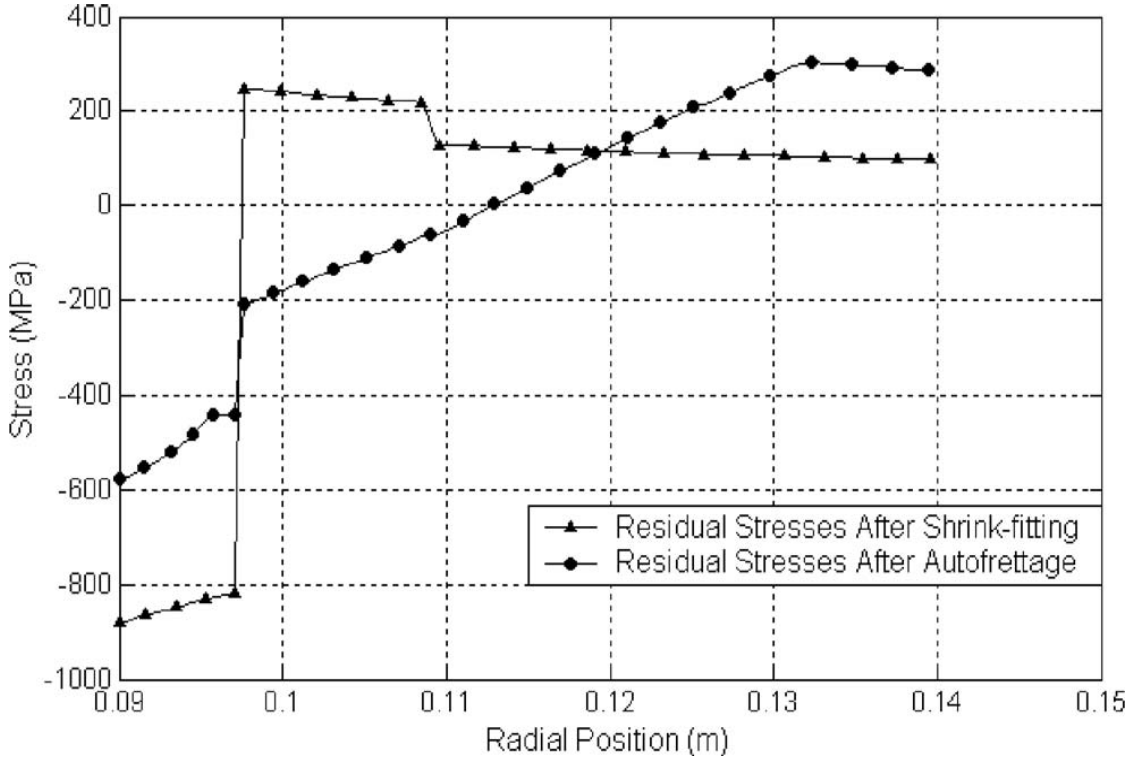

Figure 1.11: Residual hoop stresses during sequences of the third combination [25].

Lee et al. [26] studied shrink-fitted and autofrettaged cylinders based on elastic-perfectly plastic and the strain hardening materials. They proved that analysis based on strain hardening provides more reasonable results as it agreed well with experimental work, especially at the near bore region for a single autofrettage cylinder, as shown in Figure 1.12. Also, the effect of shrink-fit tolerance for different overstrain percentages of the autofrettage on the residual hoop strain is investigated. It has been found that the residual compressive stress due to strain hardening model can be considerably improved by increasing overstrain level up to 80%, as shown in Figure 1.13. They concluded that the increase of shrink-fit tolerance is harmful to the combined process.

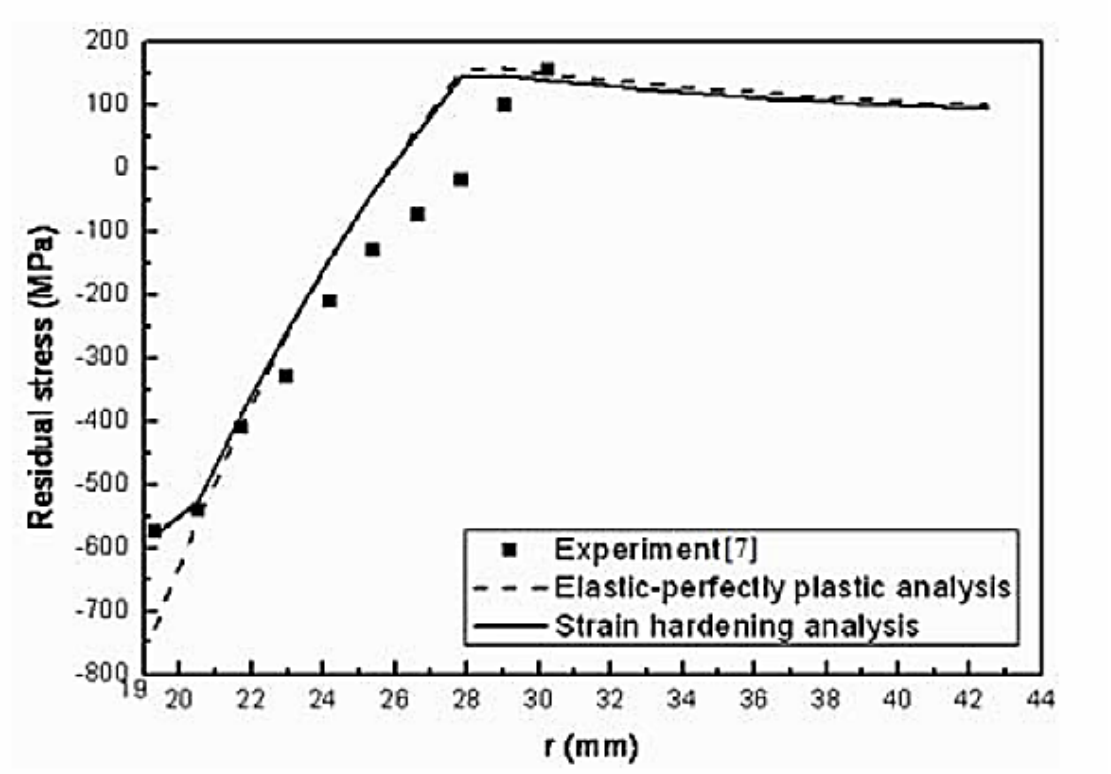

Figure 1.12: Residual stress distribution of an autofrettaged single cylinder with 35.7% overstrain level [26].

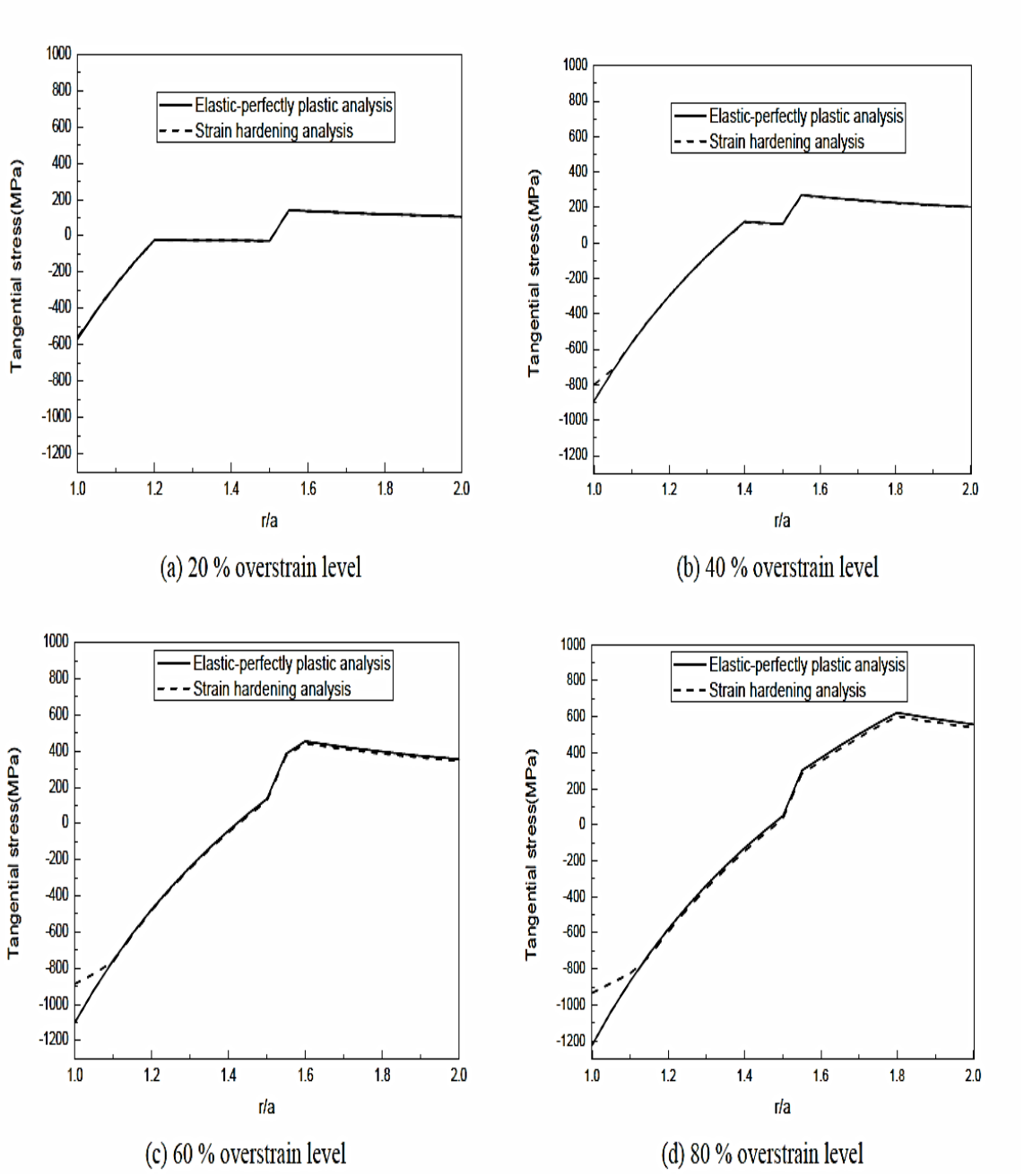

Figure 1.13: Residual hoop stress distribution of an autofrettaged compound cylinder with 0.1 mm shrink-fit tolerance under various overstrain levels [26].

1.2.5 Thermo-mechanical response of compound cylinders

In recent years, there has been an increasing interest in the importance of thermo-mechanical analysis of multilayer cylinders under simultaneous thermal and mechanical loads. Different approaches have been investigated to predict the response of multi-layer cylinders under thermal and mechanical loads. Thermo-elasticity is the branch of applied mechanics that is concerned with the effects of heat on the deformation and stresses of solid bodies. However, it is not totally reversible, as the elastic deformation due to temperature is reversed by cooling, while the thermal part may not be reversed due to energy dissipation through heat transfer. Moreover, the effect of temperature on the deformation of bodies is not reversible, but the deformation could change the temperature of bodies, demonstrating that mechanical and thermal aspects are coupled. Hence the mechanical and thermal loads should be coupled for an accurate analysis of cylinders under simultaneous thermal and mechanical dynamic excitations.

Partial and full coupling are the two main approaches mainly used to analyze thermo-mechanical problems. In the partially coupling approach, the solution to thermo-elastic problems are used to be in two separate stress fields, the thermal and mechanical fields. The temperature variation has been shown to be the most important factor for the thermal stress field, and, typically, the temperature profile through the thickness is priory defined (constant or linear) or is found by solving the Fourier heat conduction equation considering only the temperature as the external load. The majority of the work has been devoted to the analysis of partially coupled thermo-elastic problems in which temperature profile through the thickness is typically defined or obtained independent of displacement functions [27-29]. While this may be justified for static or quasi-static loading conditions,

for severe thermal and mechanical external loadings, partial treatment may generate an inaccurate temperature and stress distribution which, if overlooked, can cause catastrophic structural failure. In general, the thermo-mechanical analysis of multi-layer cylinders has not received appropriate attention by the research community, especially when dynamic cyclic thermo-mechanical loads and thermal accumulation are taken into consideration.

Chen et al. [27] investigated the one-dimensional, quasi-static partially coupled, thermo-elastic problems of an infinitely long hollow multilayer cylinder with different materials. The initial interface pressure in a multilayered cylinder caused by the heat-assembling method is considered as an initial condition for the thermo-elastic equilibrium problem. Using the Laplace transform, the general solutions of the governing equations were obtained in the Laplace domain. The solution in the time domain was then obtained using the inverse Laplace transform.

Lee et al. [28] studied the multilayer hollow cylinder as a one dimensional quasi-static thermo-elastic problem with time dependent boundary conditions under temperature and pressure loads. They also used the Laplace transform, and a finite difference technique to obtain the solution. Some simplifications, such as free-traction medium, no body force and no internal heat generation were considered to derive the governing equations. They then extended the model [29] to a two-dimensional problem and obtained the distribution of temperature along the radial directions for different time and also variation of the temperature with respect to time at different radial positions.

Few investigations have also been done on fully coupling thermo-mechanical problems in which the temperature and displacement are considered simultaneously to be the primary variables to evaluate the transient response and identify the temperature, displacement and stress distributions along all the directions. Lee [30] enhanced his work to a two-dimensional, quasi-static fully coupled, thermo-elastic model to solve the problem of a finitely long, hollow multilayered cylinder composed of two different composite materials, with axial symmetry, subjected to sudden heat at the inner and outer surfaces. The governing equations were written in terms of displacement and temperature increment. The general solution was first obtained using the Laplace transform in a complex domain, then, by using the finite difference technique and matrix operations simultaneously; the solution was transformed back to the time domain. It should be noted that depending on the fact that there might be numerical instability for the calculation of the inverse transform due to the very short time of thermal shocks, the applicability of the Laplace and Fourier transform methods in two-dimensional thermo-elastic problem is basically limited.

Ahmed and Ezzat [31] studied a one-dimension thermo-viscoelasticity problem in an isotropic medium occupying the region $-\infty < X < \infty$ using four generalized thermo-elasticity theories namely: Lord‑Shulman (L-S) [32], Green‑Lindsay (G-L) [33] and Tzou and Chandrasekharaiah (C-T) [34, 35] as well as the dynamic coupled theory. The model is subjected to thermal shock and the solution is obtained using the Laplace transform and inverse Laplace transform using the different aforementioned theories. The important phenomenon observed in this problem where the medium is of infinite extent is that the solution of any of the considered functions for the generalized theory vanishes

identically outside a bounded region of space. This demonstrates clearly the difference between the coupled and the generalized theories of thermo-elasticity.

Tian et al. [36] derived two-dimensional finite element thermo-elastic equations within the frame work of the Green‑Lindsay (G-L) theory, which contains two constants that act as relaxation times, and then modified all the equations of the coupled theory. The thermo-elastic equations were solved directly in the time domain using the principal of virtual work. They changed the meshing in the front of the heat wave propagation to obtain more reliable results.

Birsan [37] studied one of the most interesting approaches to deal with the thermo-elastic problem called Cosserat surface. In this approach, the analysis of thermal stresses through thickness is accomplished by providing two temperature fields in which one represents the absolute temperature of the middle surface and the other accounts for temperature variation along the thickness. Then dynamic thermo-mechanical analysis was accomplished, in which the thermo-mechanical coupling term acts as a thermal source, which is proportional to strain rate.

Ying and Wang [38] derived the exact solution for a two-dimensional elasto-dynamic analysis of a finite hollow cylinder excited by a non-uniform thermal shock. Non-uniform thermal shock occurs when the whole body experiences an instantaneously increasing temperature field with different amplitudes at different positions. They specified the constitutive equation as Lame's equations and determined the equations of motion for an isotropic finite simply-supported hollow cylinder. These equations were then solved into two parts: a quasi-static part which satisfies the inhomogeneous boundary conditions and

a dynamic part which is accomplished using the separation of variables technique. They presented the radial and hoop stresses through the thickness using their exact 2-D solution and demonstrated the stress wave propagation at different times. The results show that, in a thermally shocked hollow cylinder, the stress waves generate first at both internal and external surfaces and then propagate independently to the middle part.

Brischetto and Carrera [39] investigated a fully coupled thermo-mechanical analysis of a multilayer square plate, where both temperature and displacement were considered to be primary variables in the governing equations. Three different cases were discussed: 1- Static analysis under static temperature on the external surfaces. 2- Static analysis under a mechanical load, with the possibility of considering the temperature field effects. 3- A free vibration analysis considering the effect of the temperature field effects. Here, the time variation of the temperature was not taken into account, which means that the problems were investigated at equilibrium state-state conditions. Carrera's unified formulation [40] is applied to obtain several refined two-dimensional models based on Equivalent Single Layer (ESL) and Layer Wise (LW) theories to simulate the response of the multi-layer plate. For the ESL method in which the unknown variables are the same for the whole multilayer plate, the Taylor expansion was employed to approximate the variable in the thickness direction. While in LW, in which the unknown variables are considered to be independent for each layer, a combination of Legendre Polynomials was used to describe the thickness function. Constitutive equations for coupled thermo-mechanical analysis have been obtained from enthalpy density (a thermodynamic property used to calculate the heat transfer during the quasi-static process) and then the

principal of virtual work has been extended to partially and fully couple thermo-mechanical analysis.

Feldhacker and Hu [41] investigated the dynamic response of a cannon barrel to the various ballistic effects of the different round types used today using thermo-structural coupled finite element analysis.

1.2.6 Fatigue life of compound cylinders

One of the main purposes of combined autofrettage and shrink-fit in multilayer cylinders is to introduce the beneficial residual stresses in order to increase the fatigue life of the cylinder. However not many works addressing the fatigue life have been done. In particular, most of the previous works are mainly based on ASME fatigue life code and consider only cyclic inner pressure as the fatigue load. Parker and Kendall [23] calculated the fatigue life of their proposed combination of the combined autofrettage and shrink-fit multilayer cylinder using the stress intensity factor according to the ASME high pressure vessels code [42]. They found that shrink-fit prior to the autofrettage process increases the mechanical life time by 41% compared with ordinary shrink-fit. Jahed et al. [25] calculated the fatigue life for three different combinations using the same approach as that in Ref. [23]. They found that the first combination (autofrettaged each layer separately then shrink-fit) had the best fatigue life time. Jahed et al. [43] also extended their work for the stress intensity factor under the thermo-mechanical load using the weight function method for a single autofrettaged cylinder. They found that the thermal stresses reduce the life of autofrettaged cylinders by a factor of 2. Algeri et al. [44] did a

comparative study for three methods of crack growth for a wire-wound pressure vessel. The three approaches used were: (a) postulate a 1/3 semi-elliptical shape for the crack unchanged during crack growth, (b) postulate a semi-elliptical shape for the crack that is updated at the deepest point and at the surface points, and (c) calculate by numerical analysis the crack front evolution during crack growth. They found the second and the third approaches are close together compared with the first one. Nabavi and Shahani [45] calculated the stress intensity factor for a semi-elliptical surface crack in a thick-walled cylinder under transient thermal loading. The method of calculation was based on the weight function where the stress intensity factor changed along the crack front. Nabavi and Ghajar [46] found a closed form stress intensity factor for an internal circumferential crack in cylinders with various ratios of the internal and external radii using the weight function method. They then extended their work [47] by using the developed form to calculate the stress intensity factor for a pressurized cylinder under thermal loading. Lee et al. [48] studied the crack propagation kinetics for compound autofrettage and shrink-fit cylinder during firing. They then analyzed the effect of autofrettage on crack propagation of this compound cylinder and found that the fatigue life of compound cylinders are 1.1~1.3 times greater than those of single autofrettage cylinders depending on autofrettage level.

1.2.7 Design optimization of compound cylinders

Due to many possible parameters, such as sequence of combination, thickness of layers, autofrettage pressure and radial inference, design optimization of multi-layer cylinders is of paramount importance to provide optimal residual stress distribution in an attempt to

maximize the load bearing capacity and fatigue life of cylinders. Few research works have addressed design optimization of compound cylinders subjected to autofrettage and shrink-fit processes.

Amran et al. [49] investigated the optimum autofrettage pressure in a thick-walled cylinder. They found that the optimum autofrettage pressure results in the minimum equivalent stress which occurs at the elastic-plastic junction line. Jahed et al. [25] found the optimum values of the layer thicknesses, shrink-fitting pressures, and autofrettage percentages to achieve the maximum fatigue life for their proposed three different combinations. They used the simplex search method to determine the optimum values. Kumar et al. [50] studied the effect of a number of layers on the maximum hoop stress for pressurized shrink-fitted multilayer cylinders. They found that the maximum hoop stress at the inner most surface decreases with the increase of the number of layers. The optimum thickness of each layer was then obtained using Genetic Algorithm (GA) and Lagrange's Multiplier methods. Kumar et al. [51] extended their work to investigate the combined effect of autofrettage and shrink-fit in multilayered vessels. For the optimization process, the design variables were identified to be: thickness of each layer, autofrettage percentage, and diametral interference for shrink-fitting; whereas the objective function was to minimize the hoop stress distribution through the whole thickness of the cylinder when subjected to inner pressure. The Genetic Algorithm was used as the optimization algorithm to find optimal solution. They studied eight different combinations of a 3-layer vessel. They found that the lowest maximum effective hoop stress was found in the case of performing autofrettage on each layer individually and then shrink-fitting all layers sequentially, and finally applying autofrettage on the whole

assembly. Conversely, the maximum fatigue life was found in the case of performing autofrettage of the inner and outer layers individually and then shrink-fitting all the layers, followed by final autofrettage of the assembly.

It is noted that most of the prementioned work had been done based on simplified analytical formulas for shrink-fitting and autofrettage processes, such as the proposed formulas by Huang and Moan [18].

1.3 Objective and Scope of the Present Work

The main objective of this research is to fundamentally investigate compound cylinders subjected to combined autofrettage and shrink-fit processes and develop new design process and practical design optimization methodologies to enhance their fatigue life under cyclic thermo-mechanical loads. This objective has been achieved through following five stages.

In the first stage, an accurate finite element model in the environment of ANSYS has been conducted for simulating autofrettage and shrink-fit processes in thick-walled cylinder. This model has been verified with results reported in the literature and then used to produce the residual stresses for different arrangements of autofrettage and shrink-fit compound cylinders.

In the second stage, fully coupled thermo-elastic analysis is taken into consideration for the evaluation of the temperature profile through the wall thickness of the cylinder. The finite element model for the compound cylinder has been developed and then validated

with previous work in the literature and experimental study. In the experimental work, the temperature has been measured at different locations through the thickness of a two-layer shrink-fitted cylinder, subjected to quasi-static and dynamic thermal loads at the inner surface. In addition, the hoop strain at the outer surface of the cylinder has been measured for the same thermal loads. Using the developed finite element model, the hoop stress distributions through the thickness of different combinations of the compound cylinder have been calculated under different loading conditions including inner static pressure, inner cyclic thermal loads, and a combination of these loads. Different combinations of a two-layer compound autofrettage and shrink-fit cylinder have also been investigated under the prementioned loads. These combinations are: 1- Shrink-fit prior to autofrettage of the whole assembly 2- Shrink-fit of two autofrettaged layers. 3- Shrink-fit of an inner autofrettage layer with an outer virgin layer. The performance of these combinations has then been compared with that of dimensionally equivalent non-autofrettaged mono-block cylinder, autofrettaged mono-block cylinder and shrink-fitted cylinder.

In the third stage, the mechanical fatigue life has been calculated using Alternative Rules for Construction of High Pressure Vessels in Boiler and Pressure Vessel ASME codes due to cyclic inner pressure. Moreover, the Stress Intensity Factor (SIF) has been calculated for these combinations when subjected to cyclic thermal loads or cyclic thermo-mechanical loads, considering thermal accumulation. The stress intensity factors for different combinations have been compared with the critical SIF which is the fracture toughness of the material. The number of cycles until the critical SIF is reached has been counted and considered as the life time of each combination.

In the fourth stage, a new design philosophy for autofrettage process namely double autofrettage process (outer surface autofrettage pressure prior to inner surface autofrettage) has been developed. This new technique can increase the compressive residual stress at the near bore area; it also reduces the detrimental tensile stress at the outer part of the cylinder wall compared with the normal autofrettage technique. Four new different combinations have been proposed for a two-layer compound cylinder accompanying double autofrettage with single autofrettage and shrink-fit processes. The residual stresses for these new combinations have been produced and then compared with the residual stresses in the prementioned conventional combinations.

In the fifth stage, a practical design optimization methodology has been developed to identify the optimum configuration in compound cylinders subjected to autofrettage and shrink-fit processes in order to simultaneously increase the beneficial compressive residual stresses and decrease the detrimental tensile residual stresses. The design variables have been considered to be the thickness of each layer, autofrettage pressures and radial interference for shrink-fitting according to each arrangement. Design optimization based on a high fidelity finite element model is computationally very expensive and may not render accurate optimum results due to the noisy nature of the finite element response. In order to acquire objective functions, design of experiment (DOE) combined with the response surface method (RSM) has been utilized to develop smooth response functions which can be effectively used in the design optimization formulations. Genetic algorithm (GA) combined with sequential quadratic programming (SQP) technique has been utilized to find the accurate global optimum solutions. The

residual stress distributions and then mechanical fatigue life have been evaluated for the optimum configurations and then compared.

1.4 Thesis Organization

This thesis consists of six chapters. The present chapter provides the problem statement and motivation of the study. Also, it provides a literature review of the recent research showing the most important and relevant contributions that are closely related to the field of study. This chapter concludes by identifying the objective of the work together with the thesis layout.

In Chapter 2, the models and fundamentals of the main processes required to construct the autofrettaged and shrink-fitted compound cylinder have been discussed in detail. The autofrettage and shrink-fit finite element models have been developed in the environment of ANSYS. Validation of these finite element models has been accomplished through comparing the results with those of available analytical models or results from the literature. Moreover, different autofrettage and shrink-fit combinations for two-layer compound cylinder have been proposed, and then residual hoop stresses for these combinations have been evaluated and compared.

In Chapter 3, a fully coupled thermo-mechanical analysis has been conducted for a compound cylinder considering thermal accumulation. To verify the thermo-mechanical finite element model, an experimental setup has been designed for a two-layer shrink-fit cylinder under quasi-static and dynamic thermal loads. The response of the compound cylinder due to different mechanical, thermal and thermo-mechanical loads has been

calculated. Also, the fatigue life due to these prementioned loads has been evaluated for the different combinations of the compound cylinder.

In Chapter 4, a new design philosophy has been proposed named as double autofrettage process. Using proposed technique, new combinations of compound cylinders have been produced. Also the residual stresses and fatigue lives of these combinations have been evaluated and then compared together.

In Chapter 5, the design optimization of compound cylinders subjected to autofrettage and shrink-fit processes has been formulated. First, the objective functions have been developed using DOE and RSM techniques. Then, GA has been used to find the global optimum values approximately which have been then imported as initial values by SQP technique to find the accurate global optimal solutions.

Finally, Chapter 6 provides the major conclusions, the most significant outcomes and contributions and suggestions for future works.

CHAPTER 2

MODELING OF AUTOFRETTAGE AND SHRINK-FIT PROCESSES

In this chapter, autofrettage and shrink-fit processes have been studied fundamentally and their modeling has been discussed in detail. Starting with autofrettage, the most popular models used to mimic autofrettage, especially when considering the Bauchinger effect, are examined. A 3-D finite element model has been constructed in the environment of ANSYS and a kinematic hardening model has been chosen as the material behaviour during autofrettage process. The residual hoop stress has been evaluated through the thickness of cylinder and then compared with those available in the literature for validation.

Similar to autofrettage, a 3-D finite element model has been constructed to evaluate the residual stress due to the shrink-fit process and then validated with the analytical results. Finally, different combinations of autofrettage and shrink-fit processes in a two-layer compound cylinder have been considered and the residual stress distributions through the cylinder thickness have been evaluated and compared for each combination.

2.1 Modeling of the Autofrettage Process

Autofrettage is a process in which the cylinder is subjected to a certain amount of pre-internal pressure so that the inner part of its wall becomes partially plastic. The pressure is then released and the outer elastic part of the wall tries to compress the inner plastic part, causing compressive residual stresses at the inner part and tensile residual stress at the outer part of the cylinder wall, as shown in Figure 2.1 a, b [52]. These residual stresses lead to a decrease in the maximum von-Mises stress in the working loading stage at the near bore area of the cylinder. This means an increase in the pressure capacity of the cylinder.

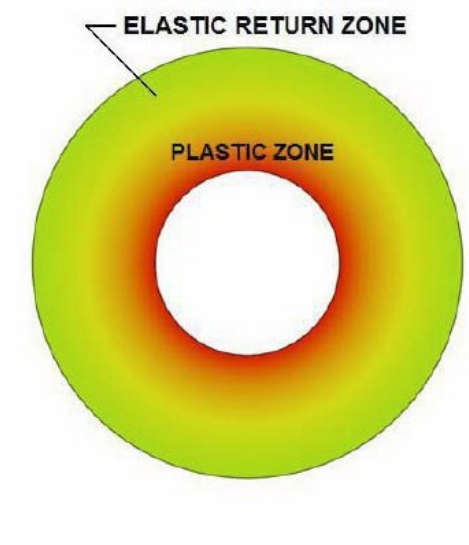

Figure 2.1-a: Stresses and deformation after applying the autofrettage pressure (loading stage) [52].

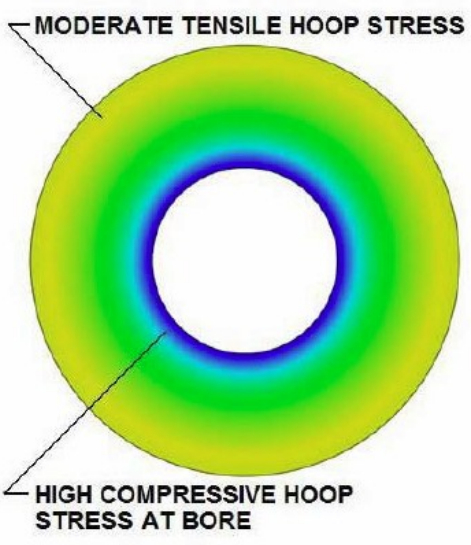

Figure 2.1-b: Residual stresses after releasing the autofrettage pressure (unloading stage) [52].

An important issue in the analysis of the autofrettage process is to find the best model which mimics the material behaviour during the loading and unloading stages while considering the Bauschinger effect.

The basic autofrettage theory assumes elastic–perfectly plastic behaviour for the material, as shown in Figure 2.2. Due to the Bauschinger effect and strain-hardening, most materials do not demonstrate elastic–perfectly plastic properties and, consequently, various autofrettage models are based on different simplified material strain-hardening models, which assume linear strain-hardening or power strain-hardening or a combination of these strain-hardening models.

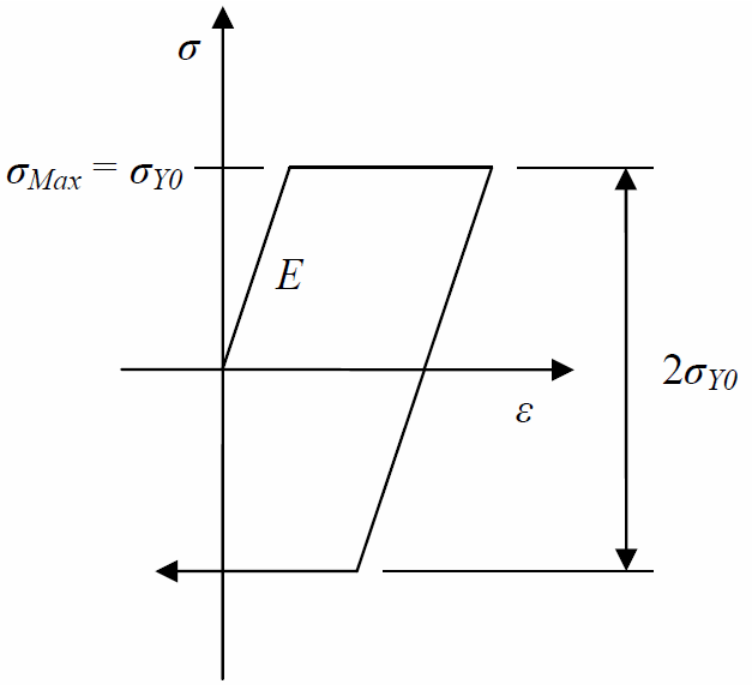

Figure 2.2: Stress-strain diagram of an elastic–perfectly plastic material.

2.1.1 The Bauschinger effect

The Bauschinger effect [53] causes a reduction in compression yield strength as a result of prior tensile plastic overload. It is important to know that the Bauschinger effect factor is a function of plastic strain. Figure 2.3 clearly demonstrates the Bauschinger-effect. Originally, the elastic tensile yield strength is equal to the compressive yield strength ($OA=OF$ or $S_{et}=S_{ec}$). Now, if the load is increased to point (B) beyond the elastic limit and then removed, the tensile strength will increase (BC); however, the compressive yield strength will decrease to S'_{ec}, as shown in Figure 2.3 [54].

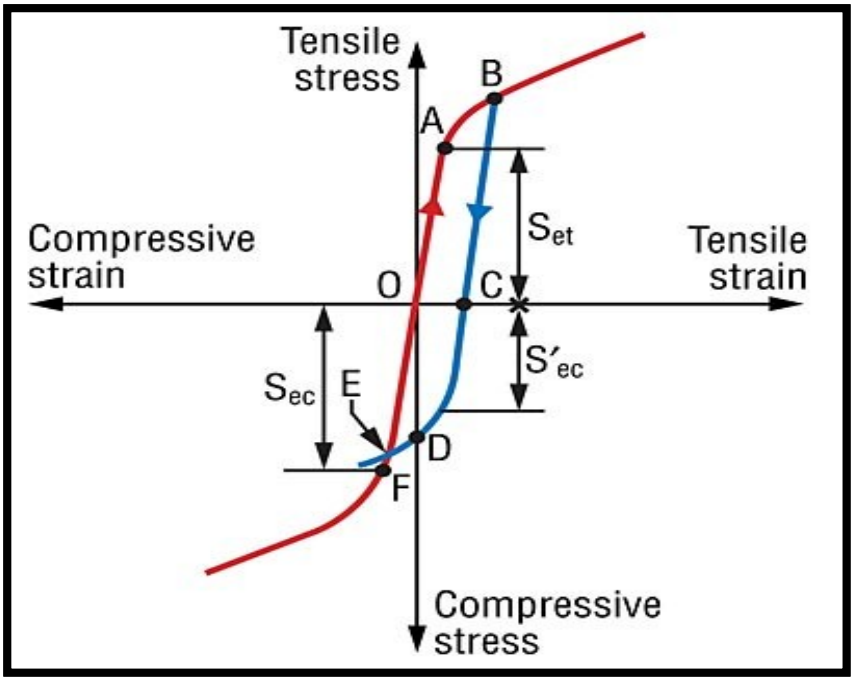

Figure 2.3: Bauchinger effect stress-strain curve [54].

The reduction of compressive yield strength within the yielded zone of an autofrettaged tube is of importance, as on removal of the autofrettage pressure, the region near the bore experiences high values of compressive hoop stress, approaching the magnitude of the

tensile yield strength of the material if the unloading is totally elastic. Now, if the combination of stresses exceeds some yield according to the Tresca or von Mises yield criterion, the tube will reyield from the bore which may cause the beneficial effect of autofrettage to be lost.

Considering this for the accurate evaluation of autofrettage residual stresses, a model that is capable of mimicking the real material behaviour, including the Bauschinger effect, should be used. Isotropic and bilinear kinematic hardening models, as shown in Figure 2.4, are the commonly used models for these purposes [55]. In view of the Bauschinger effect, the kinematic model is preferred to the isotropic one.

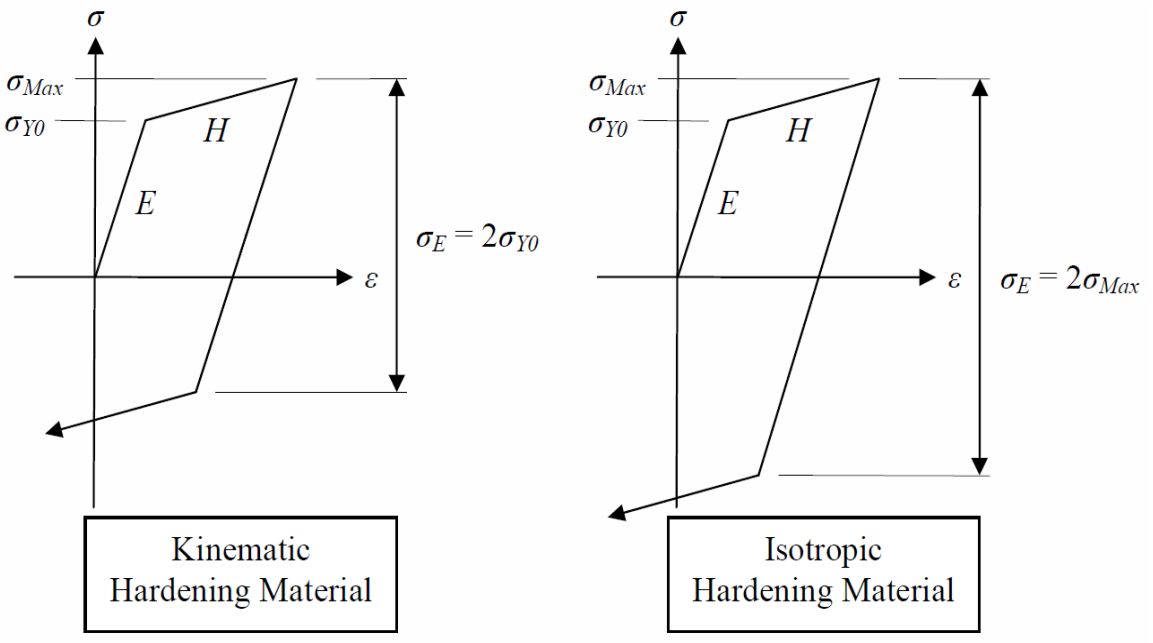

Figure 2.4: Material hardening models [55].

2.1.2 Bilinear kinematic hardening

Analysis procedure for autofrettage process involves autofrettage pressure and overstrain (defined as the proportion of the wall thickness of the tube which behaves plastically during the initial application of autofrettage pressure) which is typically based on Tresca or von Mises failure criteria. Here, using a bilinear kinematic hardening model approximating the real material behaviour (NiCrMoV125 steel) [16] as shown in Figure 2.5, and considering von Mises criteria a finite element ANSYS model is constructed to calculate the residual hoop stress in a autofrettaged mono-block cylinder. To verify the finite element model, the residual hoop stress through the wall thickness is calculated and then compared with that based on actual material behaviour presented in work by Jahed and Ghanbari [16].

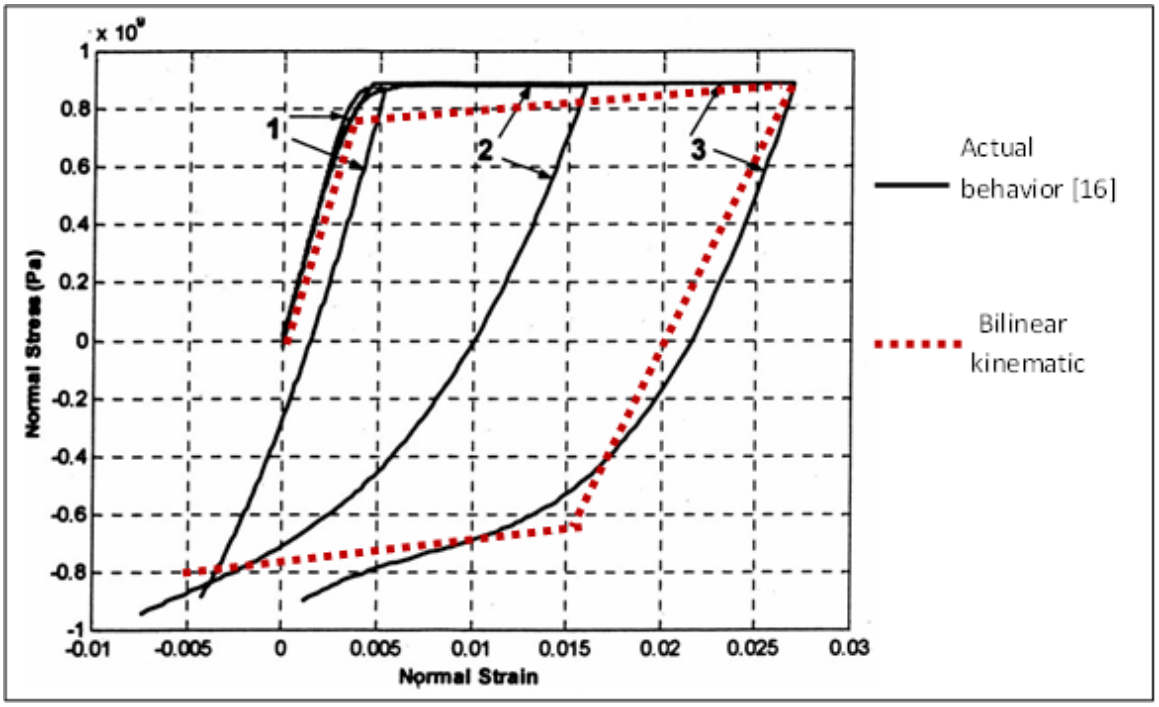

Figure 2.5: Actual and bilinear kinematic stress-strain behaviour.

2.1.3 Finite element model

The finite element model of an autofrettaged cylinder is constructed in ANSYS 12.1 WORKBENCH. The element used here is SOLID 186 which is used for 3-D solid structures, as shown in Figure 2.6. The element has 20 nodes and has three degrees of freedom at each node. The element has plasticity, stress stiffening and large strain capabilities. This element can provide different outputs as: deformations, stresses, strains, temperature, equivalent stresses and total plastic strain [56]. The finite element model of the autofrettage cylinder is shown in Figure 2.7.

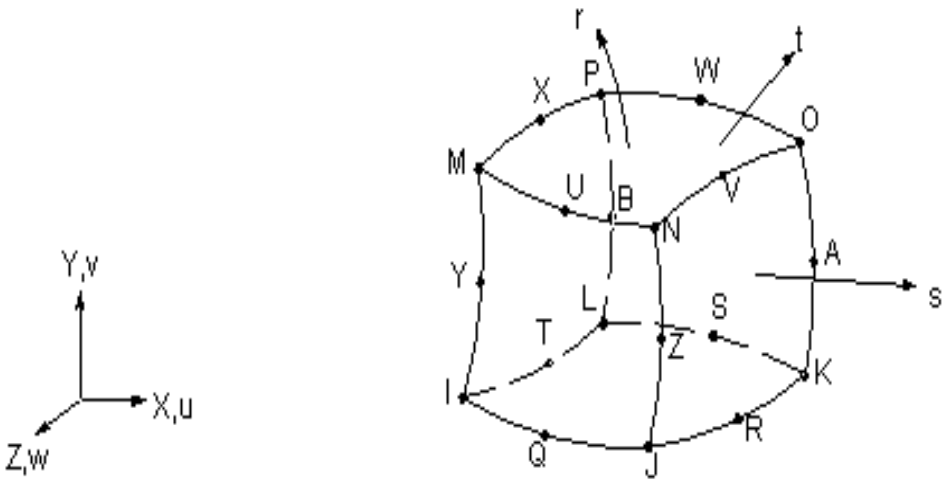

Figure 2.6: 3-D (20 node) solid 186 element [56].

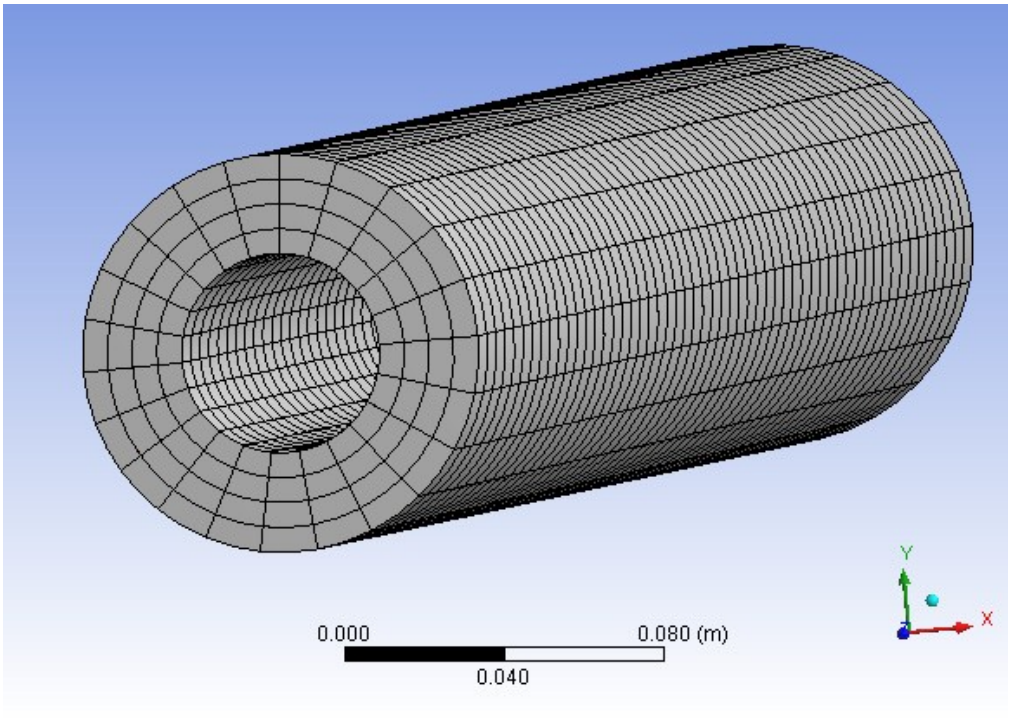

Figure 2.7: Finite element model for an autofrettaged cylinder.

2.1.4 Residual stress distribution and verification of the finite element model

It is noted that, a bilinear kinematic hardening model approximating the real material behaviour (NiCrMoV125 steel) [16]; has been used in which E is the slope of the linear line in the elastic region (modulus of elasticity) and H is the slope of the linear line in the plastic region as shown in Figure 2.4. This material's constants are as follows: E=268 GPa; H=75 GPa; $\nu = 0.29$; ρ=7800 kg/m^3; σ_y=700 MPa, where, ρ, ν, and σ_y are the density, Poisson's ratio and yield stress, respectively.

For a mono-block autofrettaged cylinder with inner and outer radii of a= 146 mm and b=305 mm, the non-dimensionalized residual hoop stress distribution through the

thickness of the cylinder has been evaluated for the autofrettage pressure of 736 MPa and then compared with that in Ref. [16], as shown in Figure 2.8.

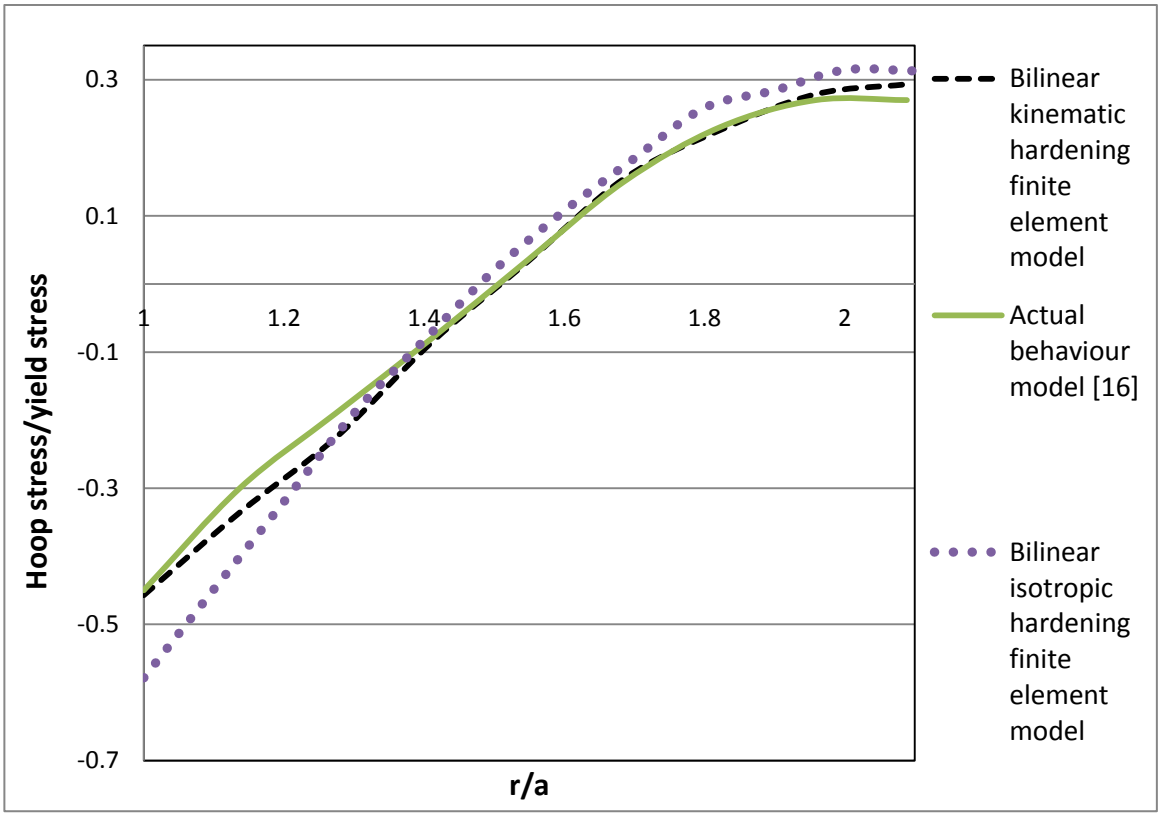

Figure 2.8: Residual hoop stress distribution for an autofrettaged mono-block cylinder using the bilinear kinematic, bilinear isotropic and the real models.

As it can be seen from Figure 2.8, the predicted residual hoop stress distribution through the thickness based on the kinematic hardening model shows very good agreement with that based on the actual material behaviour obtained by Jahed and Ghanbari [16]. However the predicted residual hoop stress distribution based on the isotropic hardening model deviates considerably from that based on the actual material behaviour especially at the near bore area. This can be attributed to the fact that the developed kinematic hardening finite element model incorporates the Bauschinger effect as shown in Figure 2.4, thus better representing the real behaviour of material. The residual hoop

stress distribution is also evaluated for a very thick-walled cylinder $\frac{b}{a} = 6$ to ensure that it decreases at the outer elastic region, as shown in Figure 2.9.

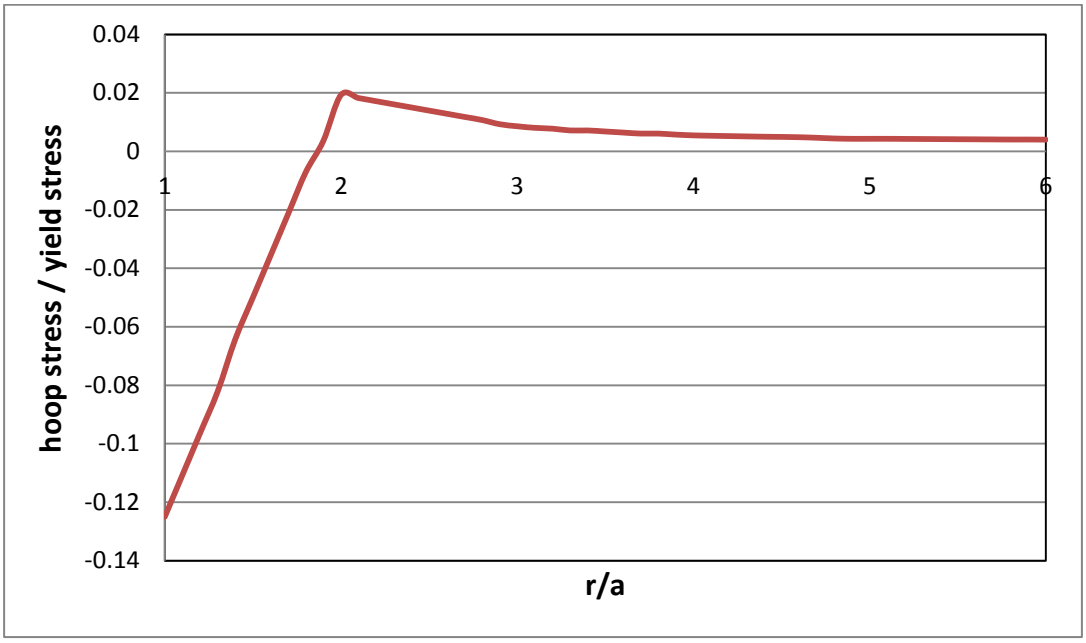

Figure 2.9: Residual hoop stresses in a single very thick autofrettaged cylinder using a finite element model.

2.2 Modeling of the shrink-fit process

Shrink-fitting in cylinders involves establishing a pressure between the inside surface of the outer layer and the outside surface of the inner layer through an interference fit. This interference pressure compresses the inner layer while expanding the outer layer. The residual stresses created by shrink-fitting pressure are shown in Figure 2.10, in which the inner layer experiences the beneficial residual compressive hoop stress, while the outer layer is under detrimental tensile hoop stress. Generally, the residual stresses developed

by the shrink-fit process have analytically been calculated using Lame's equations [57] for a thick walled cylinder.

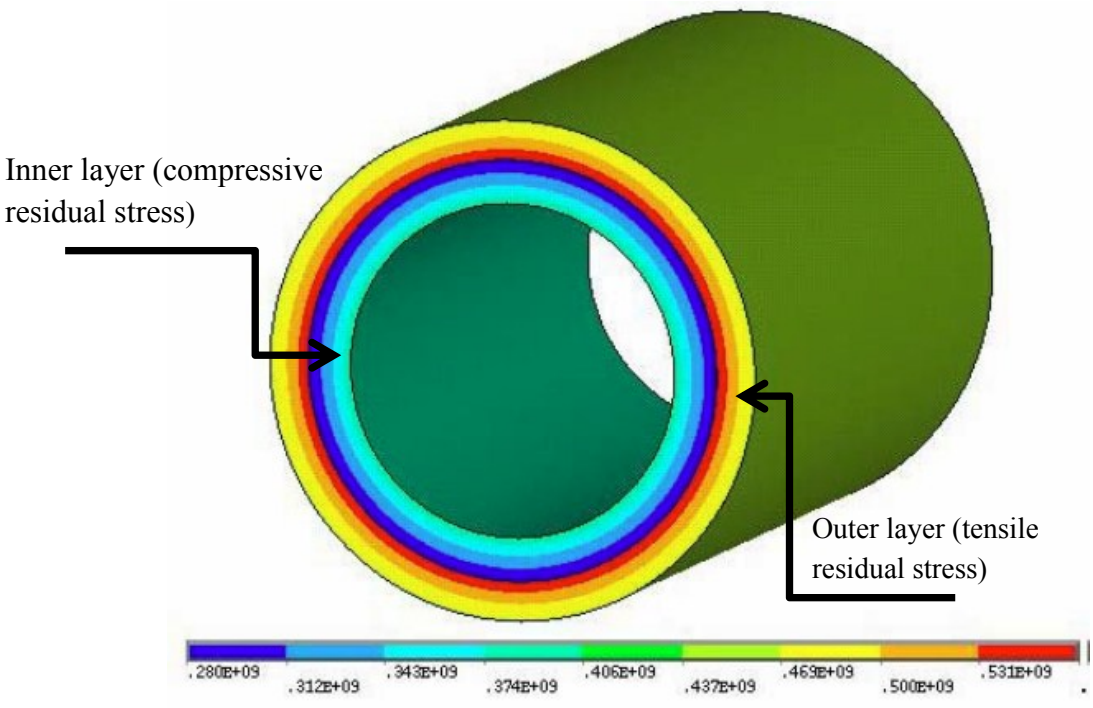

Figure 2.10: Residual hoop stresses in a shrink-fitted cylinder [58].

2.2.1 Analytical model

The interference pressure P_{sh} which is developed at the interface radius of the shrink-fitted cylinders can be calculated analytically [59] as:

$$P_{sh} = \frac{0.5\,\delta}{\frac{c}{E_o}\left(\frac{b^2+c^2}{b^2-c^2}+\upsilon_o\right)+\frac{c}{E_i}\left(\frac{a^2+c^2}{a^2-c^2}-\upsilon_i\right)} \qquad (2.1)$$

where δ is the total diametral interference, c is the interference radius, a and b are inner and outer radii, E_i, E_o and υ_i, υ_o are the modulus of elasticity and the Poisson's ratio related to inner and outer cylinders, respectively. For the shrink-fitted cylinder, the

interference pressure acts as external pressure for the inner cylinder and internal pressure for the outer cylinder which cause the residual hoop, σ_θ, and radial , σ_r, stresses along the radial position *r* for the inner and outer cylinders as:

$$\sigma_{\theta_{inner}} = -P_{sh}\frac{c^2}{c^2-a^2}\left(1+\frac{a^2}{r^2}\right) \quad (2.2)$$

$$\sigma_{r_{inner}} = -P_{sh}\frac{c^2}{c^2-a^2}\left(1-\frac{a^2}{r^2}\right) \quad (2.3)$$

$$\sigma_{\theta_{outer}} = P_{sh}\frac{c^2}{b^2-c^2}\left(1+\frac{b^2}{r^2}\right) \quad (2.4)$$

$$\sigma_{r_{outer}} = P_{sh}\frac{b^2}{b^2-c^2}\left(1-\frac{b^2}{r^2}\right) \quad (2.5)$$

2.2.2 Finite element model

The 3-D finite element model of the two-layer shrink-fitted cylinder has also been developed in ANSYS environment, as shown in Figure 2.11.

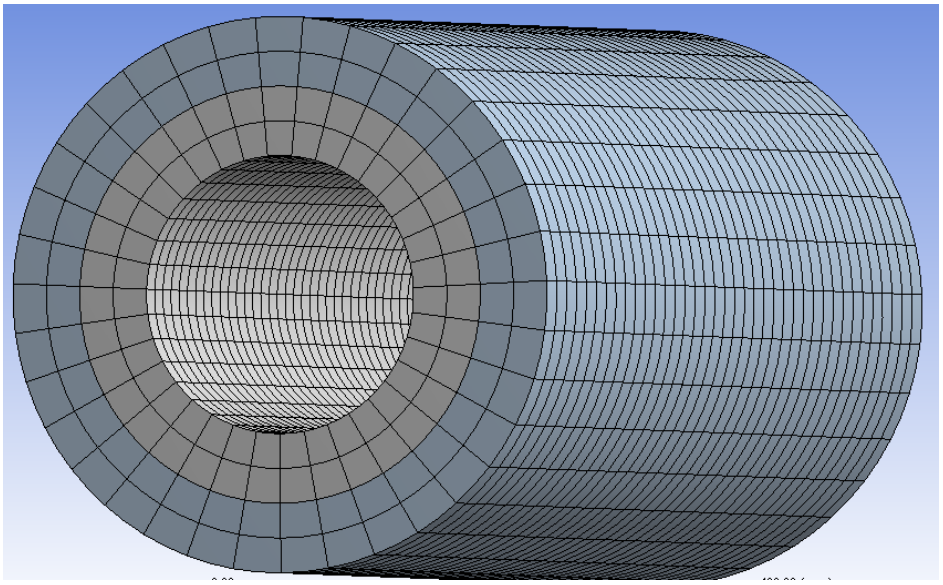

Figure 2.11: Finite element model of a two-layered shrink-fitted cylinder.

Three different elements have been used for finite element model of the shrink-fit process. The inner and outer body of cylinders are constructed using the same element SOLID 186 used for autofrettage process (Section 2.1.2.2), the outer surface of the inner layer is constructed using element CONTA 174; while the inner surface of the outer layer is constructed using TARGE 170.

In studying the contact between two bodies, the “contact-target” pair concept has been widely used in finite element simulations. The surface of one body is conventionally taken as a contact surface (outer surface of the inner layer) and the surface of the other body as a target surface (inner surface of the outer layer). Flexible-flexible contact has been considered here where both contact and target surfaces are associated with deformable bodies.

CONTA174 element is defined by eight nodes and is located on the surfaces of 3-D solid or shell elements with mid-side nodes. It has the same geometric characteristics as the solid or shell element face with which it is linked. Contact takes place when the element surface penetrates one of the target segment elements (TARGE 170) on a specified target surface [56].

TARGE170 is used to represent various 3-D "target" surfaces for the associated contact elements. This target surface is discretized by a set of target segment elements which may be line or triangle with 3, 6, or 8 nodes. Then, the element TARGE170 is paired with its associated contact surface. One can impose any translational or rotational displacement, temperature, voltage, and magnetic potential on the target segment element. Also, forces and moments on target elements can be imposed [56].

2.2.3 Residual stress distribution and verification of the finite element model

Figure 2.12 shows the variation of the residual hoop stresses normalized with respect to the yield strength through the wall thickness. Both cylinders are made of the same material (NiCrMoV125 steel) with a yield strength of 700 MPa, modulus of elasticity of 286 GPa and Poisson's ratio of 0.29. The cylinder has inner, outer and interference radii of 100 mm, 200 mm, 150 mm, respectively, and the radial interference is 0.2 mm. To validate the developed finite element model of the shrink-fitted cylinder, the results are compared with those obtained from analytical solutions using Eq.s. 2.2 and 2.4, as shown in Figure 2.12. It can be seen that excellent agreement between finite element and analytical results exist. As it can be realized, the shrink-fit process generates a high beneficial compressive residual hoop stress at the vicinity of the bore of the cylinder; however it also generates a detrimental residual tensile stress at the vicinity of the interface toward the outer surface.

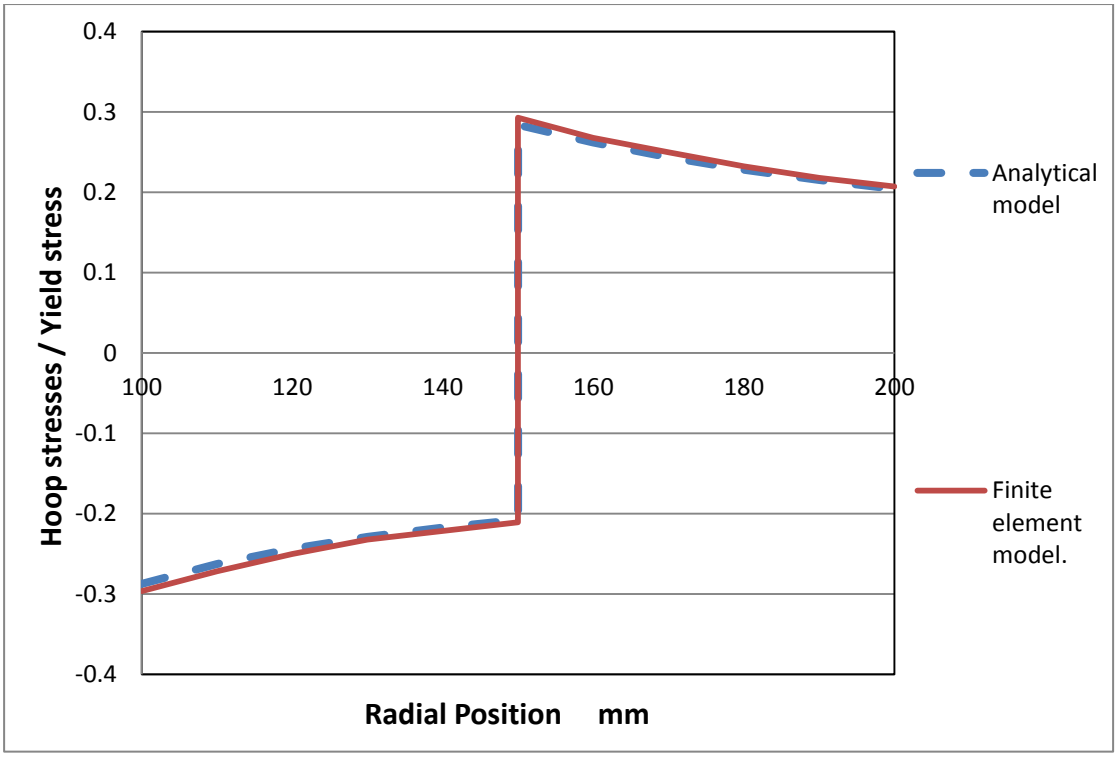

Figure 2.12: radial distribution of residual hoop stress for a two-layer shrink-fitted cylinder.

Assuming linear elasticity condition in both layers, the principle of superposition can be applied to find the hoop stress profile due to the working pressure in the shrink-fitted cylinder. For instance, for the above mentioned shrink-fitted cylinder, the hoop stress distribution due to working inner pressure of 250 MPa is shown in Figure 2.13.

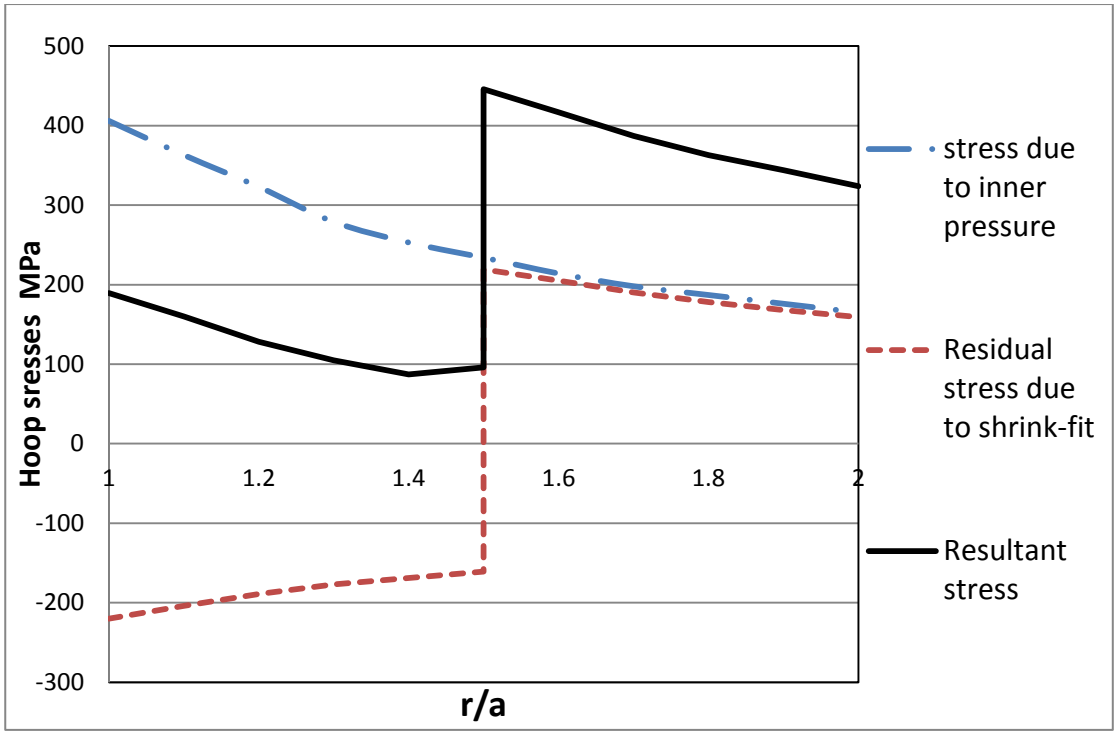

Figure 2.13: Summation of the residual hoop stress and hoop stress due to working inner pressure

2.3 Compound Autofrettage and Shrink-Fit Cylinder

As mentioned before, there are limitations associated with autofrettage and shrink-fit processes. Both techniques are generally used to introduce beneficial residual stresses into pressure vessels. Regarding the autofrettage process, the Bauschinger effect can considerably reduce this beneficial residual stress near the bore and, also, shrink-fit alone generates much less compressive residual stress compared with autofrettage in the region near the bore. Considering this, a combination of both autofrettage and shrink-fit may provide a more suitable residual stress profile and thus increase the load carrying capacity and fatigue life of the multilayer cylinder. Researchers have used different design techniques by combining the autofrettage and shrink-fit processes to enhance the residual

stress distribution and improve the fatigue life. In the following, all the possible combinations of a two-layer autofrettage and shrink-fit compound cylinder are investigated and the residual stresses for these combinations have been evaluated using the finite element model.

2.3.1 Different autofrettage and shrink-fit combinations

Here, we have investigated all possible arrangements for the two-layer autofrettaged and shrink fitted compound cylinder. These arrangements are briefly summarized as:

Combination 1: Shrink-fit of two virgin layers (non-autofrettaged layers) followed by autofrettage of the assembly.

Combination 2: Autofrettage of each layer individually then shrink-fitting them together.

Combination 3: Autofrettage of the inner layer followed by shrink-fitting the virgin outer layer.

Combination 4: Autofrettage of the outer layer followed by shrink-fitting the virgin inner layer.

For the fair comparison, all above mentioned combinations have the same inner, outer and interference radii after the autofrettage and shrink-fit processes and the same interference pressure as well. The sketches of above combinations are shown in Figures 2.14-2.17.

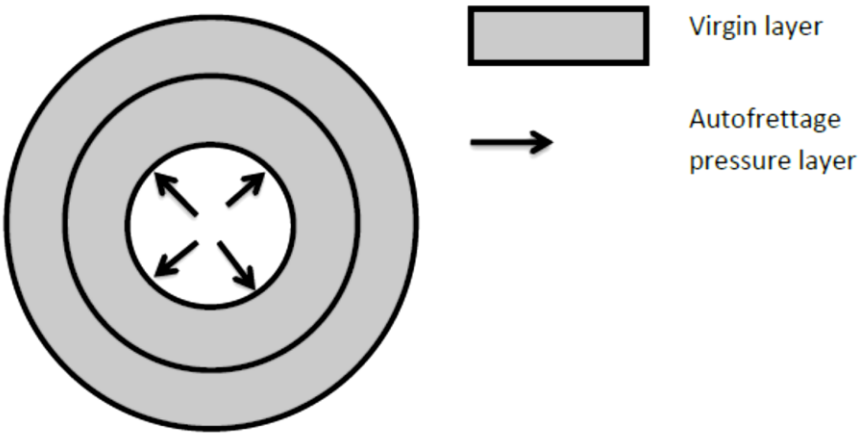

Figure 2.14: Shrink-fit of two virgin layers followed by autofrettage (combination 1).

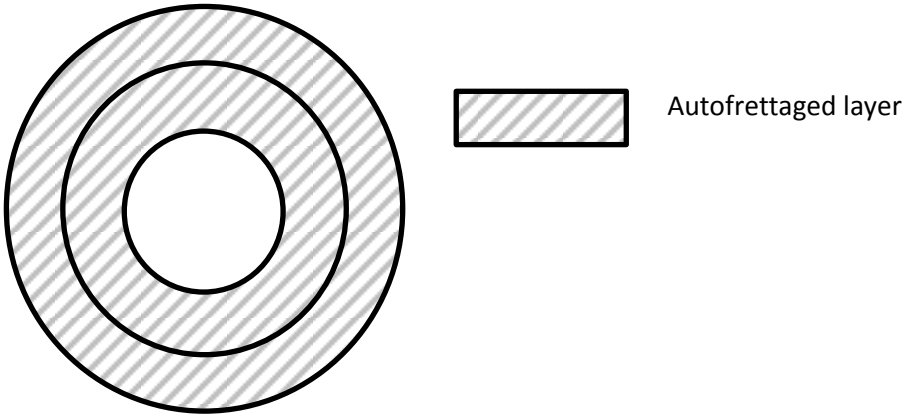

Figure 2.15: Shrink-fit of two autofrettaged layers (Combination 2).

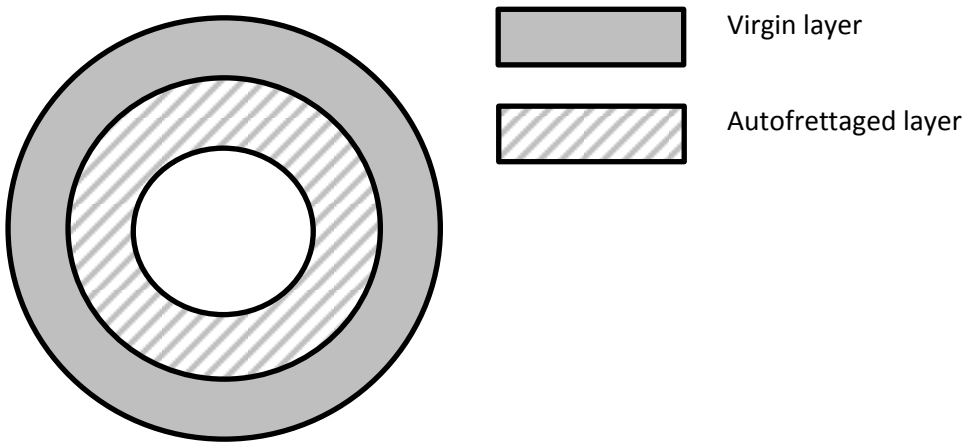

Figure 2.16: Shrink-fit of the outer virgin layer on the inner autofrettaged layer (Combination 3).

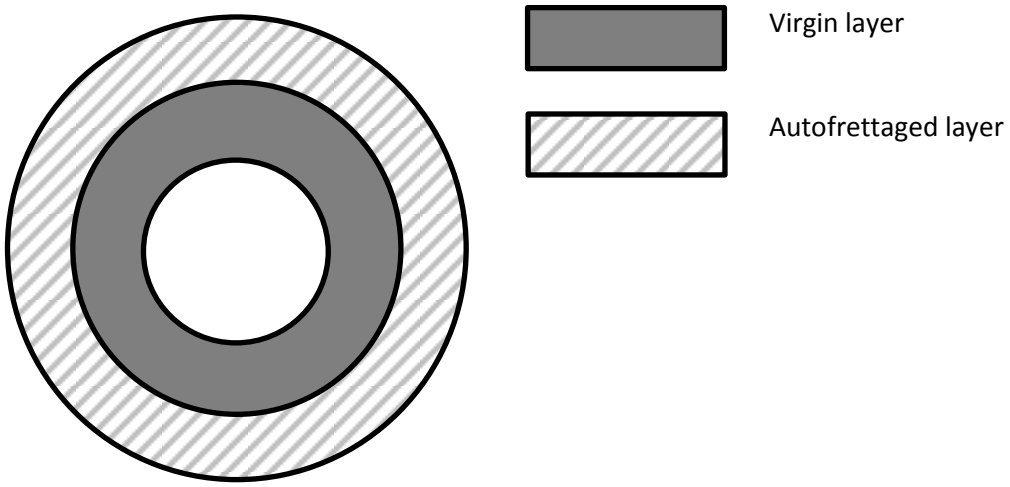

Figure 2.17: Shrink-fit of the outer autofrettaged layer on the inner virgin layer (Combination 4).

For these four combinations, it is clear that the fourth one does not add any advantage of the autofrettage procedure as the autofrettage process has been applied at the bore of outer layer. Thus, only the first three combinations have been studied.

2.3.2 Residual stress distribution in compound cylinders

Here the material properties are the same as those used in Sections 2.1.4 and 2.2.3. For fair comparison, the compound cylinders for all combinations addressed before have inner, outer and interference radii of 100 mm, 200 mm and 150 mm, respectively. The radial interference and autofrettage pressure have also been considered to be 0.2 mm and 736 MPa, for all autofrettage and shrink-fit combinations. Figure 2.18 shows the normalized residual hoop stresses for the first three combinations discussed in previous section using the developed finite element model. The results for the equivalent Autofrettaged Mono-Block Cylinder (AMBC) and Shrink-Fitted Cylinder (SFC) have also been shown for the sake of comparison.

It should be noted that autofrettage processes as discussed before have been conducted through application of hydraulic pressure. Providing that the autofrettage cylinder receives a low temperature heat treatment prior to shrink-fit process, one may model the compound cylinder subjected to autofrettage prior to shrink-fit processes elastically [60, 61].

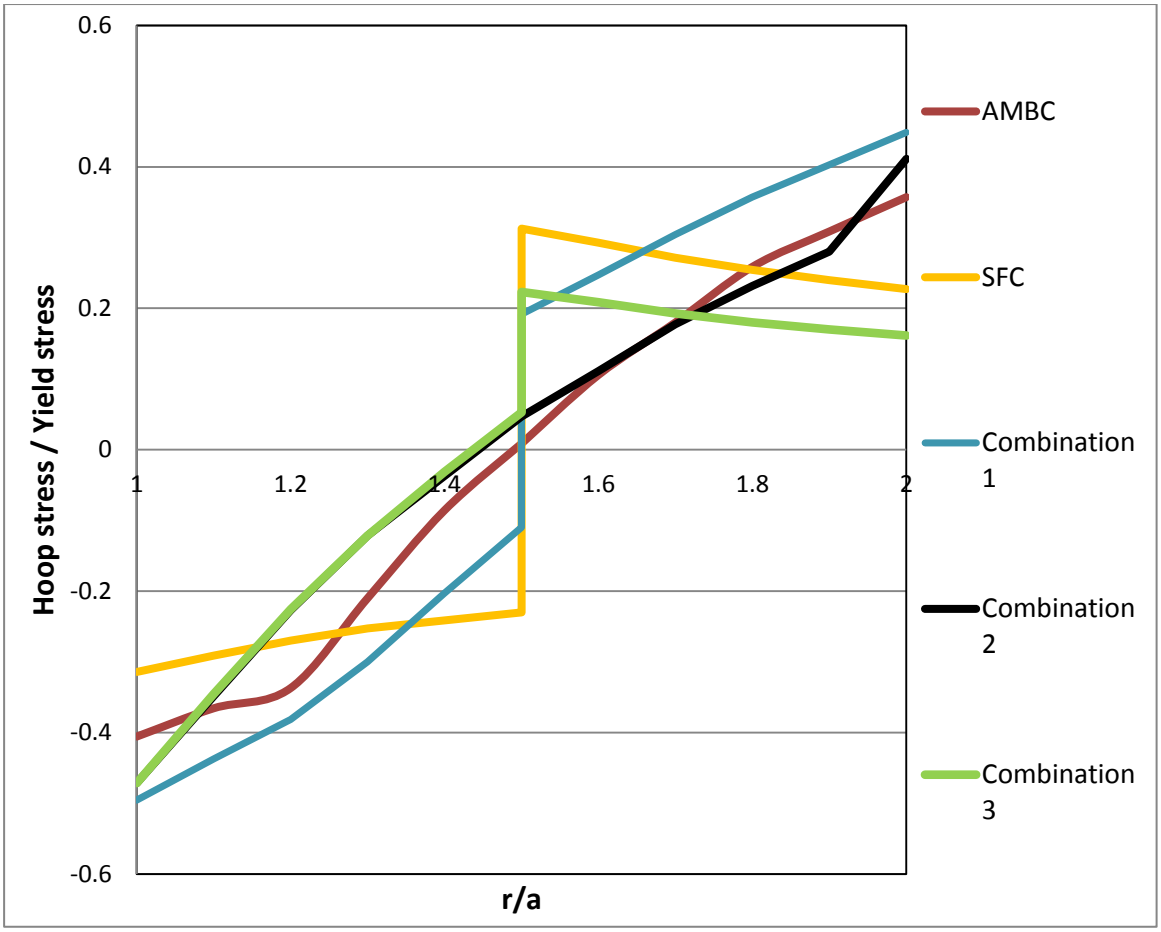

Figure 2.18: Residual hoop stresses for different combinations through the wall thickness.

Examination of Figure 2.18 reveals that the combined autofrettaged and shrink-fitted cylinders increase the compressive residual stresses considerably, especially at the inner bore area (working area). All combinations provide larger compressive residual stresses compared with the conventional shrink-fit and autofrettaged mono-block cylinders, especially at the near bore area. It is interesting to note that combinations 2 and 3 (black and green lines) give the same trend for residual compressive stress distribution (which has a beneficial effect) through the thickness of the inner layer; however, through the thickness of the outer layer, residual tensile stress distribution (which has a detrimental

effect) differs and the maximum tensile stress for combination 3 (green line) is considerably lower than that of combination 2. Nevertheless, these two combinations still generate less positive (tensile) residual stresses compared with the first combination (blue line).

2.4 Summary

In this chapter, a finite element model has been constructed to calculate the residual stresses in the autofrettaged and shrink-fitted compound cylinders. The model has been verified by comparing the results with those available in the literature and analytical model. Different combinations for two-layer compound cylinders have been investigated and the residual stress distributions through the thickness for each combination have been evaluated using the finite element model and compared with that for an equivalent autofrettaged mono-block cylinder and a two-layer shrink-fitted cylinder. It has been observed that combining autofrettage with shrink-fit processes can provide more compressive residual stresses at the near bore area of the cylinder. Also, it may reduce the detrimental tensile residual stress along the cylinder wall.

CHAPTER 3

THERMO-MECHANICAL ANALYSIS OF COMPOUND CYLINDERS CONSIDERING THERMAL ACCUMULATION

The analysis of cylindrical shells under thermal, mechanical, or combined loads has received considerable attention due to their important applications. The combinations of autofrettaged and shrink-fitted multilayer cylinders subjected to combined cyclic thermal and pressure loads have been investigated in this chapter. Fully coupled thermo-elastic analysis is taken into consideration during the calculation of the temperature profile through the wall thickness. The finite element results have been validated with previous work cited in the literature and experimental work as well. In the experimental work, the temperature has been measured at different locations through the thickness of a two-layer shrink-fitted cylinder subjected to quasi-static and dynamic thermal loads at the inner surface. In addition, the hoop strain at the outer surface of the cylinder has been measured under the same thermal loads. The finite element model has then been used to find the hoop stress distribution through the thickness of the compound cylinder subjected to different combinations of autofrettage and shrink-fit cylinders and under different loading

conditions. The mechanical fatigue life has also been calculated using ASME codes due to cyclic inner pressure. Moreover, the stress intensity factor (SIF) has been evaluated for different combinations of autofrettage and shrink-fit cylinders subjected to cyclic thermal loads or cyclic thermo-mechanical loads, considering thermal accumulation and then have been compared with the critical SIF (the fracture toughness of the material). The number of cycles until the critical SIF is reached have been counted and considered as the fatigue life time of each combination.

3.1 Thermo-Mechanical Models

Let us consider a two-layer hollow long cylinder of the inner and outer radii of *a* and *b*, respectively as shown in Figure 3.1. The cylinder is assumed to be subjected to a symmetric thermal and pressure cyclic load applied radially. Also, each layer is considered to be made of isotropic and homogenous material.

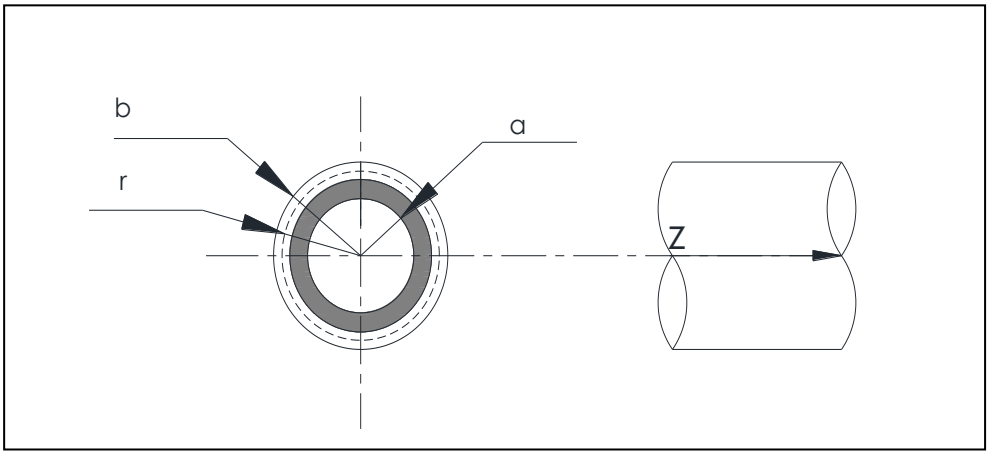

Figure 3.1: Physical model and coordinate system of multilayer long cylinder.

Here, we first formulate the governing differential equations and then cast them into the finite element form and finally validate the finite element model constructed in the ANSYS 12.1 environment.

3.1.1 Coupled thermo-mechanical model

Due to the condition of symmetry, no shear stresses exist and, thus, in the absence of body forces, one can write the following governing differential equation in radial direction as [62]:

$$\frac{\partial \sigma_r}{\partial r} + \frac{\sigma_r - \sigma_\theta}{r} = \rho \ddot{u}_r \qquad (3.1)$$

in which σ_r and σ_θ are radial and tangential normal stresses and $\ddot{u}_r$ is the radial acceleration at radius *r*.

The strain-displacement relation for the cylinder can be described as:

$$\varepsilon_r = \frac{\partial u_r}{\partial r}, \qquad \varepsilon_\theta = \frac{u_r}{r} \qquad (3.2)$$

It is noted that Eq. 3.2 provides radial and tangential strains, ε_r andε_θ, in terms of radial displacement, u_r. For the long thick-walled cylinder or cylinders with axially restrained deformation, the assumption of plain strain ($\varepsilon_z = 0$) is valid and thus stress-strain relation using generalized Hook's law considering thermal effect can be written as:

$$\sigma_r = \frac{E}{(1+\nu)(1-2\upsilon)}[(1-\nu)\varepsilon_r + \nu\varepsilon_\theta] - \frac{E\alpha}{(1-2\nu)}T \qquad (3.3)$$

$$\sigma_\theta = \frac{E}{(1+\nu)(1-2\nu)}[\nu\varepsilon_r + (1-\nu)\varepsilon_\theta] - \frac{E\alpha}{(1-2\nu)}T \qquad (3.4)$$

where T (r, t) is the change of temperature with respect to a reference temperature and is a function of radial location, r and time t. E, ν and α are Young's modulus, Poisson's ratio and the coefficient of thermal expansion of the i^{th} layer of the axisymmetric cylinder, respectively. It is noted that, due to the plain strain condition, axial stress σ_z can be stated as: $\sigma_z = \upsilon(\sigma_r + \sigma_\theta)$.

Now, substituting Eq. 3.2 into Eqs. 3.3 and 3.4 and then substituting resultant stress-displacement relations into Eq. 3.1 will yield the following governing equation of motion in terms of only displacement:

$$\frac{\partial^2 u_r}{\partial r^2} + \frac{1}{r}\frac{\partial u_r}{\partial r} - \frac{u_r}{r^2} - \frac{\alpha(1+\nu)}{(1-\nu)}\frac{\partial T}{\partial r} - \frac{\rho}{E}\frac{(1+\nu)(1-2\nu)}{(1-\nu)}\ddot{u}_r = 0 \qquad (3.5)$$

On the other hand, the coupled transient heat conduction equation for the cylinder, with no internal heat generation source can be written as [63]:

$$k^t\frac{\partial^2 T}{\partial r^2} + k^t\frac{1}{r}\frac{\partial T}{\partial r} = \rho c_p\frac{\partial T}{\partial t} + \frac{T_o E\alpha}{(1-2\nu)}\left(\frac{\partial \varepsilon_r}{\partial t} + \frac{\partial \varepsilon_\theta}{\partial t}\right) \qquad (3.6)$$

where, ρ, k^t, c_p, and T_o are the density, thermal conductivity coefficient, specific heat and initial base temperature, respectively.

Now, Eq. 3.2 is substituted into Eq. 3.6 to obtain:

$$k^t\frac{\partial^2 T}{\partial r^2} + k^t\frac{1}{r}\frac{\partial T}{\partial r} = \rho c_p\frac{\partial T}{\partial t} + \frac{T_o E\alpha}{(1-2\nu)}\left(\frac{\partial \dot{u}_r}{\partial t} + \frac{\dot{u}_r}{r}\right) \qquad (3.7)$$

Eqs. 3.5 and 3.7 are coupled partial differential equations with respect to temperature T and displacement u_r.

Using a finite element technique based on Galerking weighted residual or variational approaches, one may cast the above governing coupled thermo-elastic differential equations into the finite element form as [64]:

$$\begin{bmatrix}[m] & [0]\\ [0] & [0]\end{bmatrix}\begin{Bmatrix}\{\ddot{u}\}\\ \{\ddot{T}\}\end{Bmatrix}+\begin{bmatrix}[0] & [0]\\ [C^{tu}] & [C^{t}]\end{bmatrix}\begin{Bmatrix}\{\dot{u}\}\\ \{\dot{T}\}\end{Bmatrix}+\begin{bmatrix}[K] & [K^{ut}]\\ [0] & [K^{t}]\end{bmatrix}\begin{Bmatrix}\{u\}\\ \{T\}\end{Bmatrix}=\begin{Bmatrix}\{F\}\\ \{Q\}\end{Bmatrix} \quad (3.8)$$

where $[m]$ is the element mass matrix, $\{T\}$ is the temperature vector, $[K]$ is the element stiffness matrix, $\{F\}$ is the element pressure vector, $[C^t]$ is the element specific heat matrix, $[K^{ut}]$ is the element thermo-elastic stiffness matrix, $[C^{tu}]$ is the element thermo-elastic damping matrix and $\{Q\}$ is the thermal flux vector, described as:

$$[m] = \rho \int_V [N_s]\,[N_s]^T d(V) \quad (3.9)$$

$$[K] = \int_V [B]\,[D][B]^T d(V) \quad (3.10)$$

$$[K^{ut}] = \int_V [B]^T [D]\{\alpha\}[N_s]^T d(V) \quad (3.11)$$

$$[C^t] = \rho \int_V c_p [N_s]\,[N_s]^T d(V) \quad (3.12)$$

$$[C^{tu}] = -T_o [K^{ut}]^T \quad (3.13)$$

$$\{F\} = \int_A [N_n]^T \{P\}\, d(A) \quad (3.14)$$

$$\{Q\} = \int_A \{q\}[N_n]^T\, d(A) \quad (3.15)$$

where in the above equations, $[B]$ is the strain-displacement matrix relating strain field to the nodal displacement vector $\{u\}$, $[N_s]$ is the element shape function in the domain relating displacement function to the nodal displacement vector, $[N_n]$ is the element shape

function evaluated at the surfaces on the boundary where pressure $\{P\}$ and heat flux vectors $\{q\}$ act, $[D]$ is the elastic stiffness matrix relating stress to strain, $\{\alpha\}$ is the thermal expansion coefficient vector, and V is the element volume.

The finite element model consists of two main parts. In the first part, a coupled-field solid element SOLID226 [56] with the capability to perform coupled thermo-elastic analysis has been selected to discrete the domain and obtain the temperature profile through the thickness of the cylinder. The element has a brick geometry with 20 nodes located on each corner and middle side of the brick. For structural-thermal analysis, each node has 4 degrees of freedom (DOF), including three translational elastic displacements and temperature. It should be noted that, here, the mechanical and thermal loads are applied symmetrically in the radial direction. Thus, only displacement degrees of freedom in radial direction and temperature will be extracted. In the second part, the induced residual stresses due to shrink-fit and autofrettage processes have been evaluated (see section 2.3.2) and then combined with the thermo-mechanical results obtained from the first part.

3.1.2 Uncoupled thermo-mechanical model

It should be noted that, for the uncoupled thermo-elasticity problems, the time dependency of the strains in the heat conduction equation in Eq. 3.6 is ignored yielding the familiar uncoupled transient heat conduction equation as [65]:

$$\frac{1}{r}\frac{\partial}{\partial r}\left(k^t r\frac{\partial T}{\partial r}\right) = \rho c_p \frac{\partial T}{\partial t} \tag{3.16}$$

Solution of Eq.3.16 is obtained using the finite difference technique. If the temperature acting on the infinitesimal element at time t_j and radial distance r_i from the center of the thick-walled cylinder shown in Figure 3.2 is $T(r_i,t_j)$, then the temperature at radial distances $r_{i+1}= r_i + \Delta r$ and $r_{i-1}= r_i - \Delta r$ or time $t_{j+1}= t_j + \Delta t$ using Taylor expansion will be:

$$T(r_{i+1},t_j) = T(r_i,t_j) + \frac{\Delta r}{1!}\frac{\partial T}{\partial r} + \frac{(\Delta r)^2}{2!}\frac{\partial^2 T}{\partial r^2} + ..., \tag{3.17}$$

$$T(r_{i-1},t_j) = T(r_i,t_j) - \frac{\Delta r}{1!}\frac{\partial T}{\partial r} + \frac{(\Delta r)^2}{2!}\frac{\partial^2 T}{\partial r^2} - ...., \tag{3.18}$$

$$T(r_i,t_{j+1}) = T(r_i,t_j) + \frac{\Delta t}{1!}\frac{\partial T}{\partial t} + \frac{(\Delta t)^2}{2!}\frac{\partial^2 T}{\partial t^2} + ..., \tag{3.19}$$

where Δr and Δt are infinitesimal distance and time interval, respectively.

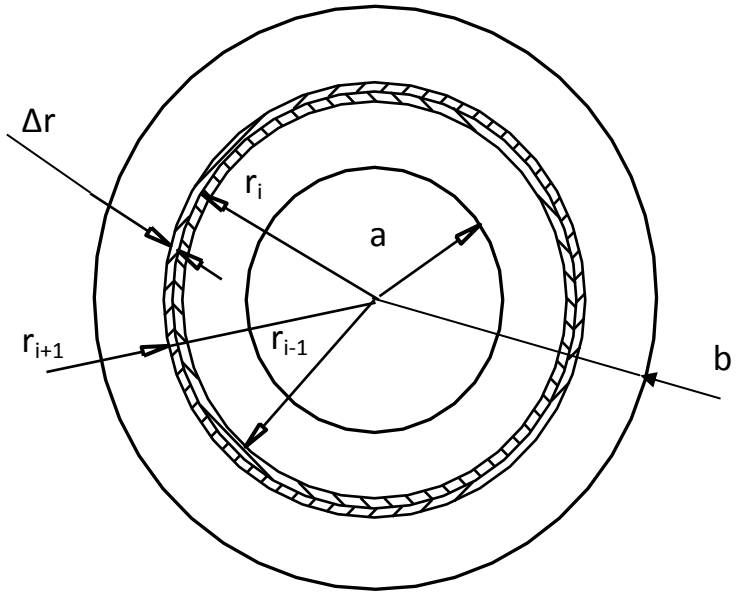

Figure 3.2: Thick-walled cylinder.

Neglecting the second-order term on the right hand side of Eq. 3.19, one can write:

$$\frac{\partial T}{\partial t} = \frac{T(r_i, t_{j+1}) - T(r_i, t_j)}{\Delta t} \tag{3.20}$$

Subtracting Eq. 3.17 from Eq.3.18 yields:

$$\frac{\partial T}{\partial r} = \frac{T(r_{i+1}, t_j) - T(r_{i-1}, t_j)}{2\Delta r} \tag{3.21}$$

While summing Eqs. 3.17 and 3.18 gives:

$$\frac{\partial^2 T}{\partial r^2} = \frac{T(r_{i+1}, t_j) + T(r_{i-1}, t_j) - 2T(r_i, t_j)}{(\Delta r)^2} \tag{3.22}$$

Now, substituting Eqs.3.20-3.22 into Eq. 3.16, the temperature at radial distance r_i and time t_{j+1} can be written as:

$$T(r_i, t_{j+1}) = T(r_i, t_j) + \frac{\alpha \Delta t}{(\Delta r)^2}\left[T(r_{i+1}, t_j) - 2T(r_i, t_j) + T(r_{i-1}, t_j) + \frac{\Delta r}{2r_i}\left(T(r_{i+1}, t_j) - T(r_{i-1}, t_j)\right)\right] \tag{3.23}$$

Eq. 3.23 is used to determine the temperature at any interior radial location r_i after time interval Δt using information at time t_j. A Matlab program has been written to solve the uncoupled thermo-mechanical model.

3.1.3 Validation of the coupled thermo-elastic finite element model and its comparison with the uncoupled model

For a better understanding of the importance of the fully coupled thermo-elastic problem, the results from the coupled thermo-elastic finite element model of the mono-block cylinder have been compared with the uncoupled model and also experimental results for the sake of comparison and validation.

The results obtained from both models have been compared with the experimental data provided in Ref. [66]. In the experiment, the outer surface temperature of a mono-block thick-walled cylinder (gun barrel) with an inner radius of 7.62 mm and outer to inner radii ratio of b/a=3 subjected to repeated thermal pulses was measured. Each thermal pulse has the amplitude of 1450 ^{o}C and time duration of 0.1 S and, also, there is no relaxation between pulses. The cylinder is made of steel with thermal and mechanical properties of k_t=28 W/m^{o}C; C=330 J/kg ^{o}C; α=6.05×10-6 1/^{o}C; E=200 GPa; $\nu = 0.3$; ρ=7800 kg/m^3.

It should be noted that, for the simulation, the thermal pulse has been considered to be in a triangular form, reaching its peak at the middle of the time duration in order to better resemble the physical testing. Results obtained by a fully coupled finite element model, the experimental results and uncoupled results obtained by solving the uncoupled heat conduction equation are provided in Table 3.1 for the sake of comparison. It should be noted that the convection boundary condition for the outer surface has been taken into consideration in modeling.

Table 3. 1: Outer surface temperature of the cylinder due to different thermal pulses.

No. of pulses	Experimental Results [Ref. 66]	Coupled model	Uncoupled model
5	43 ^{o}C	39 ^{o}C	53 ^{o}C
20	85 ^{o}C	89 ^{o}C	98 ^{o}C
30	92 ^{o}C	95 ^{o}C	101 ^{o}C

The results show that a good agreement exists between the results obtained from the coupled finite element model and the experimental results. This can be better realized by comparing the errors. The error between the coupled model and experimental results for 5, 20 and 30 thermal pulses are about 9%, 5% and 3%, respectively, while the error between the uncoupled model and experimental results are about 23 %, 15% and 10%, respectively.

Moreover, the results from the developed coupled thermo-elastic finite element model have been compared with those obtained using an uncoupled model published in Ref. [45] where the inner surface of a mono-block thick-walled cylinder was subjected to static pressure of 10 MPa and exponentially decay time-dependent temperature as T=100 $e^{-0.1t}$ ^{o}C. The cylinder has the ratio of outer to inner radii of 1.25 (b/a=1.25 with a =1 m) and is made of material with Young's modulus of E=80 GPa, Poisson's ratio of $\nu = 0.3$, thermal expansion of α=12×10-6 1/^{o}C and thermal diffusivity of $\alpha^* = k^t/(c_p\rho)$=10^{-5} m^2/s. Figures 3.3 and 3.4 show the temperature and hoop stress distribution through the thickness of cylinder for different time steps. The results clearly show that, as time increases, the temperature distribution obtained from uncoupled and

coupled models approaches each other toward the steady state condition. However as expected, considerable differences exist between these models at small time steps near the bore of the cylinder, which is the critical area.

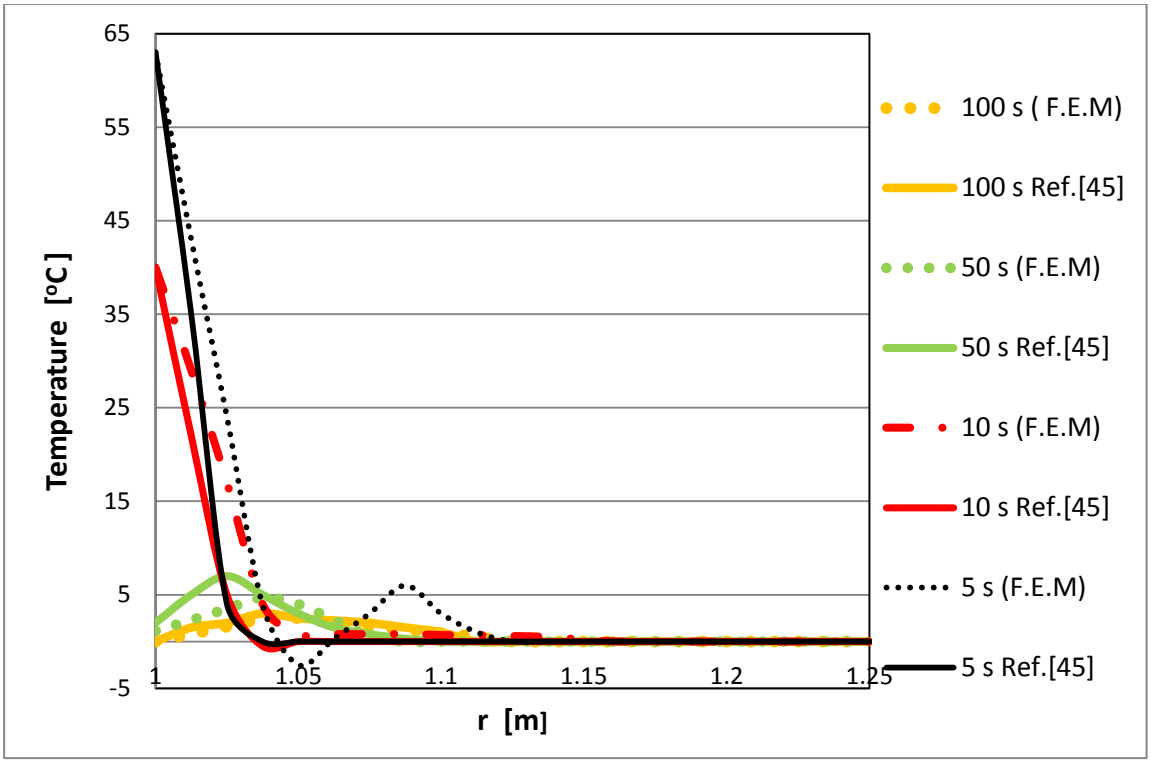

Figure 3.3: Temperature distribution through the thickness of the cylinder in Ref. [45].

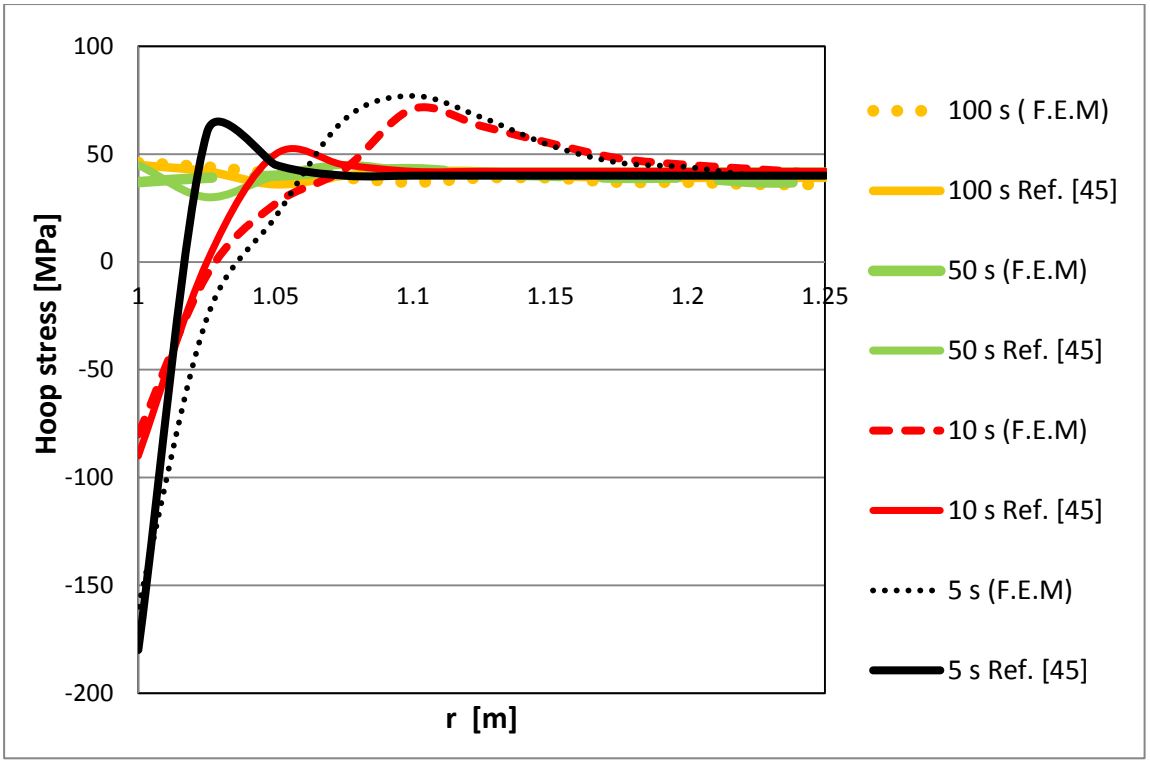

Figure 3.4: Hoop stress distribution versus radial distance for combined pressure and thermal inner loads at different times.

Now to better realize this, let us compare the uncoupled and coupled models considering different time duration of the thermal pulses. The cylinder with an outer to inner radii ratio of two (b/a=2 and a=30 mm) has been subjected to the internal thermal rectangular pulse load with an amplitude of 1500^{o}C and a time duration ranging from 0.1Sec. to 1 Sec. The cylinder is made of high alloy steel with mechanical and thermal properties of: k_t=15 W/m ^{o}C; c=480 J/kg ^{o}C; α=1.710^{-5} 1/^{o}C; E=268 GPa; $\nu = 0.29$; ρ=7800 kg/m3. Figure 3.5 shows the results for temperature distribution through the thickness.

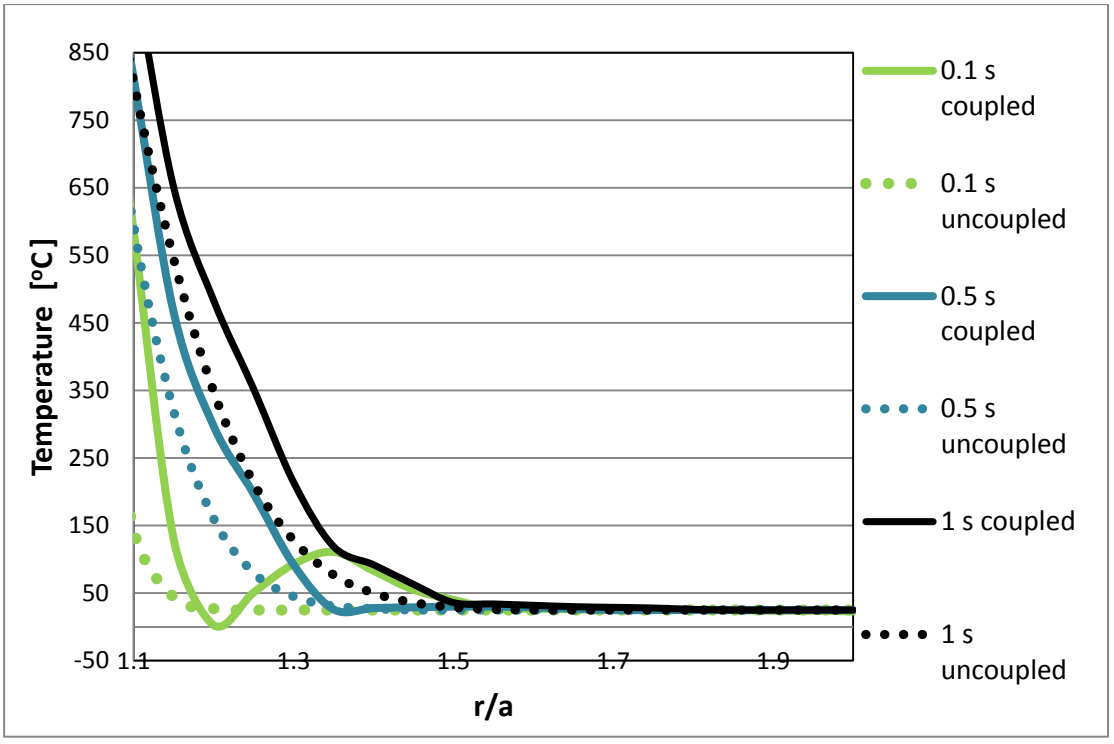

Figure 3.5: Comparison of the uncoupled and coupled model for different thermal rectangular pulse loads.

As it can be realized, significant differences exist between the results due to coupled and uncoupled models, especially at areas near the bore of the cylinder and especially when the time duration becomes shorter. The results confirm that one should conduct coupled thermo-elastic analysis for accurate analysis of temperature distribution under dynamic load with short time duration**.**

It is noted that as the time duration increases, the temperature profile approaches the steady state temperature of 1500 ^{o}C, as illustrated in Figures 3.6 and 3.7.

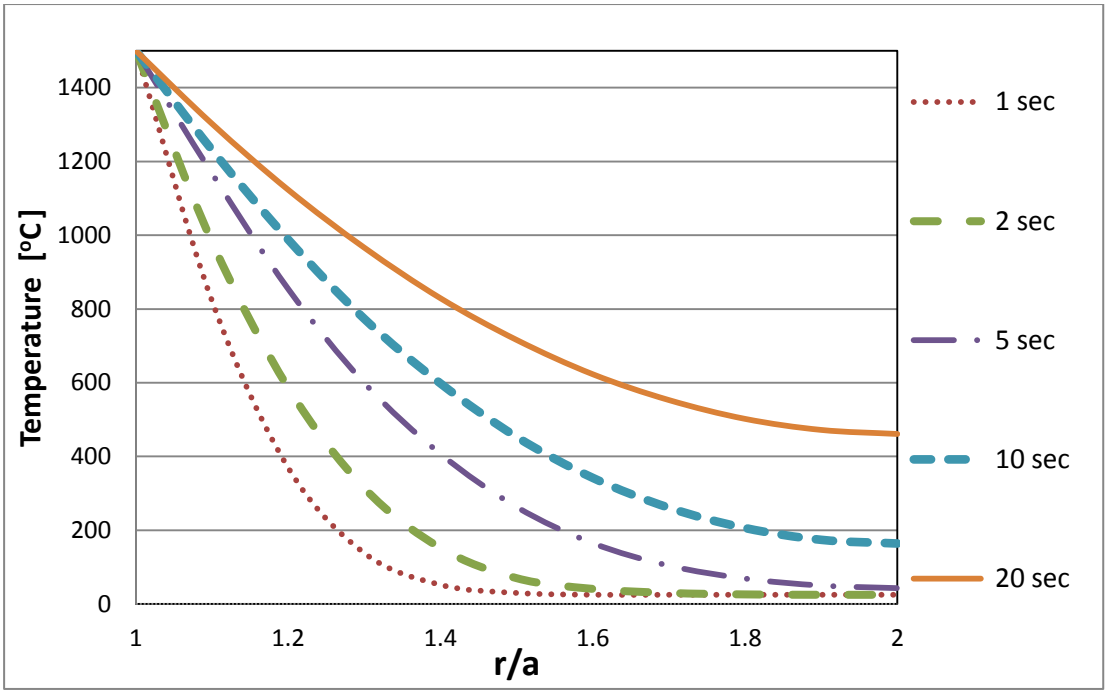

Figure 3.6: Temperature profile through the thickness of the cylinder under thermal rectangular pulse load.

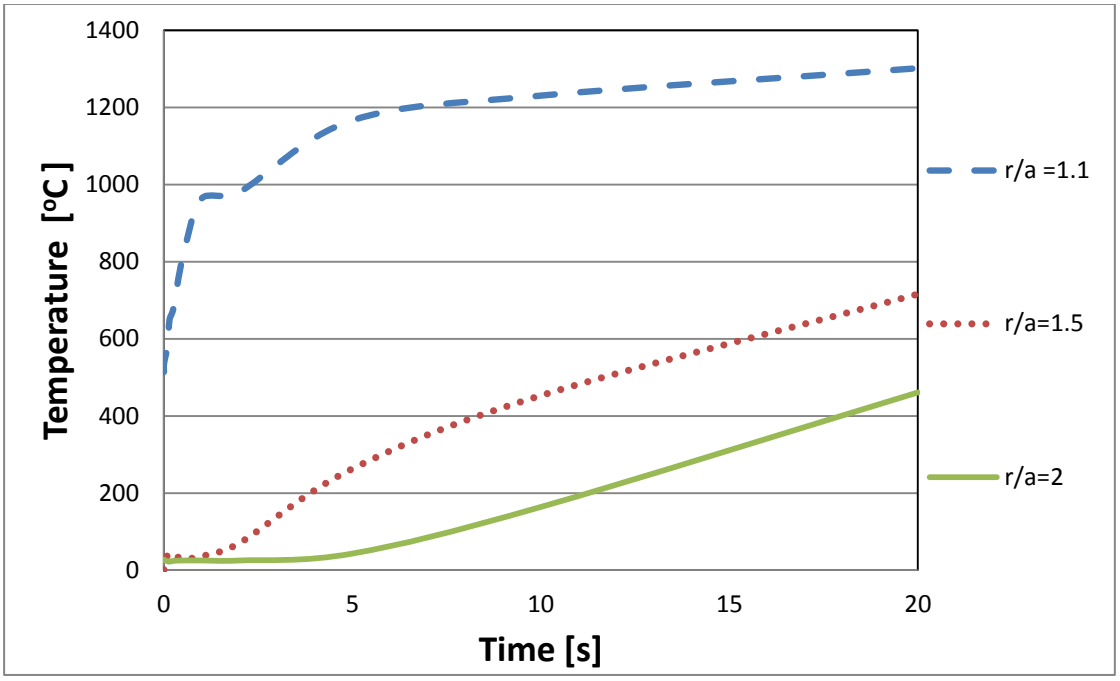

Figure 3.7: Temperature variation with time at different locations through the thickness.

3.2 Thermal Accumulation

One important issue in dynamic thermal cyclic loading (without relaxation time) is thermal accumulation which has not been appropriately investigated. Thermal accumulation can be realized as the thermal load repeats itself with no relaxation. To better realize this, the developed coupled finite element model has been used to analyze the same problem studied at the end of previous section but now considering internal thermal cyclic load. As mentioned before, the cylinder has an outer to inner radii ratio of two and inner radius of 30 mm (b/a=2 and a=30 mm) and is made of high alloy steel.

Figure 3.8 presents the thermal accumulation effect on temperature distribution due to the repeated cyclic thermal pulses without relaxation time between pulses. As shown, each pulse has been modeled as a triangular pulse with an amplitude of 1500 ^{o}C and a time duration of 0.5 Sec. It is important to mention that the temperature has been calculated at the summit point of each pulse.

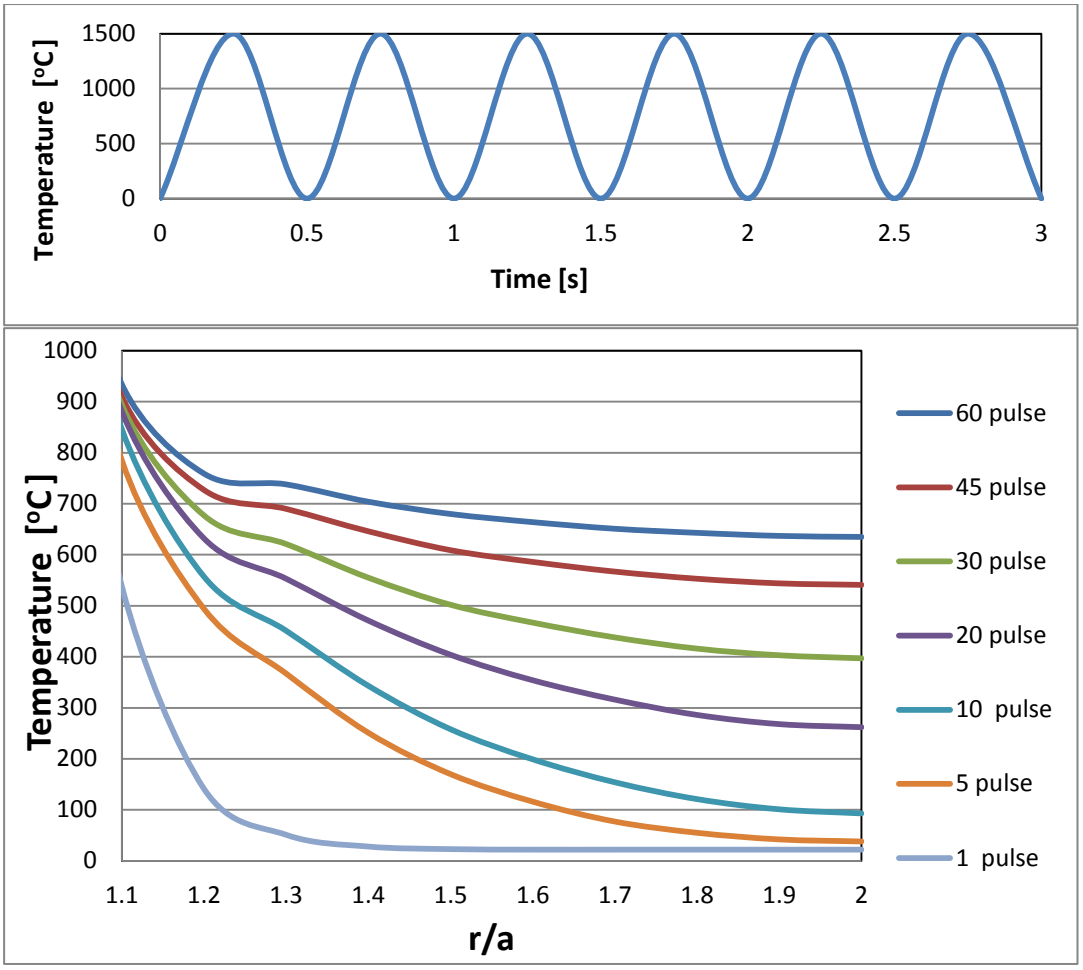

Figure 3.8: Temperature distribution through thickness due to cyclic thermal pulses.

The results, as shown in Figure 3.8, corroborate that the thermal accumulation has a significant effect on temperature distribution, which subsequently has a paramount effect on stress distribution as demonstrated in Figure 3.9 which shows the variation of hoop stress (normalized with respect to yield stress) through the thickness of cylinder for different thermal pulses.

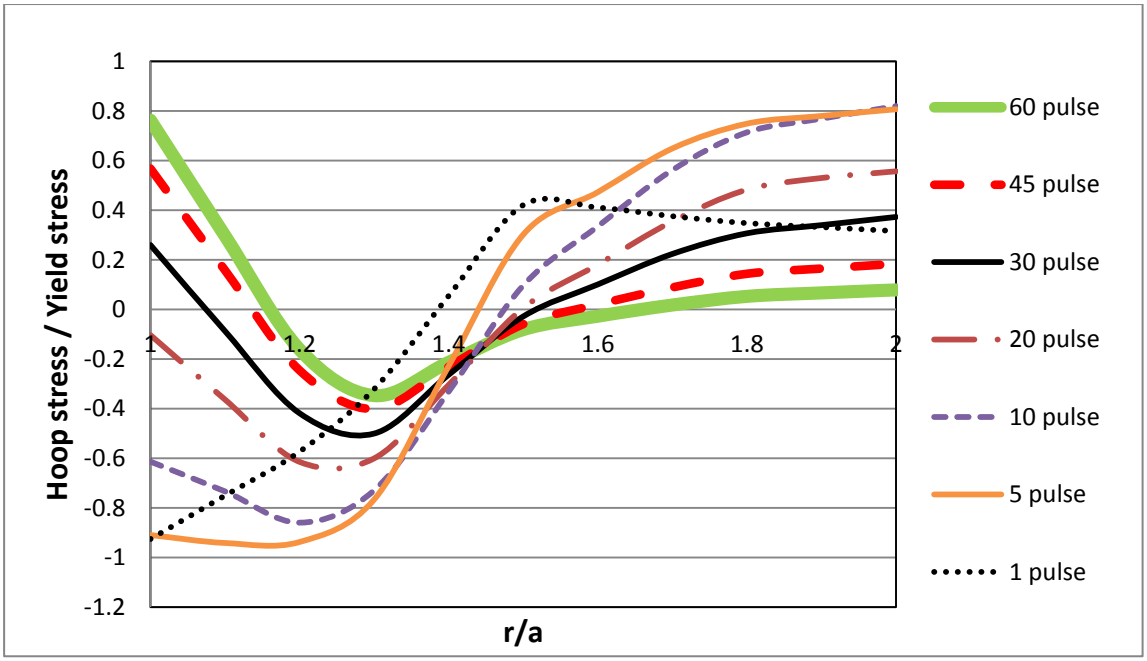

Figure 3.9: Hoop stress distribution through the thickness due to cyclic thermal pulses.

As it can be seen the hoop stress increases aggressively due to thermal accumulation at the near bore area going from a compressive to tensile state. Also, it should be mentioned that the point of calculation is at the end of the pulse where the highest hoop stresses have been found [43].

3.3 Experimental Study

The conducted experiment in this research study has two main purposes. The first goal is to observe temperature profile under dynamic load in a multilayer shrink-fitted cylinder and the second goal is to verify the developed finite element model for a multilayer

cylinder. In the following, first, the designed experimental setup has been explained and then results and comparisons with the finite element model are discussed.

3.3.1 Experimental setup

The two-layer test specimen has been made of two cylinders made of aluminum alloy. The material properties of the two cylinders are: k^t=25 W/m.^{o}C; C=896 J/kg.^{o}C; α=25.2×10^{-6} 1/^{o}C; E=68.9 GPa; $\nu = 0.339$; ρ=2700 kg/m^3 ; σ_y=280 MPa. Initially, the two cylinders were machined to be shrink-fitted together with an interference of 0.5 mm. The inner cylinder has inside and outside diameters of 15 mm and 20 mm, respectively. For the outer cylinder, the inside and outside diameters are 19.5 mm and 25 mm, respectively. The shrink fit process has been accomplished through the following steps: 1- Both cylinders were initially heated at the constant temperature of 350 ^{o}C in the furnace to have the same micro-structure; 2- The inner cylinder was then allowed to cool down to the ambient temperature and the outer one remained in the furnace at the same temperature; 3- Finally using a hydraulic axial press and a lubricant at the interference surfaces, the two cylinders were properly shrink-fitted together, as shown in Figure 3.10.

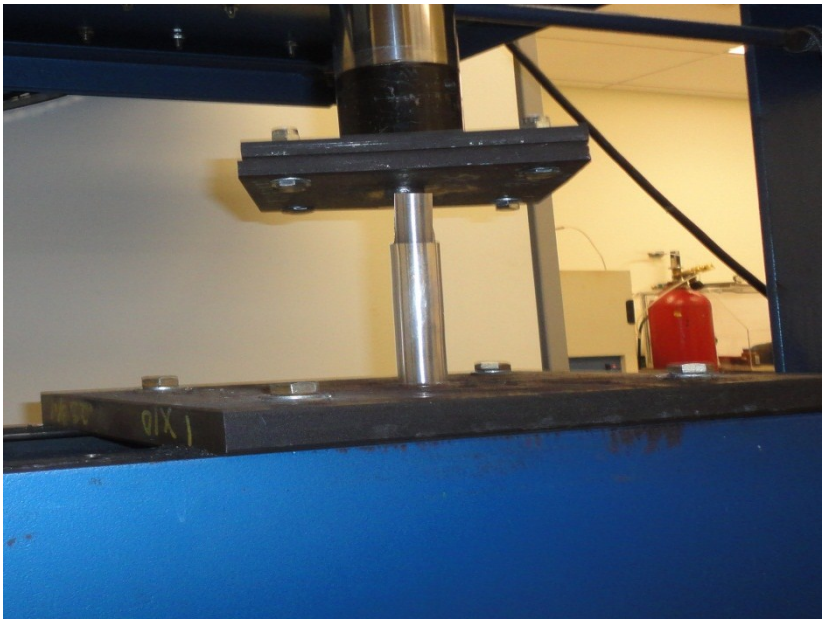

Figure 3.10: Shrink fitting process using of a hydraulic axial press.

Once the shrink fit process has been completed successfully, three holes are drilled at different distances (0.5 mm, 2.5 mm and 4.5 mm) from the outer surface of the shrink-fitted cylinder in order to accommodate thermocouples (OMEGA ® Nextel Ceramic Insulated Thermocouples) for measuring the temperature-time profile at different depth from the outer surface. Also another thermocouple has been mounted at the inner surface of the shrink-fitted cylinder to measure the inner surface temperature, which is considered as the input thermal load. Moreover, a strain gauge has been attached at the outer surface of the shrink-fitted cylinder to measure the hoop strain, as shown in Figure 3.11. The complete test rig is shown in Figure 3.12. All the thermocouples have been connected to a data acquisition system (National Instrument, SCXI – 1000) and the strain gauge has been connected as a quarter Wheatstone bridge to a strain meter. Hot air with a constant temperature has been permitted to flow inside the cylinder, which causes a time-

dependent variation of the thermal boundary condition on the inner surface of the cylinder.

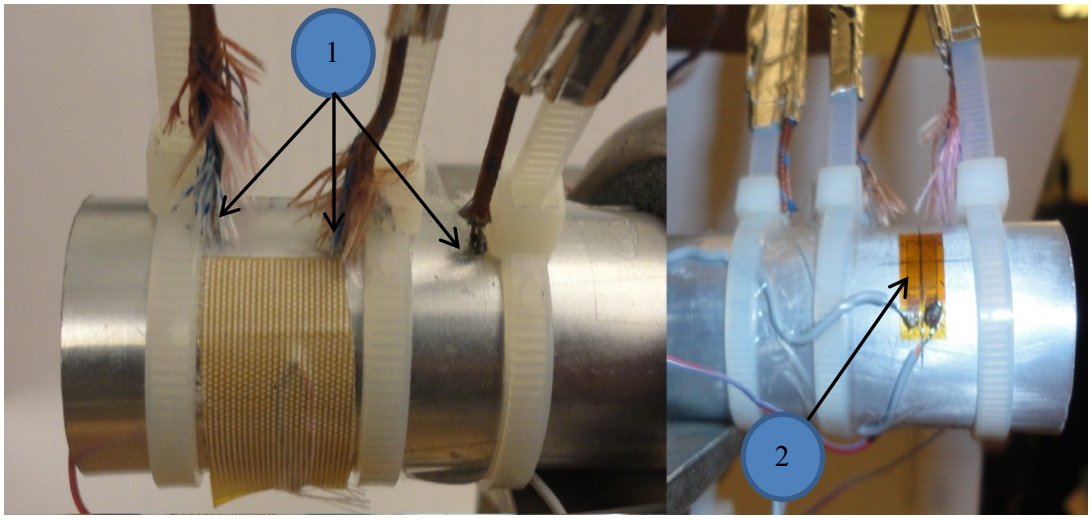

Figure 3.11: On the left, the thermocouples mounted at different depth. On the right, the strain gauge attached at the outer surface of the shrink-fitted cylinder.

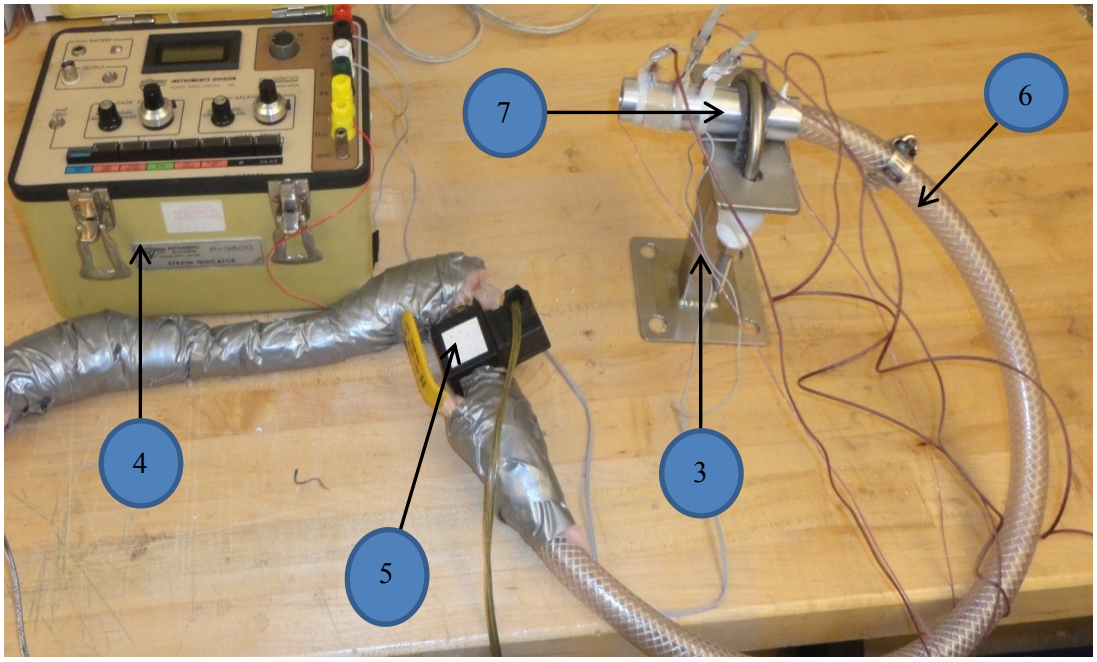

Figure 3.12: Test rig contents: strain meter, control electric valve, test specimen, and thermocouples.

In Figures 3.11 and 3.12, (1) is the thermocouples, (2) is the strain gauge, (3) is the fixture, (4) is the strain meter, (5) is the control electric valve, and (6) is the hot air pipe. The flow of the hot air is controllable; therefore it can be opened and closed to provide quasi-static or dynamic input thermal loads, as shown in Figure 3.13.

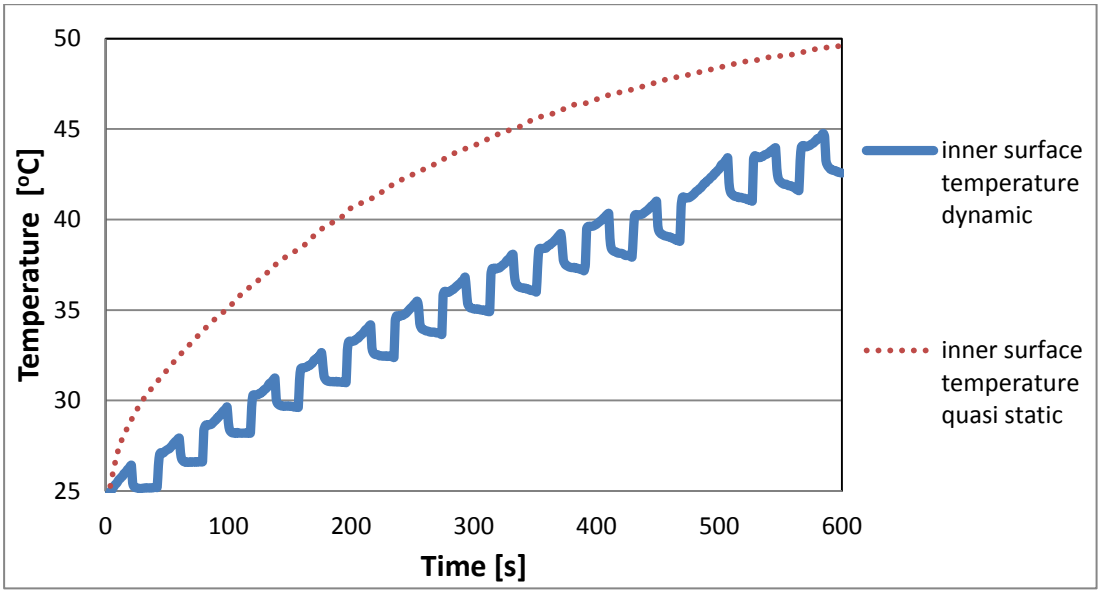

Figure 3.13: The time–dependent variation of the inner surface temperature.

It is important to note that the measured inner surface temperature has been also used as the input thermal load for the developed finite element model.

3.3.2 Experimental results and verification of the finite element model of the compound cylinder

Figures 3.14 and 3.15 present the results of the quasi-static experiment. In Figure 3.14, the measured temperature profiles with time are compared with the simulation results using the finite element model.

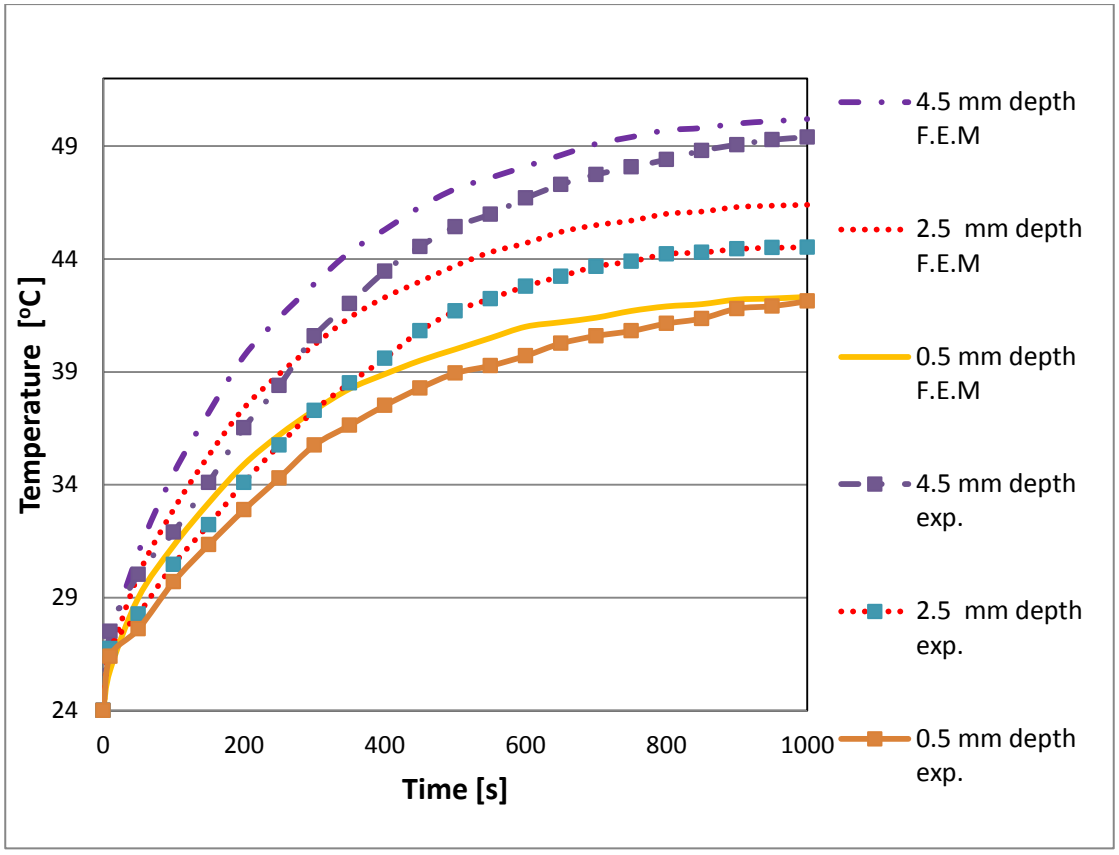

Figure 3.14: Temperature profile versus time at the three different locations in the wall thickness-Quasi-static thermal load.

Figure 3.15 also shows the temperature distribution through the thickness obtained experimentally and using the finite element model.

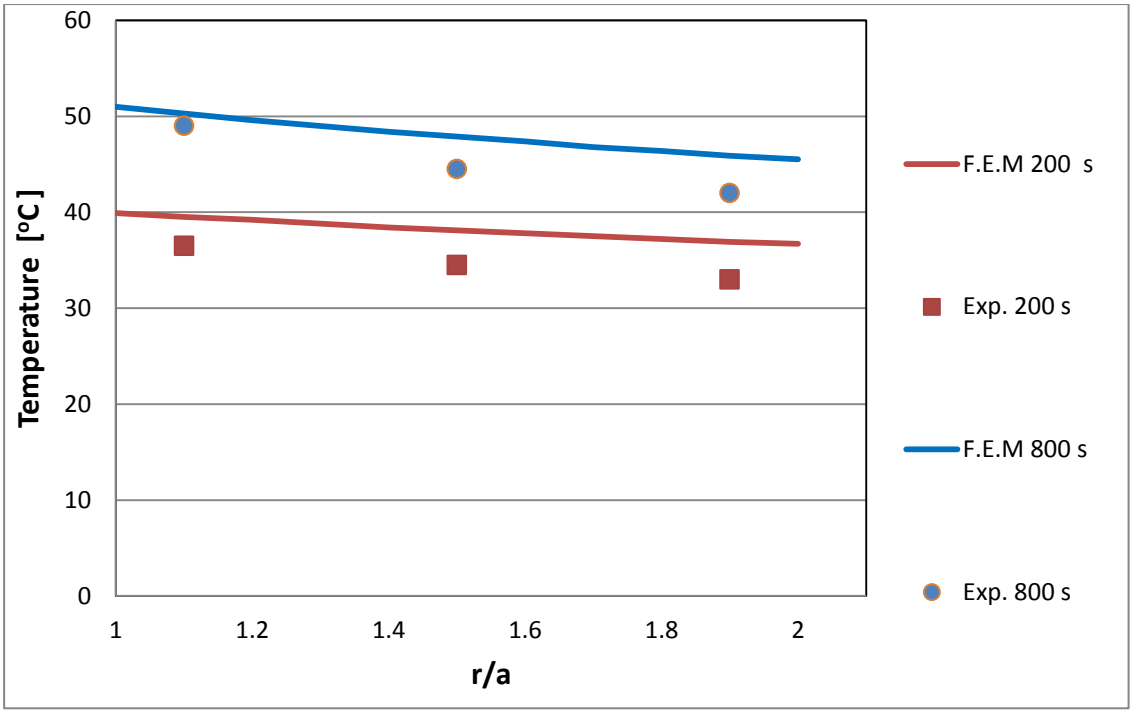

Figure 3.15: Temperature distribution through the thickness at different measuring times- Quasi-static thermal load.

The examination of results shows good agreement between the simulation and experimental results at different locations through the thickness and at different times and the Root Square Mean (RSM) error between the simulation and the experimental data does not exceed 3.5°C (9%) for all points.

In the case of dynamic thermal load, the inlet hot air flow has been controlled using the electrical control valve to provide the thermal dynamic load at the inner surface, as shown in Figure 3.13. Figures 3.16 and 3.17 illustrate the comparison between the finite element results and the experimental data for temperature-time profile at pre-mentioned depth from outer surface and temperature-distance profile at different time, respectively. As it can be realized again, very good harmony exists between the simulation and the

experimental data. Also, the RSM error in this case does not exceed 2.2 ^{o}C (6%) for all points.

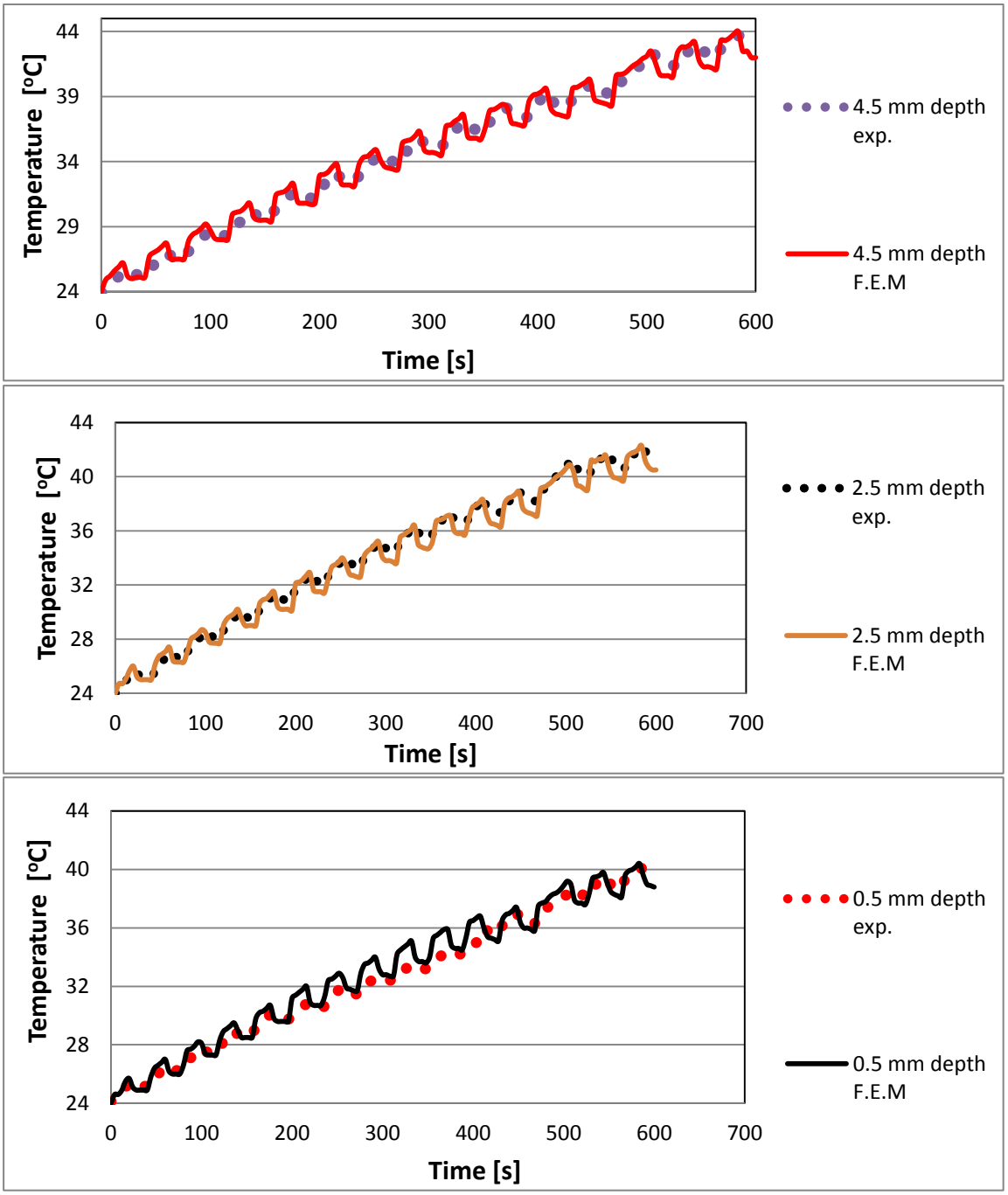

Figure 3.16: Temperature- time profiles at three different depth comparing the finite element results with the experimental data-Dynamic thermal load.

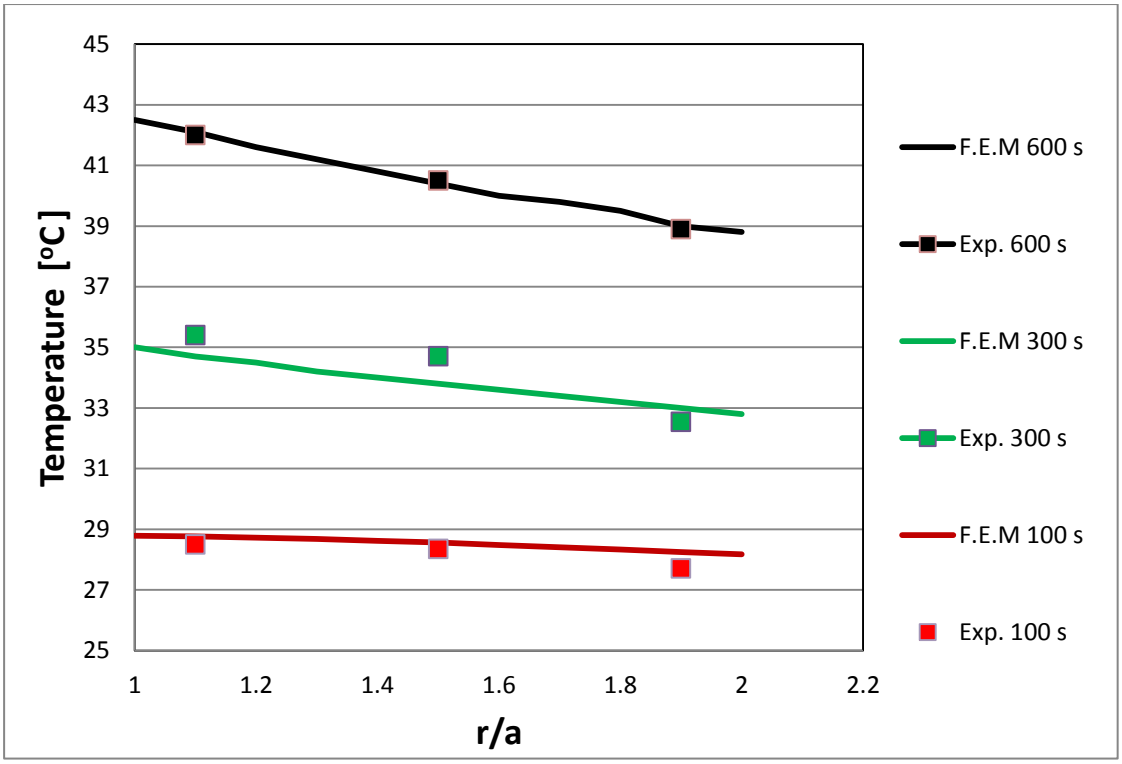

Figure 3.17: Temperature distribution through the thickness at different measuring times- Dynamic thermal load.

The hoop strain has also been measured using the strain gauge attached at the outer surface, and then compared with the thermal strain calculated using the finite element model for both the quasi-static and dynamic thermal loads in Figure 3.13. The results are provided in Tables 3.2 and 3.3.

Table 3 .2: Comparison between the measured and the simulated hoop strain at different times-Quasi-static thermal load case.

Time [s]	Strain Experimental [μstrain]	Strain F.E [μstrain]	Error [μstrain]
100	20	23	3
200	25	26	1
500	64	68.5	4.5
700	93	112.5	19.5
1000	102	120	18

Table 3 .3: Comparison between the measured and the simulated hoop strain at different times- Dynamic thermal load case.

Time [s]	Strain Experimental [μstrain]	Strain F.E [μstrain]	Error [μstrain]
100	12	15	3
200	28	33	5
300	42	47	5
400	45	48	3
600	62	70	8

The results again show that there is a good agreement between the finite element results and the measured data. The RMS error for the hoop strain does not exceed 8.05 μstrain (14.14%) and 5.13 μstrain (15.5%) in quasi-static and dynamic cases, respectively.

3.4 Hoop Stress Profiles in Compound Cylinders

The residual hoop stress through the thickness of compound cylinders induced due to shrink-fit, autofrettage or combined shrink-fit and autofrettage processes have been previously evaluated for the different combinations (see section 2.3.1). Here, the responses (hoop stress) of different combinations of the compound autofrettaged and shrink-fitted cylinders addressed before have been investigated and compared under different loads including: inner cyclic thermal load, inner static pressure, and combined thermo-mechanical load, considering thermal accumulation. Results for these combinations have also been compared with a dimensionally equivalent Mono-Block Cylinder (MBC), Autofrettaged Mono-Block cylinder (AMBC) and Shrink-Fitted Cylinder (SFC).

Material NiCrMoV125 steel with properties of k'=15 W/m.^{o}C; c=480 J/kg.^{o}C; α=1.7×10^{-5} 1/^{o}C; E=268 GPa; H=75 GPa; $\nu = 0.29$; ρ=7800 kg/m^3 and σ_y=700 MPa has been used for both layers of the compound cylinder. The inner, outer and interference radii of the compound cylinder have been considered to be 100, 200 and 150 mm, respectively for all autofrettage and shrink-fit combinations addressed before. The radial interference and autofrettage pressure have also fixed at 0.2 mm and 736 MPa.

Figures 3.18, 3.19 and 3.20 show the results for normalized hoop stress distribution through the thickness of the cylinder which is subjected to cyclic thermal pulses, static pressure, and combined cyclic pressure and thermal pulses, respectively. Static pressure has been assumed to be 250 MPa and thermal pulses, as mentioned before, have a triangular shape with amplitude of 1500 ^{o}C and 0.5 second time duration. Pressures

pulses are also similar to thermal pulses having a triangular shape with amplitude of 250 MPa and time duration of 0.5 second.

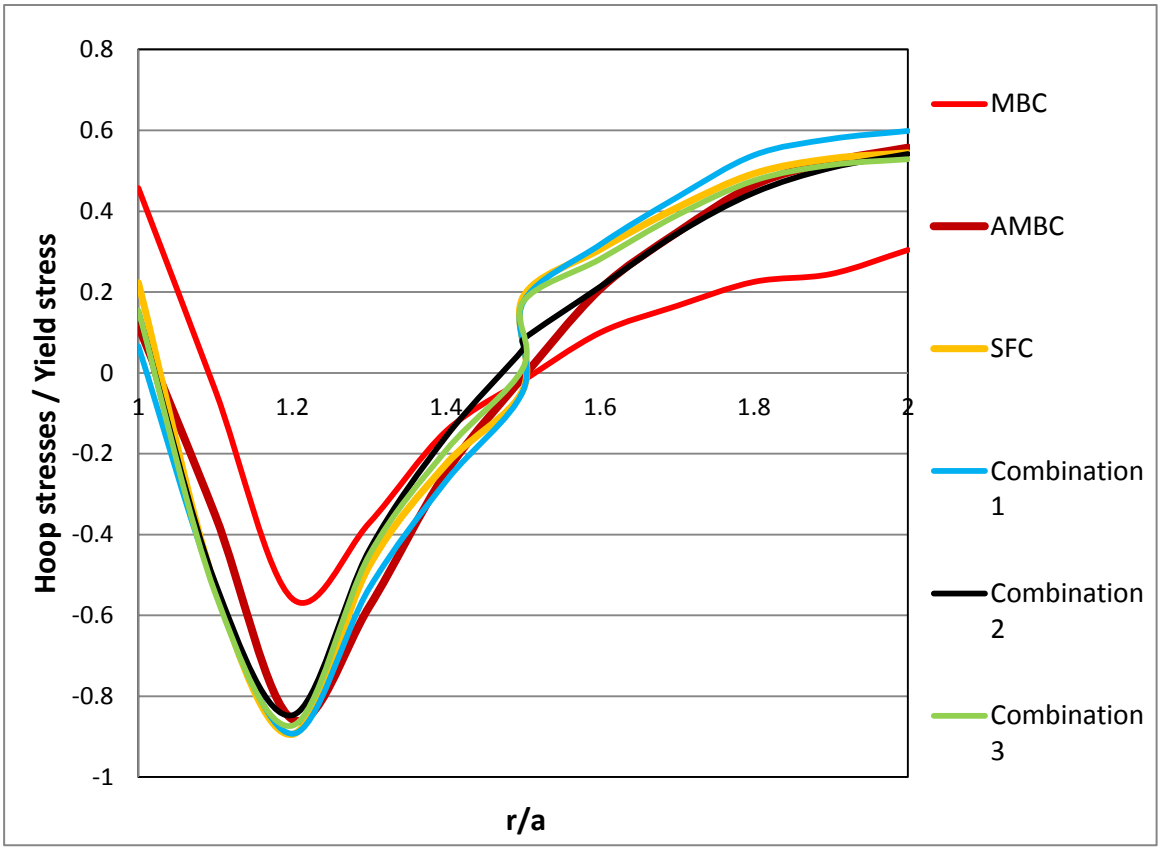

Figure 3.18: Hoop stress distribution for different combinations after 150 thermal pulses.

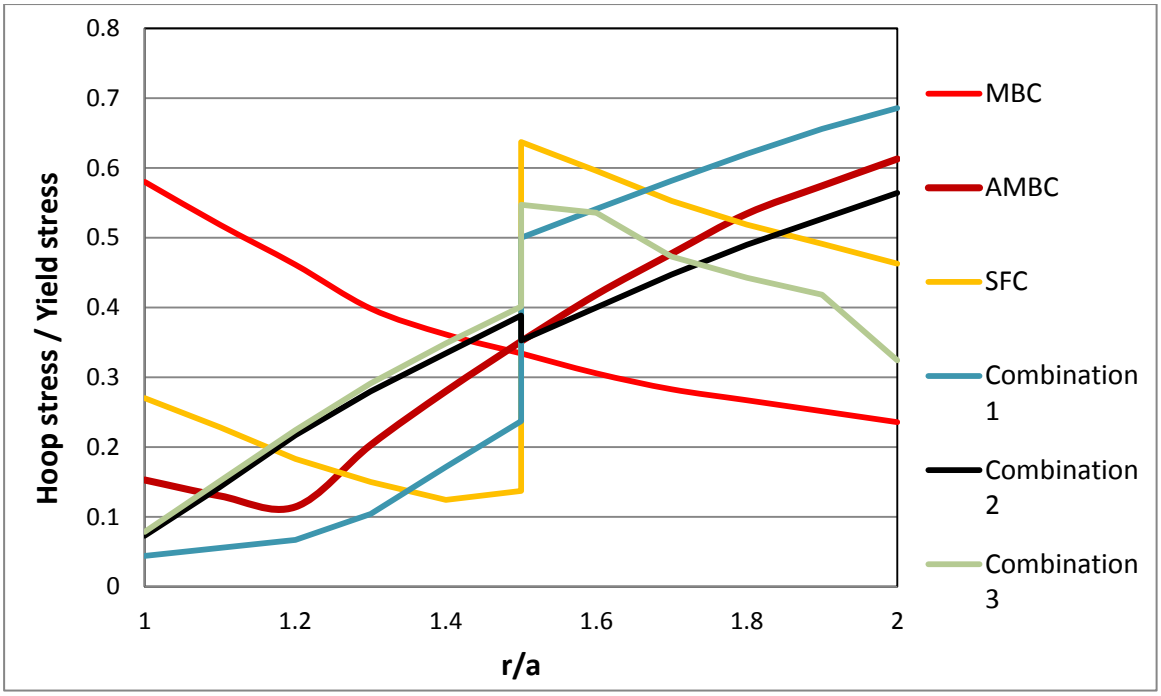

Figure 3.19: Hoop stress distribution for different combinations subjected to a static pressure of 250 MPa.

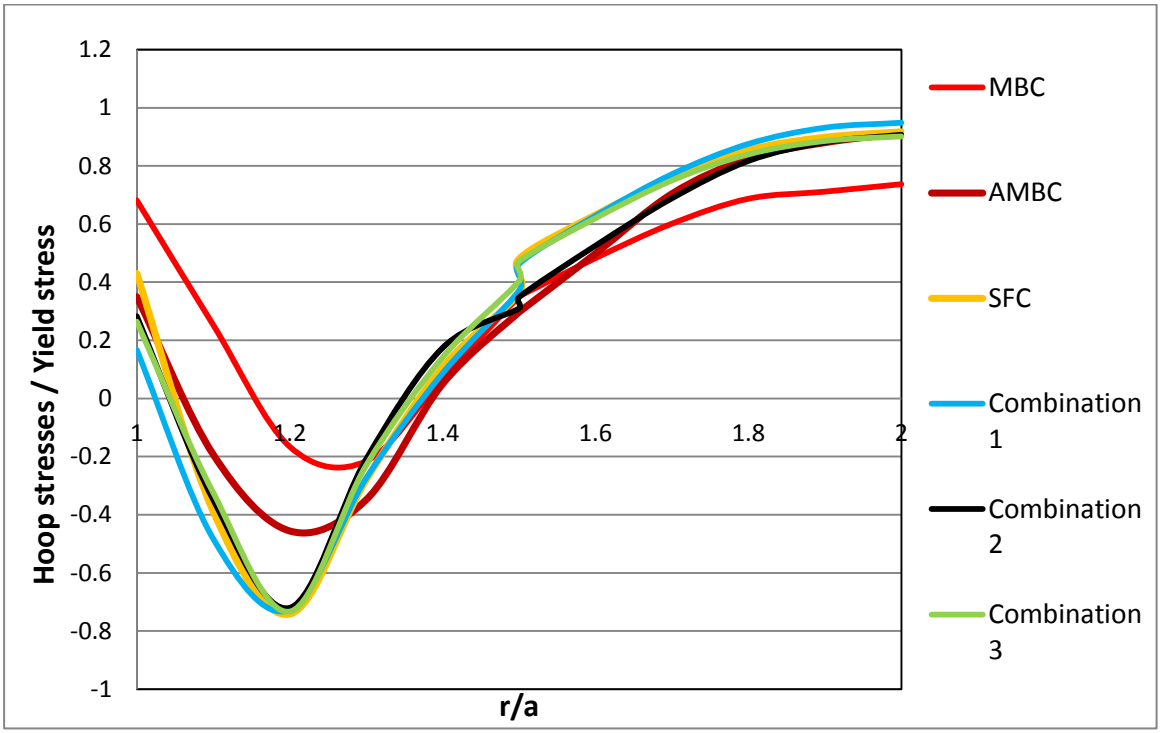

Figure 3.20: Hoop stress distribution for different combinations after 100 thermal and pressure pulses.

It should be noted that the point of calculation for pressure pulse is at the summit of the pulse, while for the thermal pulse, it is at the end of the pulse. Figure 3.21 clearly shows combined cyclic pressure and thermal loads and the locations where the calculation has been conducted. As it can be seen the calculation points are the mid points of pressure pulses where the maximum mechanical stress occurs and the end points of thermal pulses where the maximum thermal stress occurs.

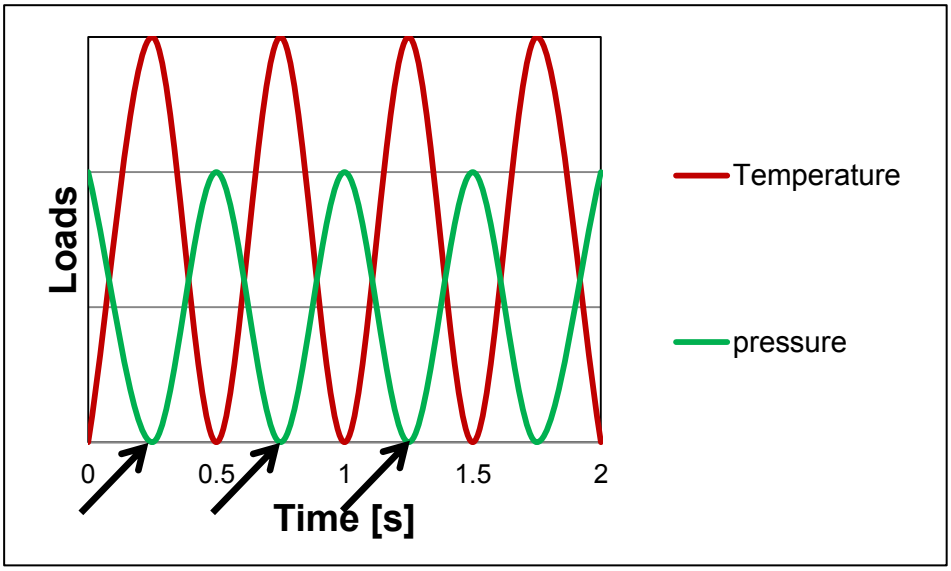

Figure 3.21: Combined pressure and thermal pulses and the points of calculation.

From examination of Figures 3.18-3.20, one can observe significant reduction in working hoop stress in region near to the bore area of compound cylinders subjected to shrink-fit or/and autofrettage processes compared with that of equivalent mono-block cylinder. This is mainly due to the fact of induced residual compressive stresses in these areas due to autofrettage and shrink-fit processes. Table 3.4 provides the percentage reduction of

the hoop stress at the bore area for different configurations with respect to equivalent mono-block cylinder for the case of combined thermo-mechanical load (Figure 3.20).

Table 3 .4: Percentage reduction of hoop stresses at the bore area with respect to mono-block cylinder subjected to combined pressure and thermal and pressure cyclic pulses.

Combination	AMBC	SFC	Combination 1	Combination 2	Combination 3
reduction %	48 %	36%	75%	57 %	58 %

As it can be realized from Table 3.4, with respect to mono-block cylinder, different shrink-fit and autofrettage combinations can considerably reduce the hoop stress at the cylinder bore subjected to cyclic pressure and thermal pulses It is important to note that the combination of shrink-fitting two layers then autofrettage of whole assembly (combination 1) can provide the highest reduction (75%) for this load case.

3.5 Fatigue Life

The main objective of using compound cylinders subjected to autofrettage and shrink-fit processes is mainly to increase the fatigue life of cylinders by inducing beneficial compressive residual stresses. Thus fatigue life can be considered as a desired performance index to evaluate different configurations of compound cylinders for design purposes. However, not many works have been reported the fatigue life for compound cylinders [23, 25 and 44-48]. Most of and the previous works mainly assume either cyclic

mechanical loads or neglect the thermal accumulation effect during the thermo-mechanical loads.

Here, first, the fatigue life of the proposed different combinations of compound cylinders subjected to inner cyclic pressure has been evaluated using ASME codes for high pressure vessel [67]. Then, using the same methodology, the stress intensity factor (SIF) has been calculated for these cylinders after each cycle of the thermo-mechanical load, and compared with the critical SIF (fracture toughness of the cylinder material). The number of cycles to reach this critical value has been considered as the life time of compound cylinders.

3.5.1 Fatigue life for compound cylinders under cyclic pressure

The evaluation of the fatigue life in the compound cylinders investigated in this study is based on the following considerations and assumptions according to ASME code, Section VIII, Division 3 [67] which is also used in Refs. [23, 25]:

1. The crack initiation stage is completed.
2. The principle of linear elastic fracture mechanics has been used to calculate the number of design cycles. This principle is modified for the plastic behavior of the material.
3. The number of design cycles is the only cause to propagate these initial cracks to the allowable final depth.

4. The residual stresses introduced due to the manufacturing processes, such as shrink-fit and autofrettage, will be taken into consideration during calculations.

5. A surface crack not associated with a stress concentration shall be assumed to be semielliptical with an initial ratio of depth to surface length of 1:3.

To evaluate the fatigue life, the first step is to assume the initial depth a_{c_o} for a semielliptical crack shown in Figure 3.22 and then present by the curve fitting process the stress distribution normal to the plane of the crack using a third degree polynomial function as [67]:

$$\sigma = A_o + A_1\left(\frac{x}{a_c}\right) + A_2\left(\frac{x}{a_c}\right)^2 + A_3\left(\frac{x}{a_c}\right)^3 \qquad (3.24)$$

where x is the distance through the wall measured from the inner surface of the layer in (mm) and A_i are the polynomial coefficients.

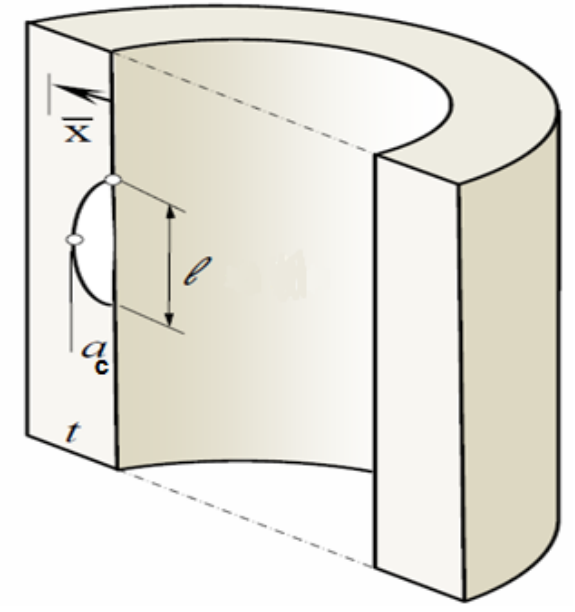

Figure 3.22: Semielliptical crack in a single layer [44].

Eq. 3.24 may be transferred to another form using an alternating method according to ASME, Section VIII, Division 3, code D-401.1 [67] as:

$$\sigma = A'_o + A_1{}'\left(\frac{x}{t}\right) + A_2{}'\left(\frac{x}{t}\right)^2 + A_3{}'\left(\frac{x}{t}\right)^3 \quad (3.25)$$

where t is the layer thickness in terms of diameter ratio, the values of $A_i{}'$ are converted to the A_i values as follows:

$$A_o = A'_o, \quad A_1 = A'_1(\frac{a_c}{t}), \quad A_2 = A'_2(\frac{a_c}{t})^2, \quad A_3 = A'_3(\frac{a_c}{t})^3 \quad (3.26)$$

The polynomial coefficients A'_i in Eq. 3.25 are to be determined using curve fitting of the hoop stress distribution along the whole thickness of the cylinder, then substitute in Eq. 3.26 to determine the A_i values.

The second step is to calculate the stress intensity factor (SIF) K_I according to the ASME code D-401 as:

$$K_I = [(A_0 + A_p)G_o + A_1G_1 + A_2G_2 + A_3G_3]\sqrt{\frac{\pi a_c}{Q_c}} \quad (3.27)$$

where A_i are coefficients given in Eq. 3.26, A_p is the internal vessel pressure in (MPa) if the pressure acts on the crack surfaces for the inner layer and it is equal to radial stress for the other layers, G_i are the free surface correction factors which depends on material and provided in Ref. [67], Tables D-401.1 and D-401.2 and Q_c is the flaw shape parameter described as:

$$Q_c = 1 + 4.593(\frac{a_c}{l})^{1.65} - q_y \quad (3.28)$$

where l is the major axis of the flaw in (mm), a_c/l is the flaw aspect ratio (assumed initially 1:3) and q_y is the plastic zone correction factor, which may be set to zero for fatigue crack growth calculations.

The third step is to use Paris relation where the crack growth rate da_c/dN is a function of the range of the stress intensity factor ΔK_I and the stress intensity ratio R_K which can be stated as:

$$\frac{da_c}{dN} = C_f[f(R_K)](\Delta K_I)^{m_f} \tag{3.29}$$

$$R_K = \frac{K_{Imin}+K_{Ires}}{K_{Imax}+K_{Ires}} \tag{3.30}$$

$$\Delta K_I = K_{Imax} - K_{Imin} \tag{3.31}$$

where K_{Ires}, K_{Imin} and K_{Imax} are the stress intensity factors (SIFs) due to residual stress, initial inside pressure and working pressure, respectively. C_f and m_f are crack growth rate factors which can be found in Ref. [67], Tables KD.430. The function of R_K is different for positive and negative values of R_K and for different materials. For materials listed in Table D-500 [67], the following functions of $f(R_K)$ may be used:

For $R_K \geq 0$, $\quad f(R_K) = 1 + C_3 R_K$ (3.32)

and for

$R_K < 0$, $\quad f(R_K) = [C_2/(C_2 - R_K)]^{m_f}$ (3.33)

where C_2 and C_3 are material factors extracted from Ref. [67], Table D-500.

Finally, the number of design cycles is obtained by the numerical integration of Eq. 3.29 and assuming that ΔK_I is constant over an increment change of the crack depth Δa_c as [44]:

$$\Delta N = \frac{\Delta a_c}{C_f[f(R_K).(\Delta K_I)^{m_f}]} \tag{3.34}$$

The calculation is then repeated with renewing the values of Δa_c in Eq. 3.34 until it reaches the final allowable crack depth.

3.5.2. Numerical results for fatigue life-cyclic pressure

Material, geometrical parameters and cyclic pressure load are all the same as those used in Section 3.4. All material factors according to the ASME code [67] are found to be: C_f=3.64×10^{-12} mm/cycle, m_f=3.26, C_2=1.5, C_3=3.53, G_o=0.90289, G_1=0.12851, G_2=0.04263, G_3=0.01942.

The inner, outer and interference radii of the compound cylinder have been considered to be again 100, 200 and 150 mm, respectively for all autofrettage and shrink-fit combinations. The radial interference and autofrettage pressure are 0.2 mm and 736 MPa, respectively and cyclic pressure has the amplitude of 250 MPa. Initial crack depth, a_{c_o}, is assumed to be 0.5 mm.

The maximum number of design cycles N for combinations 1-3 described in Section 2.3.1 and shrink-fit cylinder (SFC) has been found assuming that the crack exists at the inner surface of both inner and outer layers. The results are provided in Table 3.5.

Table 3. 5: Fatigue life as number of cycles for different combinations of compound cylinders under cyclic pressure.

Combination	SFC	Combination 1	Combination 2	Combination 3
No. of cycles (N)	4800	6900	29200	7520

As it can be realized the shrink-fitting of two autofrettaged cylinders (combination 2) has the maximum number of life cycles. It has also been observed that the outer layer always has the minimum number of life cycles compared with the inner layer for all combinations. This can be attributed to the existence of detrimental tensile residual stresses in the outer layer.

It is important to mention that the von-Mises stress for all prementioned combinations have been calculated at 250 MPa working pressure to assure that re-yielding does not occur the compound cylinder behaves elastically under operational load. Appendix A provides von-Mises stress distribution along the wall thickness of the cylinder.

Now assuming the initial crack exits only at the inner surface (working surface) of the compound cylinders and the critical crack depth is 25% of the whole thickness of the cylinder. The results for fatigue life for different combinations have also been compared with that of the equivalent mono-block cylinder (MBC) and autofrettaged mono-block cylinders (AMBC). The results are provided in Table 3.6.

Table 3. 6: Fatigue life as number of pressure cycles assuming the crack is only at the inner surface

Combination	MBC	AMBC	SFC	Comb. 1	Comb. 2	Comb.3
No. of cycles (N)	4.9×10^3	1.01×10^4	9.3×10^3	1.38×10^4	1.19×10^4	1.19×10^4

Examination of results in table 3.6 reveals that the first combination (shrink fir prior to autofrettage) has the maximum number of fatigue life cycles. It is noted that the combination 1 has the maximum compressive residual stress at the inner surface.

3.5.3. Fatigue life for compound cylinders under cyclic thermo-mechanical loading

For thermal or thermo-mechanical loading the generated hoop stresses in the compound cylinder are not repeated for each cycle (see Figure 3.9) as the temperature gradient through the cylinder thickness changes at the beginning of each new cycle due to the thermal accumulation effect. In this research study, in order to evaluate the fatigue life of compound cylinders for this loading condition, the SIF has been calculated using the same technique described in section 3.5.1 after each cycle of thermal or thermo-mechanical pulses. Figures 3.23 and 3.24 present the SIF versus number of thermal and thermo-mechanical pulses, respectively for different configurations of the compound cylinders described before. The material and geometrical parameters are exactly the same as those in Section 3.4. Now the number of pulses required to reach the critical SIF (K_{Ic}) has been evaluated and considered to be the fatigue life time for each configurations. It is

noted that pressure and thermal pulses have the same magnitude as those mentioned in Section 3.4.

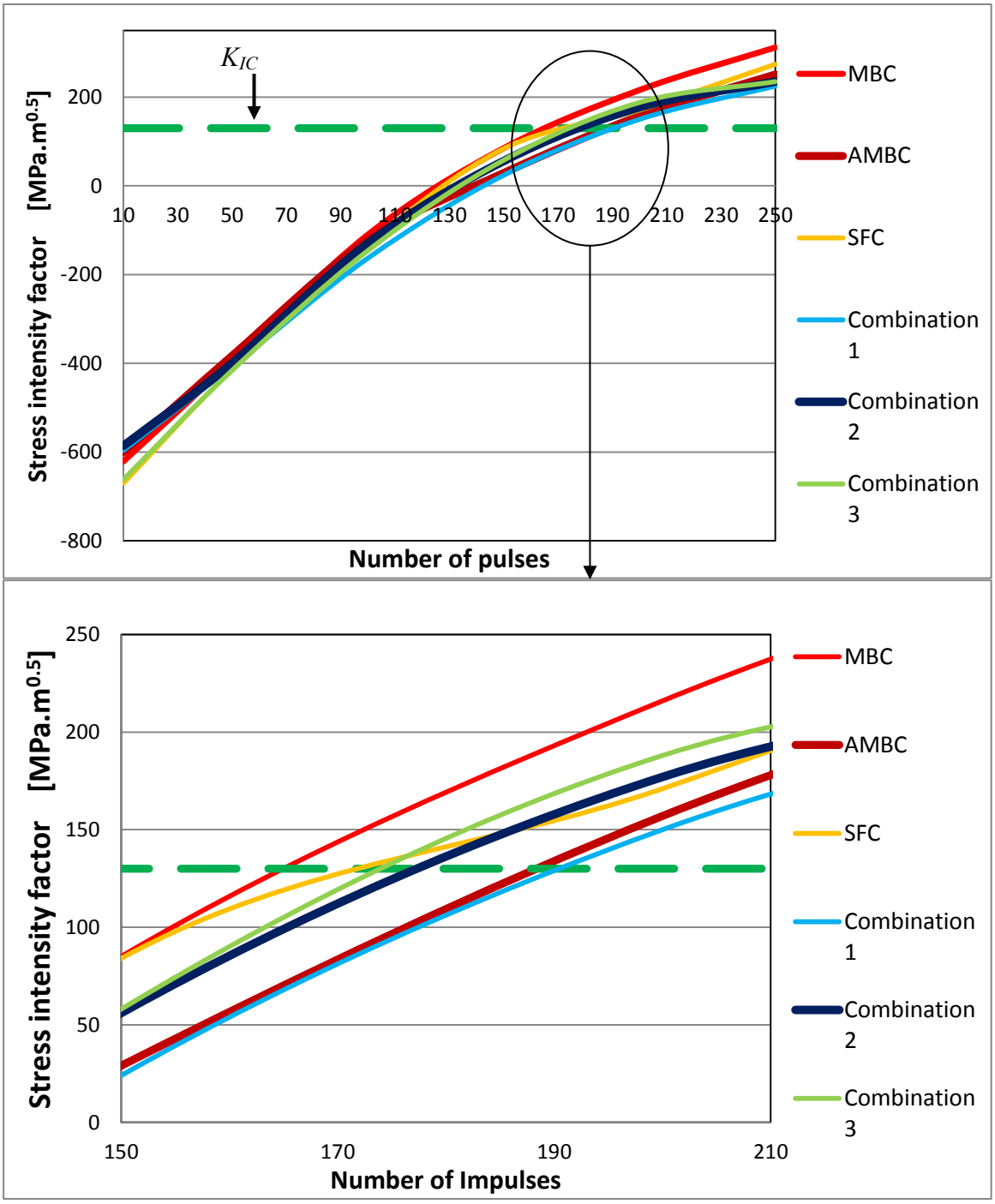

Figure 3.23: SIF versus number of pulses for different combinations subjected to cyclic thermal pulses.

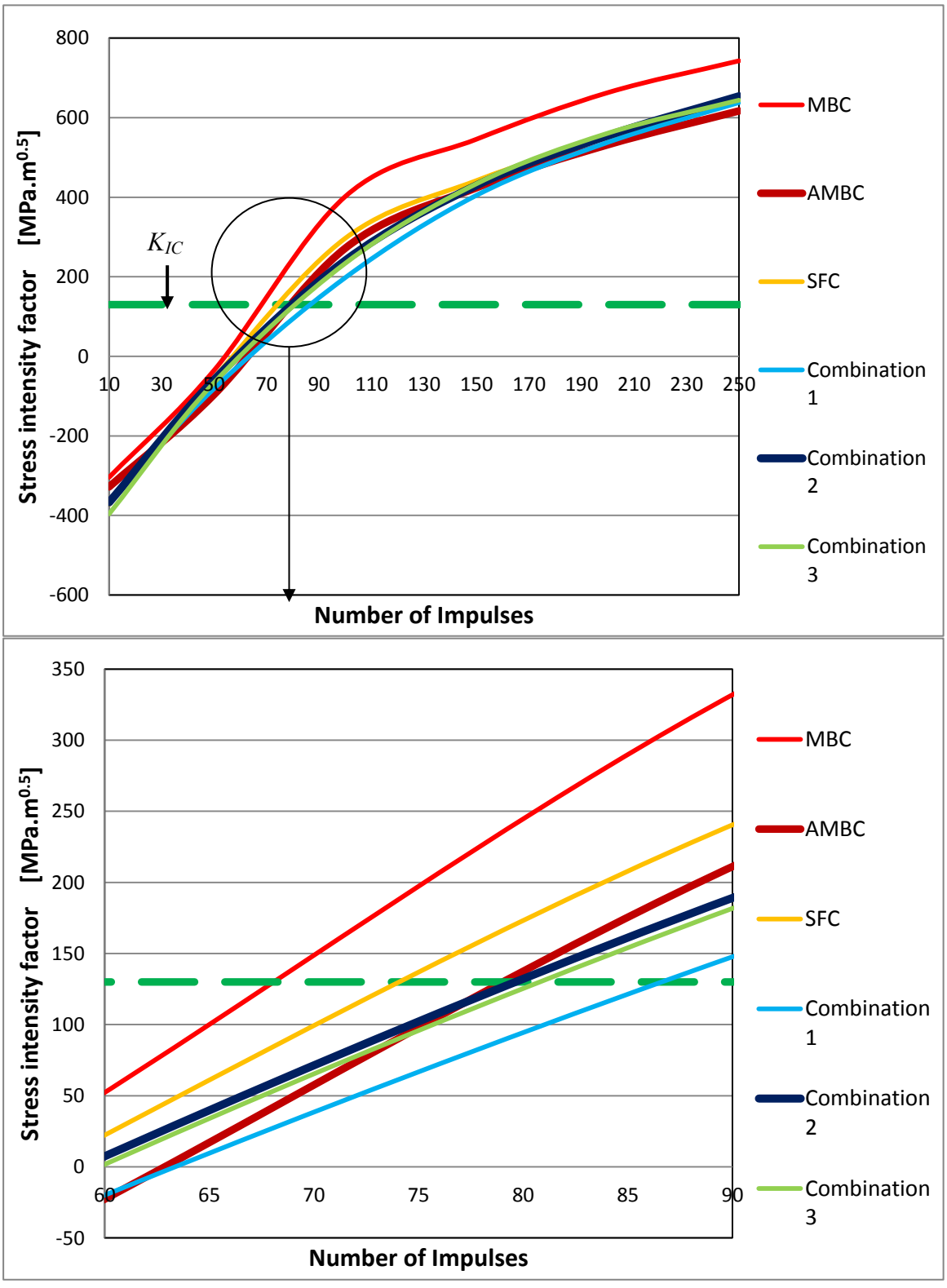

Figure 3.24: SIF versus number of pulses for different combinations subjected to cyclic thermo-mechanical pulses.

The percentage increase in fatigue life of compound cylinders subjected to shrink-fit and/or autofrettage processes with respect to the mono-block cylinder are tabulated in Tables 3.7 and 3.8 for cyclic thermal and cyclic thermo-mechanical pulses, respectively. It is important to note that that, for calculation of SIF, the initial crack has been assumed only at the inner surface (working surface) of the cylinder for all configurations.

Table 3.7: Percentage increase of fatigue life with respect to mono-bock cylinder subjected to cyclic thermal pulses.

Combination	SFC	AMBC	Combination 1	Combination 2	Combination 3
Enhancement % compared with virgin cylinder	4%	12%	14%	9%	6%

Table 3.8: Percentage increase of fatigue life with respect to mono-bock cylinder subjected to cyclic thermo-mechanical pulses.

Combination	SFC	AMBC	Combination 1	Combination 2	Combination 3
Enhancement % compared with virgin cylinder	7%	14.6%	29.4%	14.7%	17.6%

Examination of Tables 3.7 and 3.8 reveals that a compound multilayer cylinder could significantly enhance the fatigue life time compared with the equivalent single layer mono-block cylinder. Specifically, shrink-fitting of two layers then autofrettage of the assembly (combination 1) provides the largest increase in the fatigue life for both thermal and thermo-mechanical loading conditions. As mentioned before, the combination 1 has the maximum compressive residual stress at the inner surface.

3.6 Summary

This chapter addresses the response of autofrettaged and shrink-fitted compound cylinders under internal cyclic pressure, internal cyclic thermal pulses, and internal cyclic pressure and thermal pulses considering thermal accumulation. It has been shown that the fully coupled thermo-elastic model is much more accurate than the partially coupled one, especially when the component is subjected to thermal shocks. In addition, the thermal accumulation has a significant effect on the thermal stresses. The different combination of the compound cylinders can reduce the hoop stress at the near bore area up to 75%, compared with the equivalent mono-block cylinder.

For the fatigue life, the SIF has been calculated using ASME code for high pressure vessel. All the combinations of compound cylinders could enhance the fatigue life, which has been found under the effect of the different loads as:

1- For the case of internal cyclic pressure, the shrink-fitting of two autofrettaged layers (Combination 2) is found to be the best combination and could enhance the fatigue life significantly compared with the equivalent mono-block cylinder. The outer layer is the critical layer in this case.

2- For the case of internal cyclic thermal loads, the shrink-fitting of two layers then autofrettage of the assembly (Combination 1) is found to be the best combination and could enhance the fatigue life by 14% compared with the equivalent mono-block cylinder.

3- For the case of combined pressure and thermal loads, also the shrink-fitting of two layers and then autofrettage of the assembly (Combination 1) is found to be the best

combination and it could enhance the fatigue life by 29.4% compared with the equivalent mono-block cylinder.

CHAPTER 4

OUTER SURFACE PRIOR TO INNER SURFACE DOUBLE AUTOFRETTAGE PROCESS

The autofrettage and shrink-fit processes are used to enhance the load carrying capacity and fatigue life of the pressure vessels subjected to thermal, mechanical, or combined thermo-mechanical loads. All the previous works were only concerned with increasing the magnitude of compressive residual stress at the inner layer or the near bore area of the thick-walled cylinders, not considering the harmful high tensile residual stress at the outer part of the cylinder, which can reduce the fatigue life. Also, the idea of multiple or re-autofrettage had been only used at the inner surface of the cylinder to increase the magnitude of compressive residual stress at the near bore area regardless of the tensile residual stress at the outer part of the cylinder. On the basis of these findings, a methodology to reduce the magnitude of positive residual stresses at the outer part of the combined cylinders without affecting the negative residual stresses in the near bore area has been proposed here.

In this chapter, a new design philosophy is examined by applying an autofrettage cycle on the external surface of the cylinder prior to an autofrettage cycle on the internal surface of the cylinder. It is shown that these external and internal autofrettage cycles not only increase the magnitude of compressive residual stress at the near bore area but also decrease the tensile residual stress at the near outer surface area. Moreover, this double (external prior to internal) autofrettage process has been combined with shrink-fit and standard inner surface autofrettage processes to produce new combinations of the compound thick-walled cylinders. The residual stresses for these new combinations have been evaluated and then the mechanical fatigue life has been calculated to verify the improvement while using the double autofrettage process.

4.1 Definition of Double Autofrettage

As discussed, all of previous investigations were mainly focused on inducing beneficial residual stresses at the near bore area, neglecting the outer part. However, the results show that autofrettage and shrink-fit basically induce harmful tensile residual stress at the outside layer of the cylinder, which may affect the fatigue life and carrying load capacity of the cylinder.

In double autofrettage, the process starts by performing autofrettage pressure on the outer surface of the cylinder, which causes a partial plastic deformation of the inner part of the cylinder. Thus, after unloading this pressure, the inner part now has tensile residual stress and the outer part has compressive residual stress, as shown in Figure 4.1. After the first autofrettage process, a second autofrettage pressure applies at the inner surface of the

cylinder that causes another partial plastic deformation of the inner part of the cylinder, and, after unloading, the inner part of the cylinder now has a higher compressive residual stress and the outer part has a lower tensile residual stress, as shown in Figure 4.2, compared with the case of performing a single autofrettage process on the inner surface only.

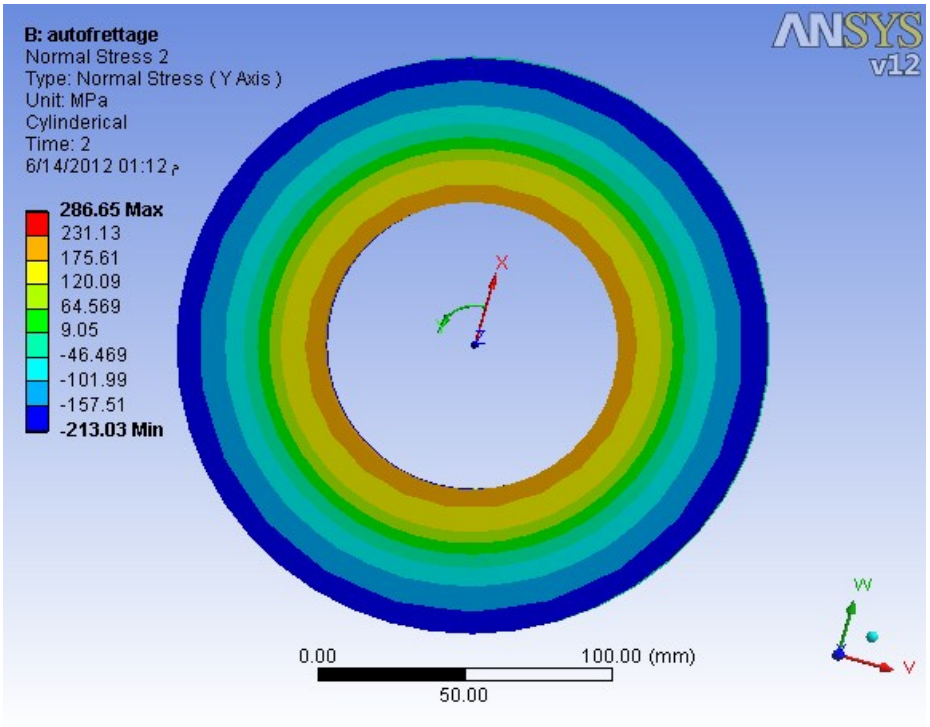

Figure 4.1: Residual stress after the outer surface autofrettage process.

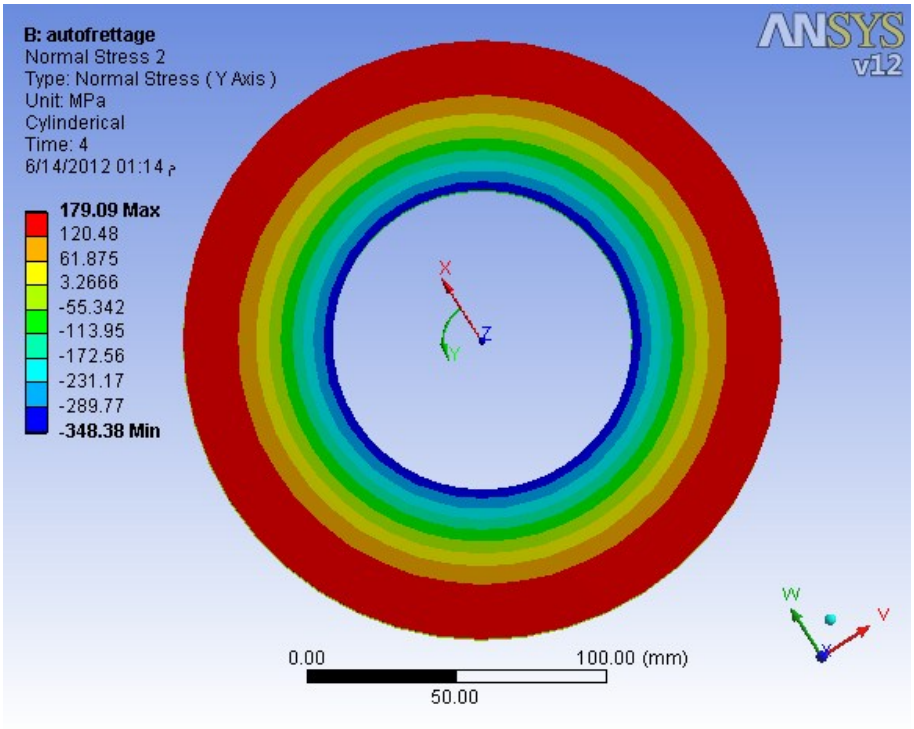

Figure 4.2: Total residual stress after the outer surface followed by the inner surface autofrettage processes.

4.2 Comparison between the Double and Standard Autofrettage Processes in Mono-Block Thick-Walled Cylinders

For the same cylinder used in section 3.4, the residual stress has been evaluated using the finite element model after performing a double autofrettage process on the cylinder and then compared with that of the conventional inner autofrettage process (single autofrettage). Figure 4.3 demonstrates the developed residual hoop stress distribution through the thickness of the compound cylinder subjected to the proposed double autofrettage process compared with that of conventional autofrettaged cylinder, which experiences the same inner autofrettage pressure. Figure 4.4 shows the same compassion

for working hoop stress distribution when the compound cylinder is subjected to internal static pressure of 250 MPa.

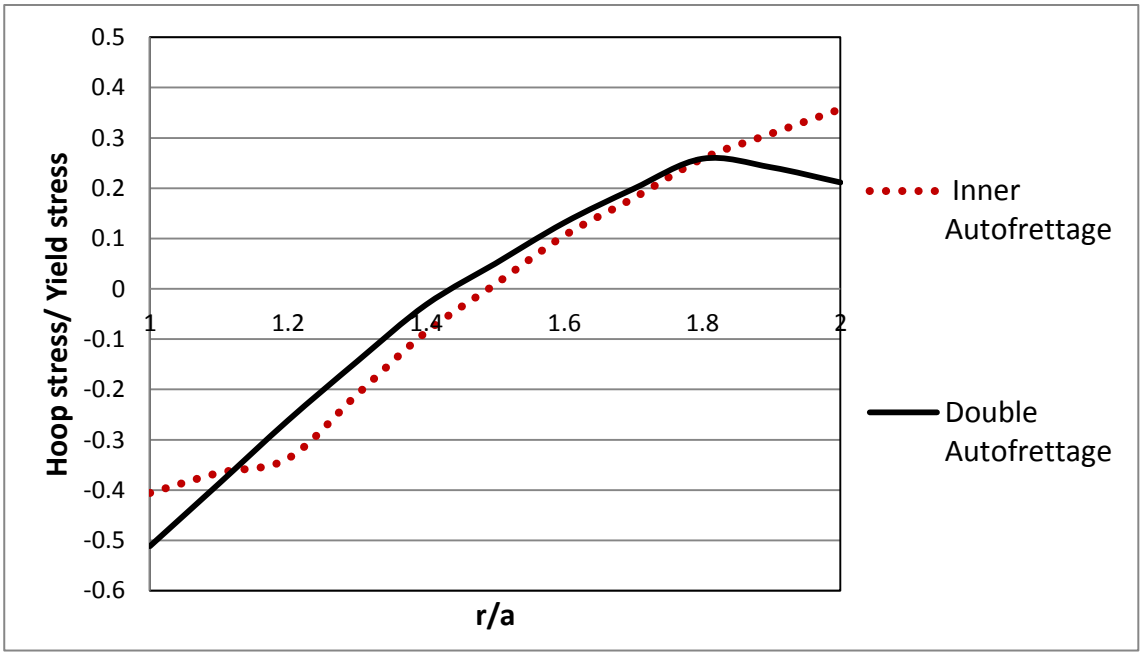

Figure 4.3: Residual hoop stresses for single and doubled autofrettage.

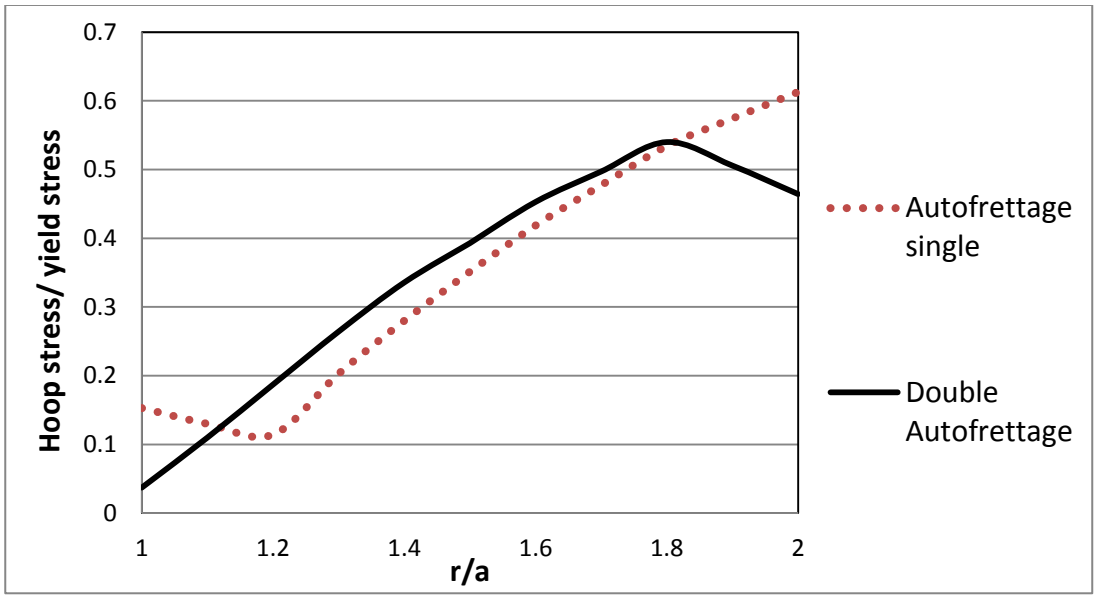

Figure 4.4: Hoop stresses for conventional and doubled autofrettage processes due to 250 MPa internal static pressure.

The results shown in Figures 4.3 and 4.4 are very promising and clearly demonstrate that the double autofrettage at the inner and outer surfaces will not only provide more compressive residual stresses at the near bore area, but also decrease the detrimental effects of the tensile residual stresses at the area close to the outer surface.

4.3 New Combinations of Compound Cylinders

Using the proposed double autofrettage process, new combinations of autofrettaged and shrink-fitted compound cylinders have also been proposed. These new combinations can be summarized as:

Combination 4: Double autofrettage of the inner layer and conventional autofrettage of the outer layer followed by shrink-fitting the outer layer on the inner layer.

Combination 5: Double autofrettage of the inner layer followed by shrink-fitting the virgin (non-autofrettaged) outer layer.

Combination 6: Shrink-fit of two layers followed by double autofrettage of the assembly.

Combination 7: Double autofrettage of each layer individually then shrink-fit them together.

For the sake of clarity, the sketch of these combinations has been shown in Figures 4.5-4.8. It should be noted that all combinations have the same inner, outer and interference radii after the autofrettage and shrink-fit processes and the same interference pressure as well.

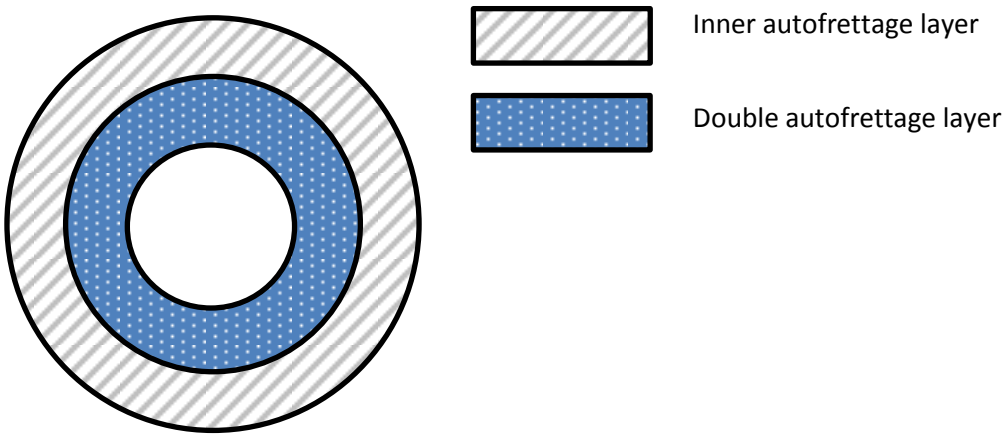

Figure 4.5: Shrink-fitting the conventional autofrettaged outer layer on the double autofrettaged inner layer (combination 4).

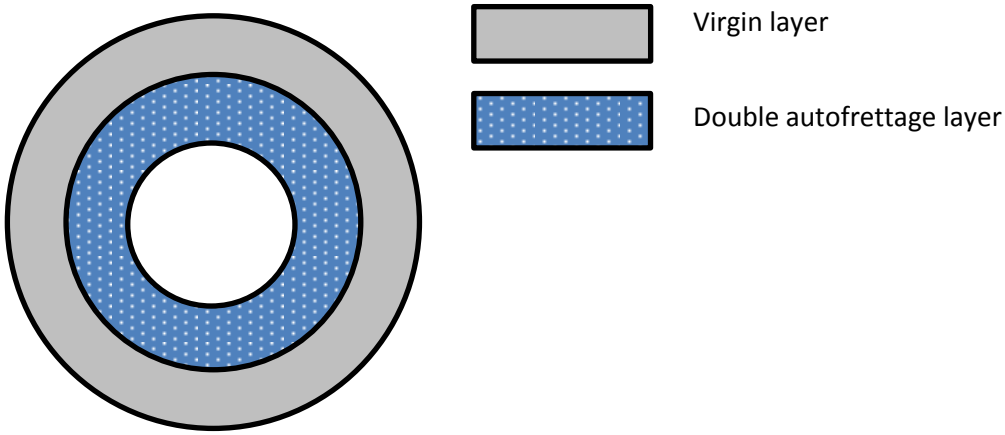

Figure 4.6: Shrink-fitting the virgin outer layer on the double autofrettaged inner layer (Combination 5).

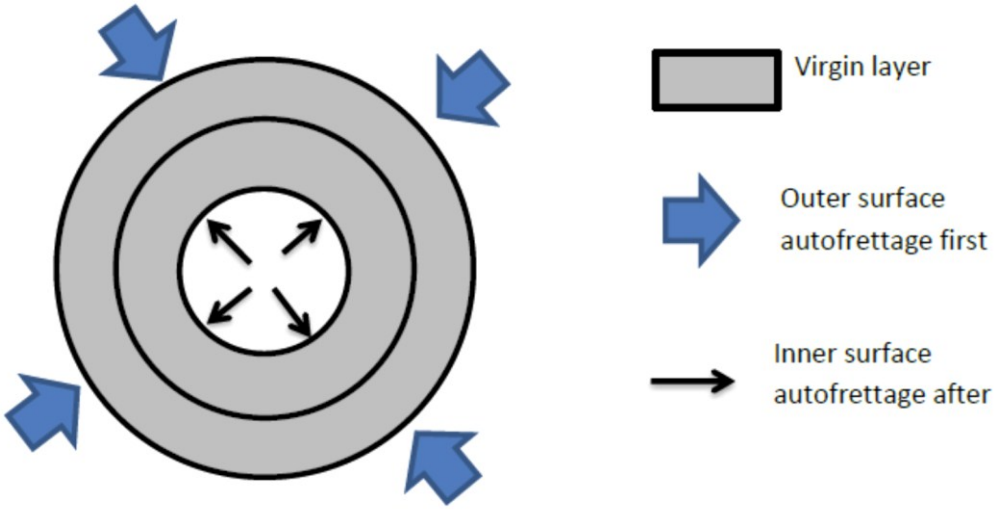

Figure 4.7: Shrink-fitting of two virgin layers followed by double autofrettaged of the assembly (Combination 6).

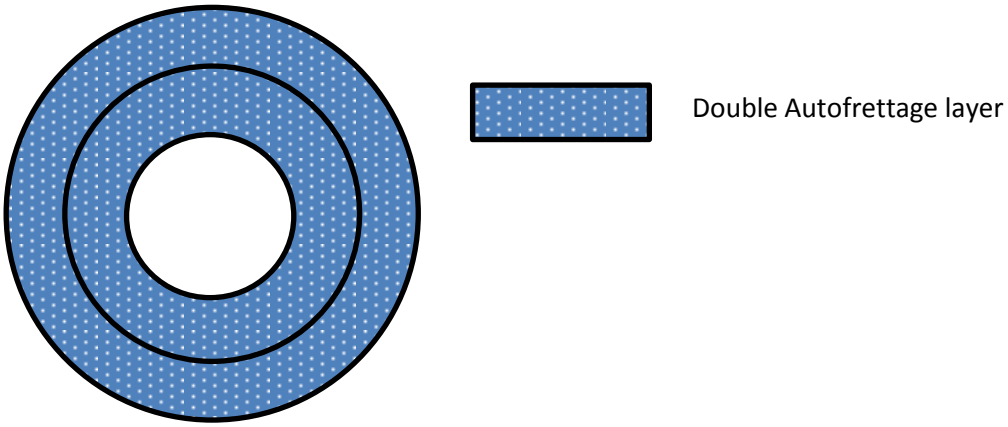

Figure 4.8: Shrink-fitting the two double autofrettaged layers (Combination 7).

4.3.1 Residual stress distribution in the proposed combinations

Figure 4.9 shows the normalized residual hoop stress distribution through the thickness for the four new combinations of the compound cylinder addressed in previous section using the finite element analysis. The residual stress for the equivalent Double Autofrettaged Mono-Block Cylinder (DAMBC) has also been provided for the sake of comparison. It is noted that the material and geometrical parameters are the same as those used in Section 3.4.

Examination of Figure 4.9 reveals that the new combinations increase the compressive residual stresses considerably, especially at the inner bore area (working area). It has been observed that combinations 4 and 5 have the same trend for residual compressive stress distribution through the thickness of the inner layer; however, through the thickness of the outer layer, residual tensile stress distribution differs and maximum tensile stress for combination 4 (yellow line) is lower than that of combination 5. It is also interesting to note that combination 7 (black line) has a desirable trend in the outer layer where the tensile residual stress at the area near to interface is lower than other combinations. Nevertheless, combination 6 (blue line) generates the best compressive residual stresses among combinations 4-7; however it also generates the highest value of the harmful tensile residual stress.

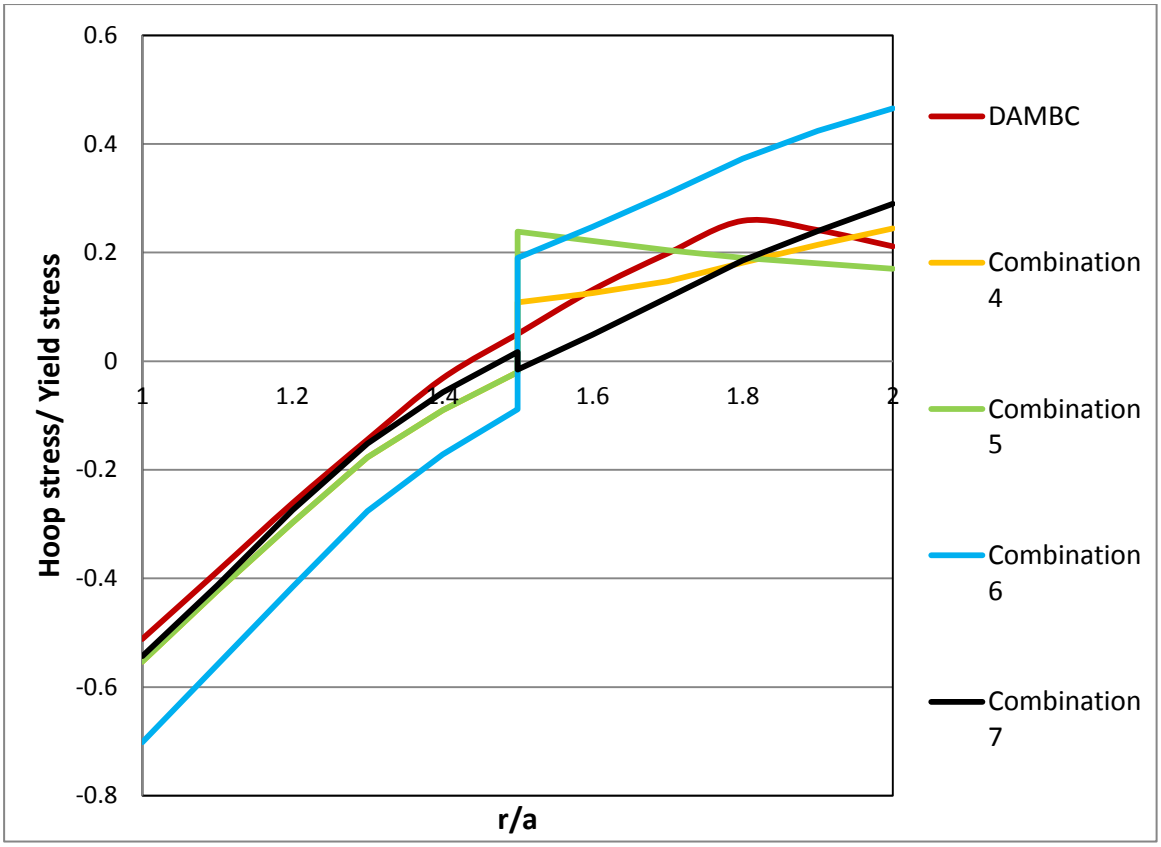

Figure 4.9: Residual stress distribution for the new combinations of compound cylinders using the double autofrettage process.

Moreover, the residual stress distribution in the compound cylinders subjected to the proposed combinations 4-7 using double autofrettage and shrink-fit processes have also been compared with those in the compound cylinders subjected to combinations 1-3 (based on conventional autofrettage and shrink-fit processes) investigated in Chapter 2 as shown in Figure 4.10.

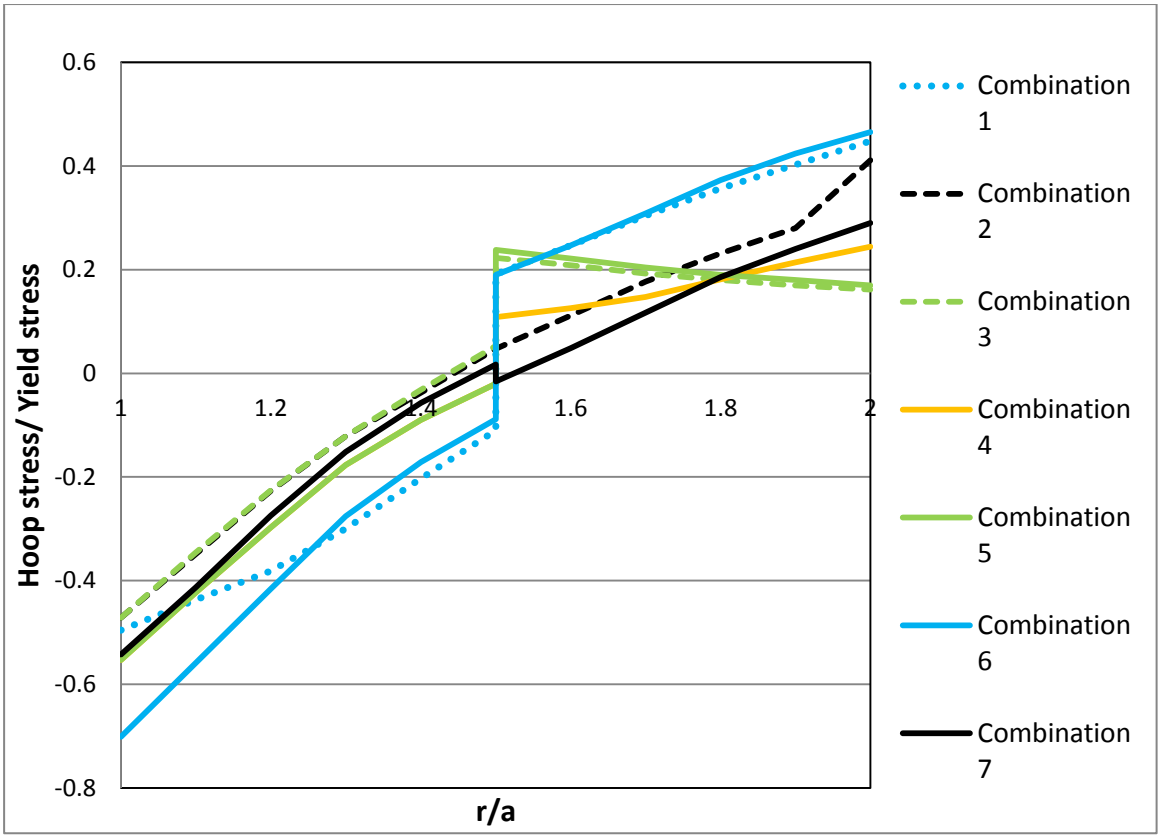

Figure 4.10: Residual stress for the new double autofrettage combinations (combinations 4-7) compared with that of standard autofrettage combinations (combinations 1-3) of compound cylinders.

Combinations 1 and 6 (dotted and continuous blue lines) which involves shrink-fitting of two virgin (non-autofrettaged) layers followed by conventional autofrettage and proposed double autofrettage processes, respectively can be fairly compared. It is noted that combination 6 because of double autofrettage process can significantly enhance the residual stresses at the near bore area without inducing more harmful tensile residual stress at the outer part of the cylinder. Also combinations 3 and 5 (dashed and continuous green lines) which involves shrink-fitting the outer virgin layer on the conventional autofrettaged inner layer and double autofrettaged inner layer, respectively may be

compared together. It is again noted that the double autofrettage process in Combination 5 can improve the residual compressive stresses at the near bore area while inducing less maximum tensile residual along the thickness of outer layer. In similar, combinations 2 and 7 (dashed and continuous black lines) involving shrink-fitting of two conventional autofrettaged and double autofrettaged layers, respectively are compared. As it can be seen, tensile residual stress through the whole thickness of outer layer in combination 7 is considerably lower than that in combination 2 while compressive residual stress distribution in the lower layer is nearly the same.

Combination 4 (yellow line) which involves the shrink-fitting of conventional autofrettaged outer layer on the double autofrettaged inner layer provides nearly similar compressive residual stress distribution compared with combinations 3 and 5. However it provides better tensile residual stress distribution in good portion of the outer layer thickness.

4.3.2 Effect of induced residual stress on working hoop stress

To investigate the effect of the induced residual stresses due to the proposed new combinations on the compound cylinder response, the working hoop stress distributions in the compound cylinders under inner static pressure of 250 MPa have been evaluated and then compared with equivalent mono-block cylinder (MBC) and equivalent double autofrettaged mono-block cylinder (DAMBC), as shown in Figure 4.11.

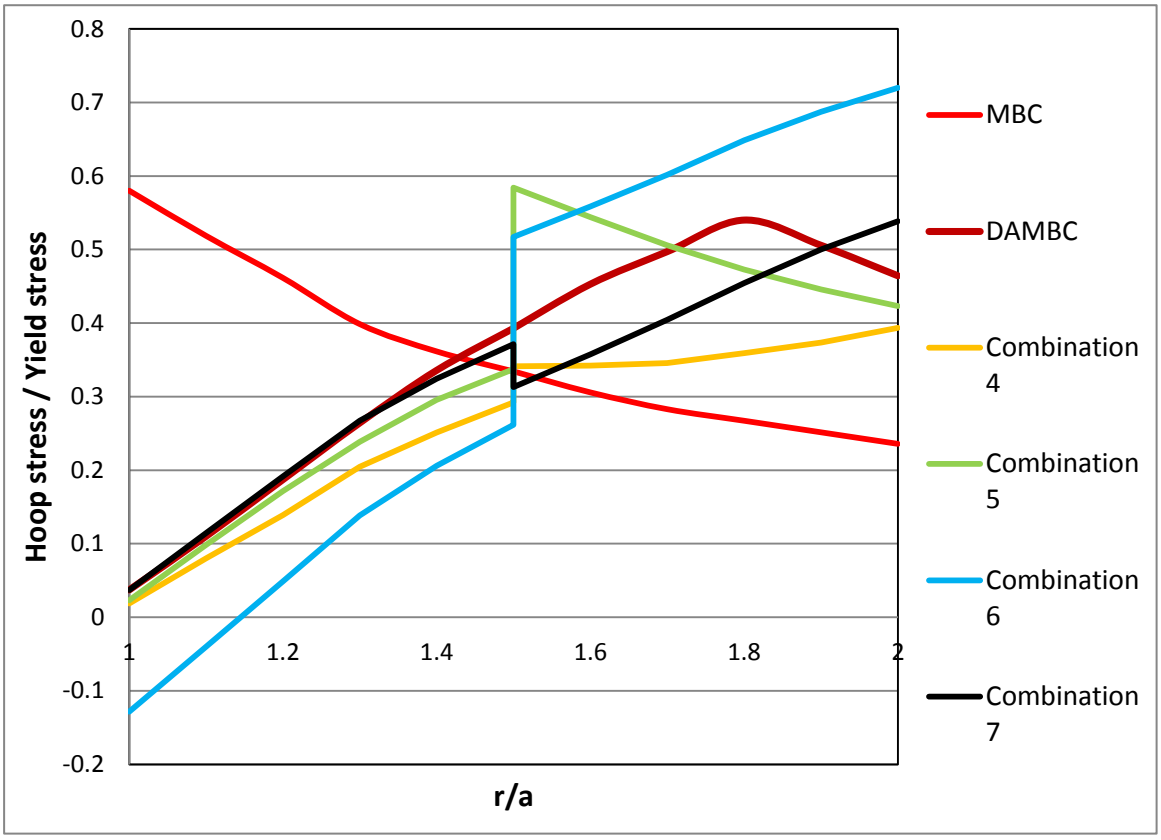

Figure 4.11: Hoop stress distribution in compound cylinder subjected to new combinations 4-7 involving double autofrettage process under static pressure of 250 MPa.

It is apparent from Figure 4.11 that combination 4 has the smallest value of maximum hoop stress along the whole thickness of the compound cylinder. It should be noted that while combination 6 generates the maximum magnitude of compressive hoop stress, it develops the maximum tensile hoop stress along the whole wall thickness.

To better compare the effect of different combinations based on double autofrettage process, Table 4.1 provides the percentage reduction of the hoop stress at the inner surface of the compound cylinders subjected to proposed combinations 4-7 with respect

to the hoop stress in the equivalent mono-block cylinder under inner static pressure load of 250 MPa.

Table 4. 1: Percentage reduction of hoop stresses at the inner surface of compound cylinders with respect to mono-block cylinder for static pressure of 250 MPa.

Combination	DAMBC	Combination 4	Combination 5	Combination 6	Combination 7
reduction %	93 %	96%	96%	122 %	93 %

From Table 4.1, one can observe that the new combinations involving the double autofrettage process can significantly reduce the hoop stress at the near bore area (working area) of a cylinder when subjected to inner static pressure, compared with that for equivalent mono-block cylinder. It has also been realized that the combination of shrink-fitting two layers followed by double autofrettage of the assembly (combination 6) can provide the maximum reduction for the hoop stress.

Table 4.2 also shows the percentage reduction of the maximum hoop stress in the compound cylinder subjected to new combinations 4-7 with respect to the maximum hoop stress in the equivalent mono-block cylinder under inner pressure load of 250 MPa. As it can be realized combinations 4 and 7 and the DAMBC provide good percentage reduction of the maximum hoop stresses along the whole thickness of the cylinder. On the contrary, combinations 5 and 6 provide an increase in the maximum hoop stress with respect to that of mono-block cylinder.

Table 4.2: Percentage reduction of the maximum hoop stresses in compound cylinders with respect to the mono-block cylinder under inner static pressure of 250 MPa

Combination	DAMBC	Combination 4	Combination 5	Combination 6	Combination 7
reduction %	6.8 %	41 %	-0.06 %	- 24.1 %	8.6 %

It is interesting to note that percentage reduction compared with the mono-block cylinder is very high at the inner surface, while it is very low or even negative regarding the maximum value of the hoop stress along the whole thickness of the cylinder, which is considered as a limitation of increasing the cylinder pressure capacity.

4.3.3 Fatigue life of compound cylinders subjected to the proposed double autofrettage and shrink-fit processes

For better understanding of the effect of the residual stress due to proposed new combinations of compound cylinders, the fatigue life is evaluated assuming a semielliptical crack at the inner surface of each layer of the cylinder. Using the fatigue life criteria described in Section 3.5.1, the mechanical fatigue life (fatigue life due to cyclic pressure load) has been obtained for all new combinations (Combinations 4-7) and compared with that of conventional autofrettage combinations (Combinations 1-3), as provided in Table 4.3. It is noted that the material and geometrical parameters are the same as those used in Section 3.4. Also the inner, outer, interference radii and initial crack depth for each layer are the same for all combinations. Initial crack depth and static

cyclic pressure are the same as before in Section 3.5.2 and assumed to be 0.5 mm and 250 MPa, respectively.

Table 4. 3: Fatigue life of compound cylinders for all combinations at both inner and outer layers when subjected to inner cyclic pressure.

Combination	Fatigue life (cycles)	
	Inner layer	Outer layer
1	6.4×10^4	2.3×10^4
2	1.02×10^5	1.4×10^4
3	2.6×10^4	7.7×10^3
4	1.5×10^5	7.2×10^3
5	1.3×10^5	2.4×10^3
6	8.7×10^5	3.25×10^3
7	1.1×10^5	1.6×10^4

The results in Table 4.3 can be clearly compared using bar chart shown in Figure 4.12. Examination of Table 4.3 and Figure 4.12 reveals that the highest fatigue life time for the inner layer occurs for the sixth combination while the highest fatigue life time for the outer layer occurs for the first combination. Moreover, the seventh combination provides a high fatigue life time in both layers at the same time compared with the other combinations. These results indicate that there is a need to optimize these combinations to reach the optimum configuration for each combination to enhance the residual stress at the near bore area while avoiding the increase of the tensile residual stress at the outer part of the cylinder. The optimization problem will be discussed in detail in the next chapter.

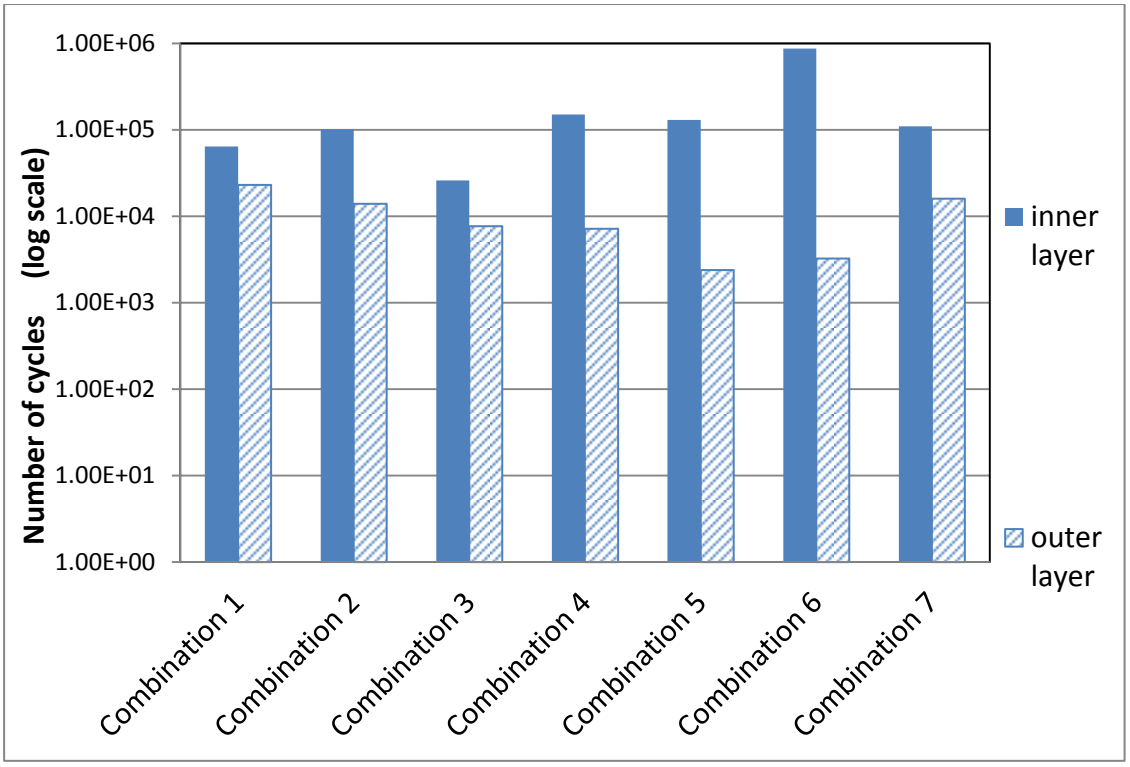

Figure 4.12: Fatigue life of inner and outer layers of the compound cylinder subjected to different combinations.

It should be noted that as in section 3.5, the von-Mises stress developed in compound cylinders under working pressure of 250 Mpa have been evaluated (please see Appendix A), in order to assure that re-yielding does not occur and compound cylinders subjected to new combinations 4-7 behave elastically.

4.4 Summary

This chapter addresses the new design philosophy of using the autofrettage process named as the double autofrettage process, in which an external surface autofrettage process is performed prior to the conventional inner surface autofrettage process. This

process can improve not only the compressive residual hoop stress at the near bore area of the cylinder, but also can decrease the detrimental residual tensile stress at the outer part of the cylinder.

The proposed double autofrettage process, combined with the conventional autofrettage and shrink-fit processes, can provide new combinations of the autofrettaged and shrink-fitted compound cylinders. The residual stresses developed due these new combinations have been calculated and then compared with those due to the shrink-fit and conventional autofrettage combinations. It is found that these new combinations could enhance the residual hoop stress over the whole thickness of the cylinder wall.

Under applied static pressure, the hoop stress at the near bore area of the compound cylinder subjected to the double autofrettage and shrink fit combinations is significantly lower than that of equivalent mono-block cylinder. Regarding mechanical fatigue life, the results indicate that the combination of shrink-fitting of two virgin (non-autofrettaged) layers followed by double autofrettage of the assembly has the highest fatigue life only at the inner layer of the cylinder, while the combination of double autofrettage for each layer individually followed by shrink-fitting them together can provide a high fatigue life in both layers.

CHAPTER 5

DESIGN OPTIMIZATION OF COMPOUND CYLINDERS

In this chapter, a design optimization methodology has been proposed to identify the optimal configuration of a two-layer cylinder subjected to the different prementioned combinations of shrink-fit, single autofrettage and double autofrettage processes. The objective is to find the optimal thickness of each layer, the autofrettage pressures and diametral interference for each shrink-fit and autofrettage combinations in order to increase the fatigue life of the compound cylinder by maximizing the beneficial and minimizing the detrimental residual stresses induced by these processes. Using the finite element model developed in Chapter 2, the hoop stress profile through the thickness of the cylinder has been accurately evaluated. Design optimization based on a full finite element model is computationally very expensive and may not render accurate optimum results due to the noisy nature of the finite element response. Considering this here, the design of experiment (DOE) and response surface method (RSM) have been utilized to develop smooth response functions which are explicitly related to selected design variables. These functions can then be effectively used in the design optimization formulation instead of the high fidelity finite element model. The DOE has been basically used to identify optimal location of assigned design variables (design points) in the given

design space. The responses (maximum magnitude of compressive and tensile residual stresses) at theses design points will be evaluated using the finite element model. Using DOE information, RSM has been then utilized to develop smooth response functions which explicitly relate the design variables to the relative responses. Finally, the developed objective functions have been utilized in design optimization problems to identify the optimal configuration of shrink-fitted and autofrettaged compound cylinders. Optimization is based on combined Genetic Algorithm (GA) and Sequential Quadratic Programming (SQP) technique. First GA which is a popular stochastic based global optimizer has been employed to find the near global optimum solution. Then, the optimal results obtained from GA have been transferred as initial values into the SQP technique which is a powerful gradient based local optimizer to find the accurate global optimum solution. The residual stress distributions and the mechanical fatigue life based on the ASME code for high pressure vessels have then been calculated and compared for optimal configurations.

5.1 Design Optimization Formulation

In the optimization problem, objectives are identified as the maximization of the magnitude of beneficial compressive residual hoop stress at the bore area, minimization of the maximum detrimental tensile residual hoop stress and simultaneous maximization of the compressive residual stress at the bore area and minimization of the maximum tensile residual hoop stress.

The design variables have been considered to be the thickness of each layer, autofrettage pressures at the inner surfaces, autofrettage pressures at the outer surfaces (if any), and the diametral interference for shrink-fitting. Also, constraints in the form of upper and lower bounds have been assigned for each design variable.

5.1.1 Design Variables for each Autofrettage and Shrink-fit Combinations

Here, the design variables associated with seven combinations discussed in chapters 2 and 4 are addressed in Table 5.1. The complete design variables are the thickness of the inner layer t_1, thickness of the outer layer t_2, the autofrettage pressure at the inner surface of the inner layer P_{1in}, the autofrettage pressure at the outer surface of the inner layer P_{1out}, the autofrettage pressure at the inner surface of the outer layer P_{2in}, the autofrettage pressure at the outer surface of the outer layer P_{2out}, and the diametral interference for shrink-fitting δ. Thus, for instance, according to Table 1, for Combinations 1 and 3, the identified design variables are t_1, t_2, δ, P_{1in}, while for Combination 7 all complete design variables t_1, t_2, δ, P_{1in}, P_{1out}, P_{2in} P_{2out} are considered.

Table 5. 1: Design variables for different shrink-fitting and autofrettage combinations.

DVs / Combinations	t_1,	t_2	δ	P_{1in}	P_{1out}	P_{2in}	P_{2out}
1	√	√	√	√	-	-	-
2	√	√	√	√	-	√	-
3	√	√	√	√	-	-	-
4	√	√	√	√	√	√	-
5	√	√	√	√	√	-	-
6	√	√	√	√	-	-	√
7	√	√	√	√	√	√	√

5.1.2 Constraints of each Autofrettage and Shrink-fit Combination

As mentioned before, here, side constraints in the form of upper and the lower boundaries on design variables have been considered. Table 5.2 provides the lower and upper limits for design variables in each combination addressed in Table 5.1. It is noted that, in Table 5.2, the first number is the lower bound and the second number is the upper bound.

Table 5. 2: Boundaries of design variables for each combination.

DVs / Combination	t_1 ,mm	t_2, mm	δ, mm	P_{1in}, MPa	P_{1out}, MPa	P_{2in}, MPa	P_{2out}, MPa
1	30-55	30-55	0.18-0.22	630-700	-	-	-
2	30-55	30-55	0.18-0.22	468-572	-	252-308	-
3	30-55	30-55	0.18-0.22	468-572	-	-	-
4	30-55	30-55	0.18-0.22	225-275	468-572	252-308	-
5	30-55	30-55	0.18-0.22	225-275	468-572	-	-
6	30-55	30-55	0.18-0.22	500-600	-	-	660-808
7	30-55	30-55	0.18-0.22	225-275	468-572	225-275	468-572

5.1.3 Derivation of Objective Functions

The full finite element model has been effectively used to evaluate accurately the residual stress distribution through the thickness of the compound cylinder for each combination of autofrettage and shrink-fit processes. As mentioned before, the established objectives are: maximization of the magnitude of compressive residual stress at the bore area, minimization of the maximum tensile residual stress and simultaneous optimization of both. To formulate the design optimization problems, one may combine the full finite element model with optimization algorithms; however, this would be computationally

very expensive due to the iterative nature of the optimization problem in which, at each iteration, the objective functions may be evaluated (running the full finite element model) several times. Besides, the optimal results may not be accurate due to the possible noisy nature of the output response and also it may be difficult to establish the derivative of the objective functions required for higher order optimization algorithms.

Considering above, in this study design of experiment (DOE) and response surface method (RSM) combined with the developed finite element model are effectively used to derive the desired objective functions which will be explicitly related to the design variables for each combination of autofrettage and shrink-fit processes [68-69]. The DOE has been used to identify the best location of design variables (design points) to accurately map the given design space for each combination of autofrettage and shrink-fit processes. Once the DOE matrix has been established, the maximum values of the response magnitude (hoop stresses) have been calculated using the finite element model for each row (design point) in the DOE matrix. Then, RSM based on the fully quadratic response function has been used to relate the variations of hoop stresses with respect to different design variables for each combination. Finally, these response functions have been effectively utilized as objective functions in the design optimization problems.

In the following, brief discussion regarding DOE and RSM to derive DOE matrix and response are presented, respectively.

5.1.3.1 Design of Experiments (DOE)

Design of experiments is basically a technique to develop an experimentation strategy that maximizes learning using a minimum of resources. In many applications, the scientist is constrained by resources and time, to investigate the numerous factors that affect complex processes using trial and error methods. Instead, DOE is an influential tool that permits multiple input factors to be manipulated, determining their effect on a desired output (response) [70-71]. By manipulating multiple inputs at the same time, DOE can recognize important interactions that may be missed when experimenting with one factor at a time. All possible combinations (full factorial) or only a portion of the possible combinations (fractional factorial) can be investigated [72]. In full factorial design, the number of combinations of k design variables in which each design variable, can take a value from l values (level), is l^k combinations. The number of combinations increases exponentially with the number of design variables.

In fractional factorial design, a fraction of the full factorial design is considered. The number of combination is l^{k-p}, where p is a number that defines the size of the fraction. There are many methods used in fractional factorial design to minimize the number of combinations in the full factorial design such as Koshal Design, Factorial Design, Central Composite Design, Box- Behnken Design and D-Optimal Design. An excellent review of the different design types can be found in Myers et al. [73].

In this study, Box–Behnken design based on three-level full factorial technique [74, 75] has been used in which each factor is placed at one of three equally spaced values. This technique gives ($2k$ (k-1) $+C_o$) different combinations before removing the repeated points, in which k is the number of the design variables and C_o is the number of central

points, which is considered to be unity at this study. Here, using the statistical Matlab toolbox, the DOE matrix, which has the dimension of $[(2k\ (k\text{-}1)\ +C_o) \times k]$, has been established for each combination of autofrettage and shrink-fit processes. Then, using the full finite element model, the responses (maximum magnitude of compressive and tensile residual stresses) for each design point (row) in the DOE matrix have been evaluated. Thus, considering the output responses, the DOE matrix would have a dimension of $[(2k\ (k\text{-}1)\ +C_o) \times (k+2)]$. Table 5.3 provides the DOE matrix for the first combination, as described in Table 5.1. It is noted that for all combinations the inner radius of compound cylinder is kept constant at 100 mm.

Table 5.3: DOE Matrix for the first combination.

Number of experiments	t_1	t_2	δ	P_{1in}	Max. residual compressive stress MPa	Max. residual tensile stress MPa
1	30	30	0.2	700	-166	182
2	30	55	0.2	700	-280	269
3	55	30	0.2	700	-252	315
4	55	55	0.2	700	-449	291
5	42.5	42.5	0.22	630	0.34	300
6	42.5	42.5	0.22	770	-250	277
7	42.5	42.5	0.18	630	-373	297
8	42.5	42.5	0.18	770	-243	274
9	30	42.5	0.2	630	-266	260
10	30	42.5	0.2	770	-203	205
11	55	42.5	0.2	630	-446	311
12	55	42.5	0.2	770	-297	319
13	42.5	30	0.22	700	-224	276
14	42.5	30	0.18	700	-216	262
15	42.5	55	0.22	700	-379	303
16	42.5	55	0.18	700	0.31	300
17	30	42.5	0.22	700	-239	244
18	30	42.5	0.18	700	-229	235
19	55	42.5	0.22	700	-370	328
20	55	42.5	0.18	700	-363	324
21	42.5	30	0.2	630	-251	290
22	42.5	30	0.2	770	-175	240
23	42.5	55	0.2	630	-468	265
24	42.5	55	0.2	770	-270	297
25	42.5	42.5	0.2	700	-267	292

Similar tables have also been established for all other combinations and provided in the Appendix B.

Figures 5.1 and 5.2 show the variation of maximum compressive and tensile residual stresses versus the design points identified by DOE, respectively.

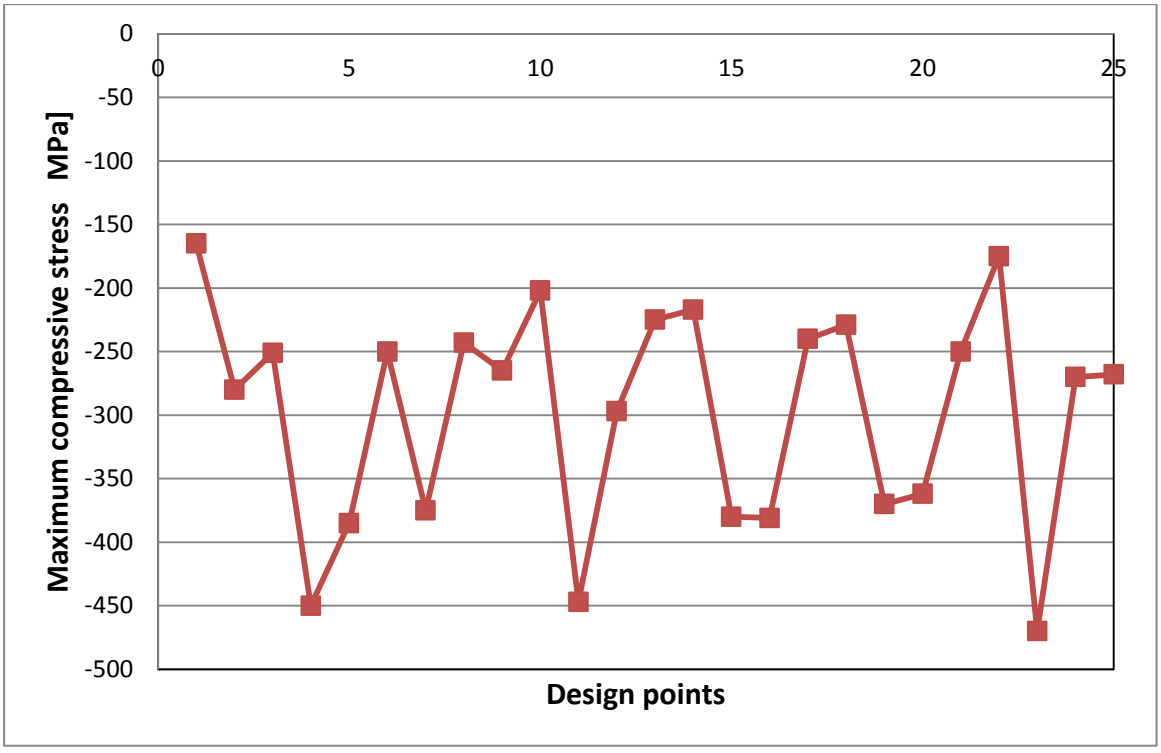

Figure 5.1: Variation of magnitude of maximum compressive residual stresses versus the design points obtained by DOE for the first combination.

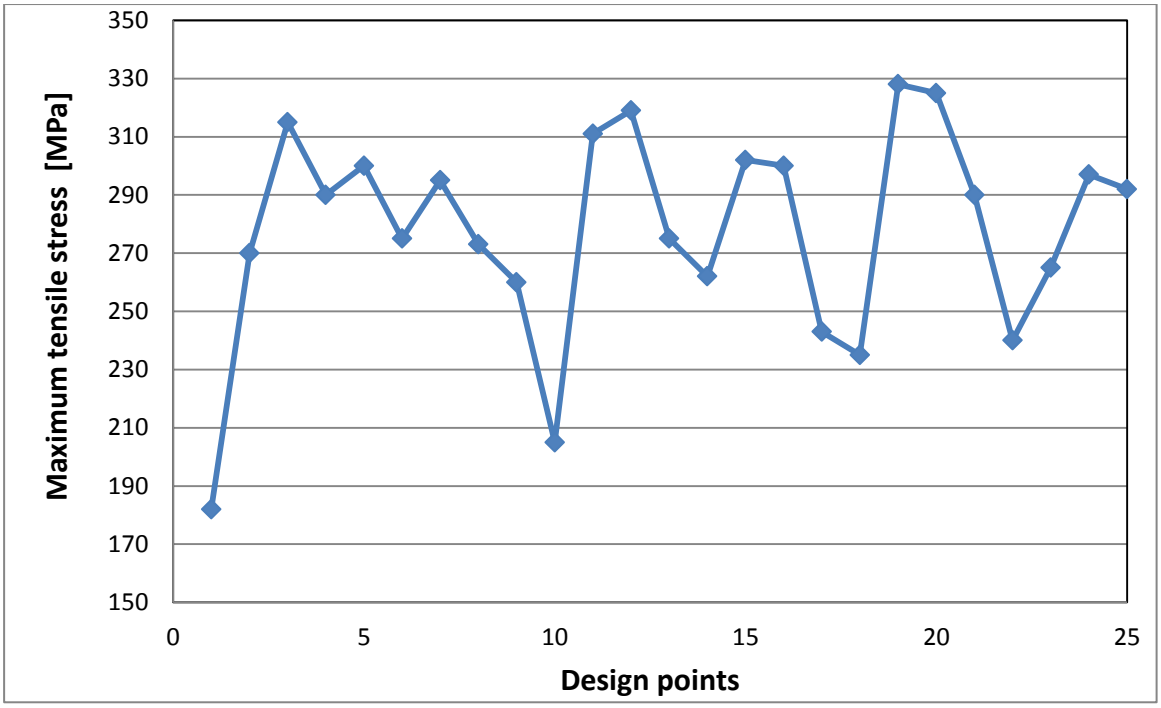

Figure 5.2: Variation of maximum tensile residual stresses versus the design points obtained by DOE for the first combination.

From Figures 5.1 and 5.2, one can realize that the responses (maximum compressive or maximum tensile residual stresses) vary significantly with respect to design points scattered in the design space. Similar behaviors have also been observed for all other combinations.

5.1.3.2 Response Surface Method (RMS)

The main objective of the RSM is to examine the relationship between the response and design variables [76, 77]. This requires having a good fitting model that provides an appropriate representation of the response over the whole design space. Generally, the RSM depends on the nature of the fitted model, which can be obtained using regression

analysis to formulate a polynomial function. There are four different types of these fitting models: a linear model with only basic variables, a linear model with interaction, pure quadratic model which includes constant, linear and square terms, and a full quadratic model with interactions terms [78]. A full quadratic model has been employed here in order to accurately map the whole design space.

For the case of first combination, which has four design variables according to Table 5.1, the full quadratic response surface equation can be written as:

$$f = a_o + a_1 t_1 + a_2 t_2 + a_3 \delta + a_4 P_{1in} + a_5 t_1 t_2 + a_6 t_1 \delta + + a_7 t_1 P_{1in} + a_8 t_2 \delta + a_9 t_2 P_{1in} + a_{10} P_{1in} \delta + a_{11} t_1^2 + a_{12} t_2^2 + a_{13} \delta^2 + a_{14} P_{1in}^2 \quad (5.1)$$

It should be noted that the number of unknown coefficients, p, in the full quadratic response surface function can be related to the number of design variables, k, as:

$$p = 1 + k + \frac{1}{2}(1 + k)k \quad (5.2)$$

Thus, for the first combination with four design variables (k=4), we have p=15, unknown coefficients.

Similar quadratic response functions can be written for other combinations as well. The unknown model coefficient vector $\{a\}$ can be identified through regression analysis in order to minimize the error between the true response (obtained using the finite element model) and its approximation using the response surface method. In other words, for a given design vector of $\{x\}$ evaluated at design points generated by the DOE process with n number of experiments, one may write [79]:

$$\{y\} = [X]\{a\} + \{e\} \quad (5.3)$$

in which $\{\hat{y}\} = [X]\{a\}$ represents the approximate response vector, $\{y\}$ is the true response vector obtained by the finite element analysis and [*X*] is the *n* ×*p* design matrix. The problem is now to find the unknown coefficient vector $\{a\}$ that minimizes the error $\{e\}$. This can be easily achieved using the least square method. The least square function can be defined as the summation of the squared errors for all *n* design points generated by the DOE process as:

$$LS = \sum_{i=1}^{n} e_i^2 = \{e\}^T \{e\} = (\{y\} - [X]\{a\})^T (\{y\} - [X]\{a\}) \quad (5.4)$$

Now minimizing the least square function *LS* with respect to the unknown vector $\{a\}$ and equating the resultant to zero will yield:

$$\{a\} = ([X]^T [X])^{-1} [X]^T \{y\} \quad (5.5)$$

Using the above procedure the unknown model coefficient vector has been obtained for all combinations described before. Figures 5.3- 5.6 show the variation of response functions over design space for the first combination. In Figure 5.3, variation of maximum compressive residual stress with respect to outer and inner layer thicknesses has been shown (radial interference and inner surface autofrettage pressure are kept contact), while for Figure 5.4, its variation has been shown with respect to radial interference and inner surface autofrettage pressure (outer and inner layer thicknesses are kept constant). Similarly Figure 5.5 shows the variation of maximum tensile residual stress with respect to outer and inner layer thicknesses, while Figure 5.6 provides this variation with respect to radial interference and inner surface autofrettage pressure.

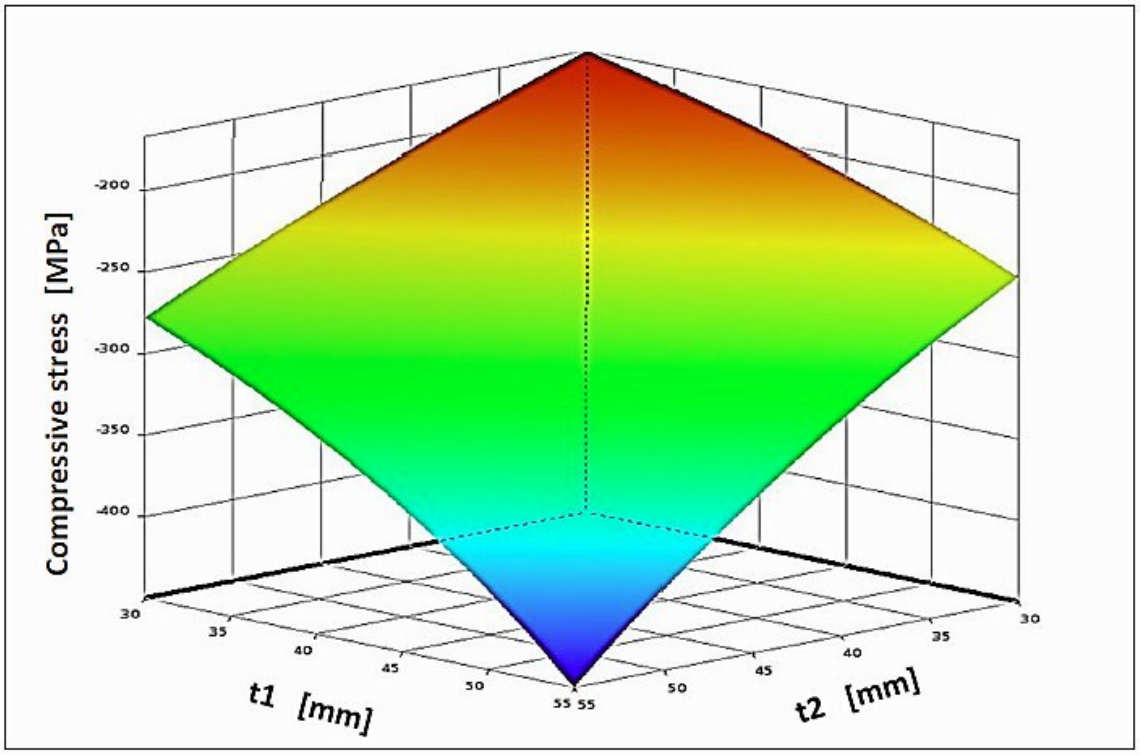

Figure 5.3: Maximum compressive residual stress variation with respect to the thickness of inner and outer layers for the first combination.

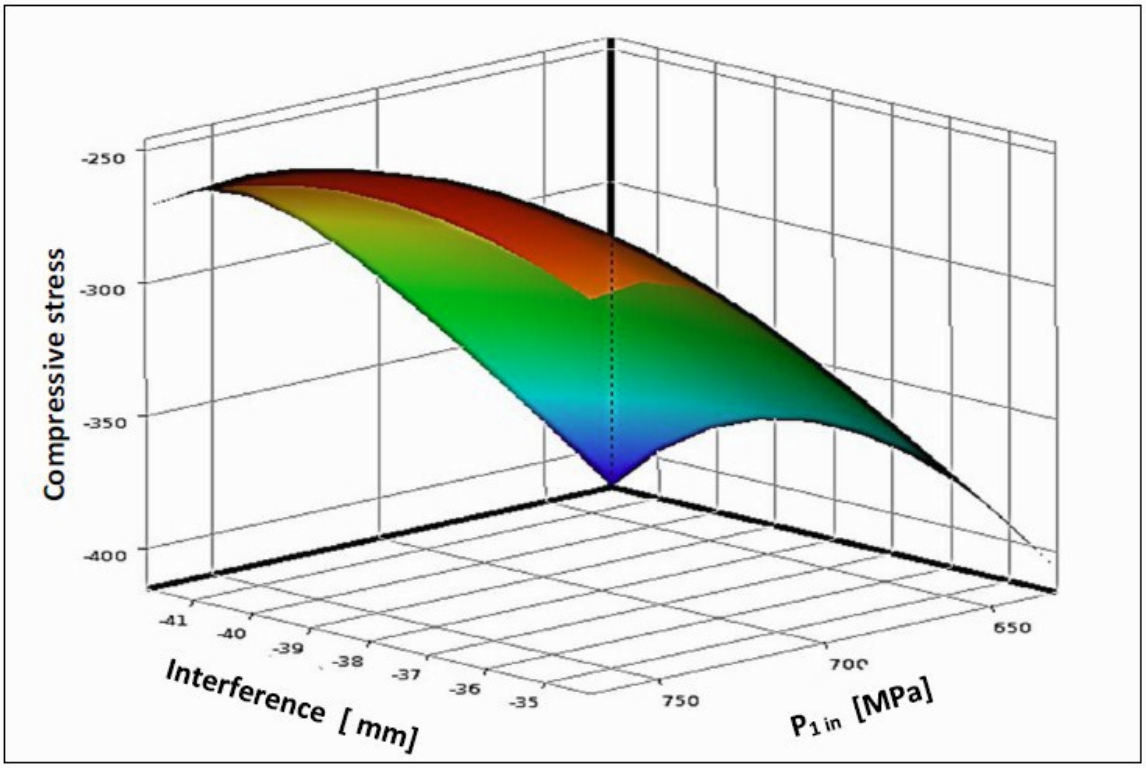

Figure 5.4: Maximum compressive residual stress variation with respect to the radial interference and the inner surface autofrettage pressure for the first combination.

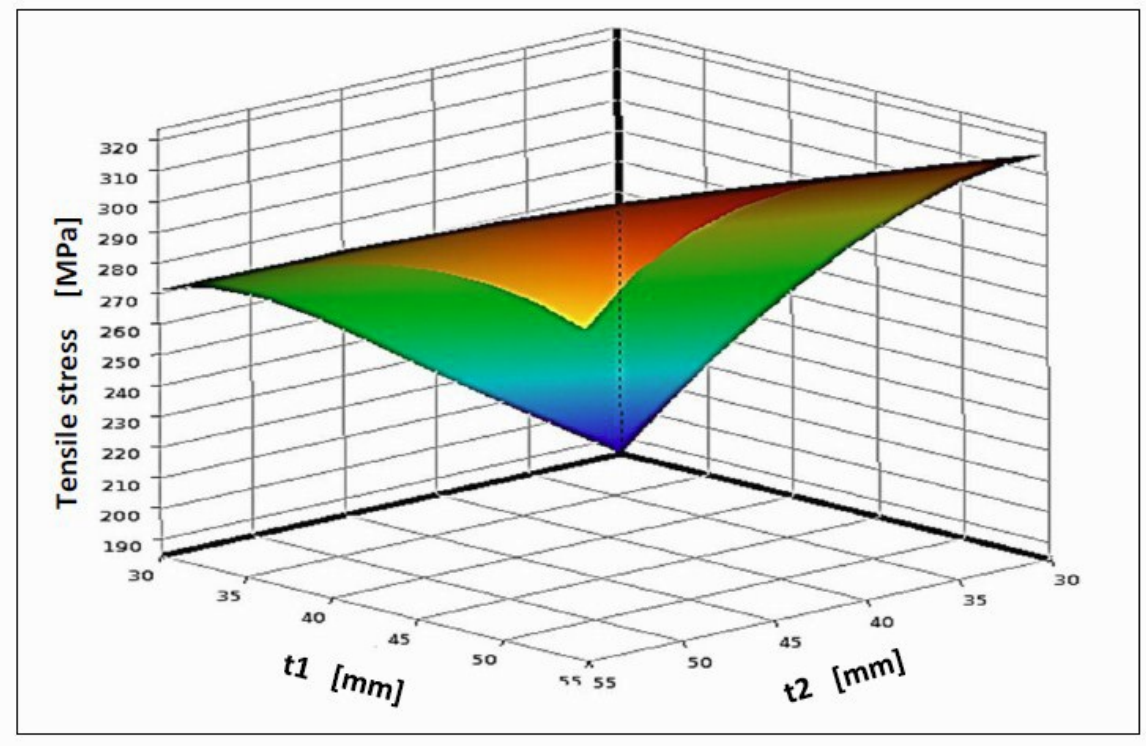

Figure 5.5: Maximum tensile residual stress variation with respect to the thickness of inner and outer layers for the first combination.

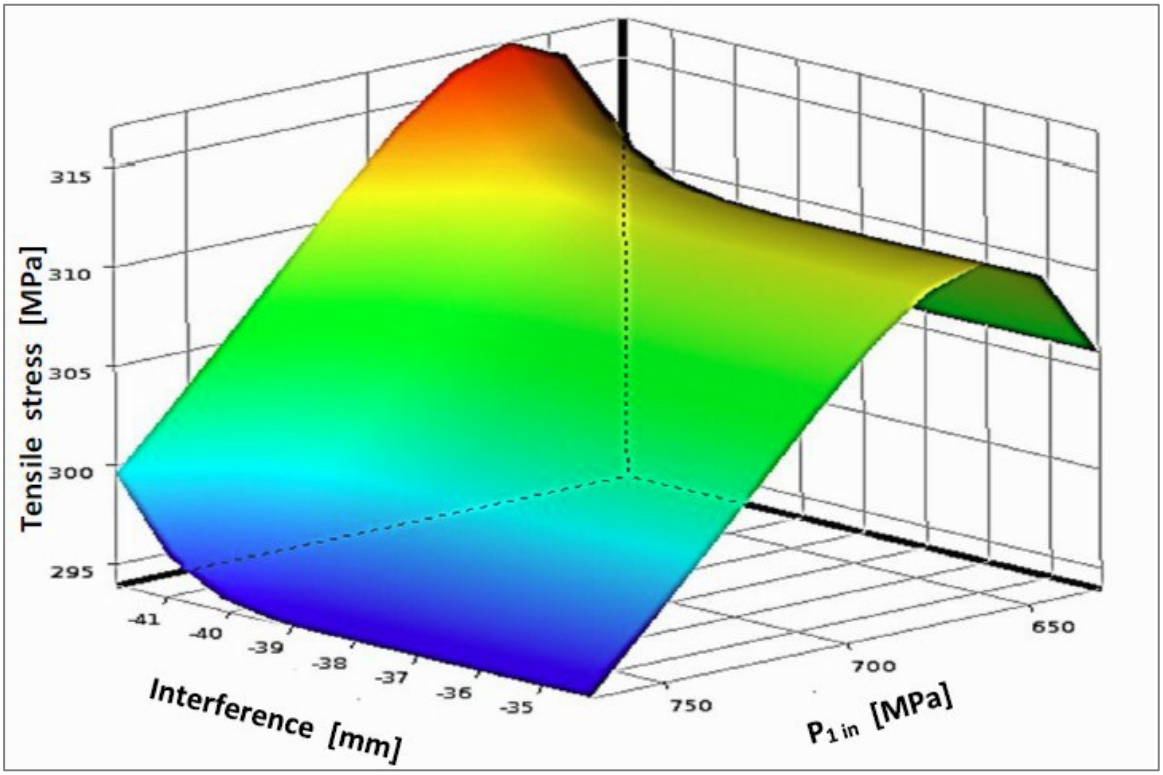

Figure 5.6: Maximum tensile residual stress variation with respect to the radial interference and the inner surface autofrettage pressure for the first combination.

The sensitivity of the output responses with respect to the change in design variables has also been investigated. For instance, Figure 5.7 shows the result for the first combination.

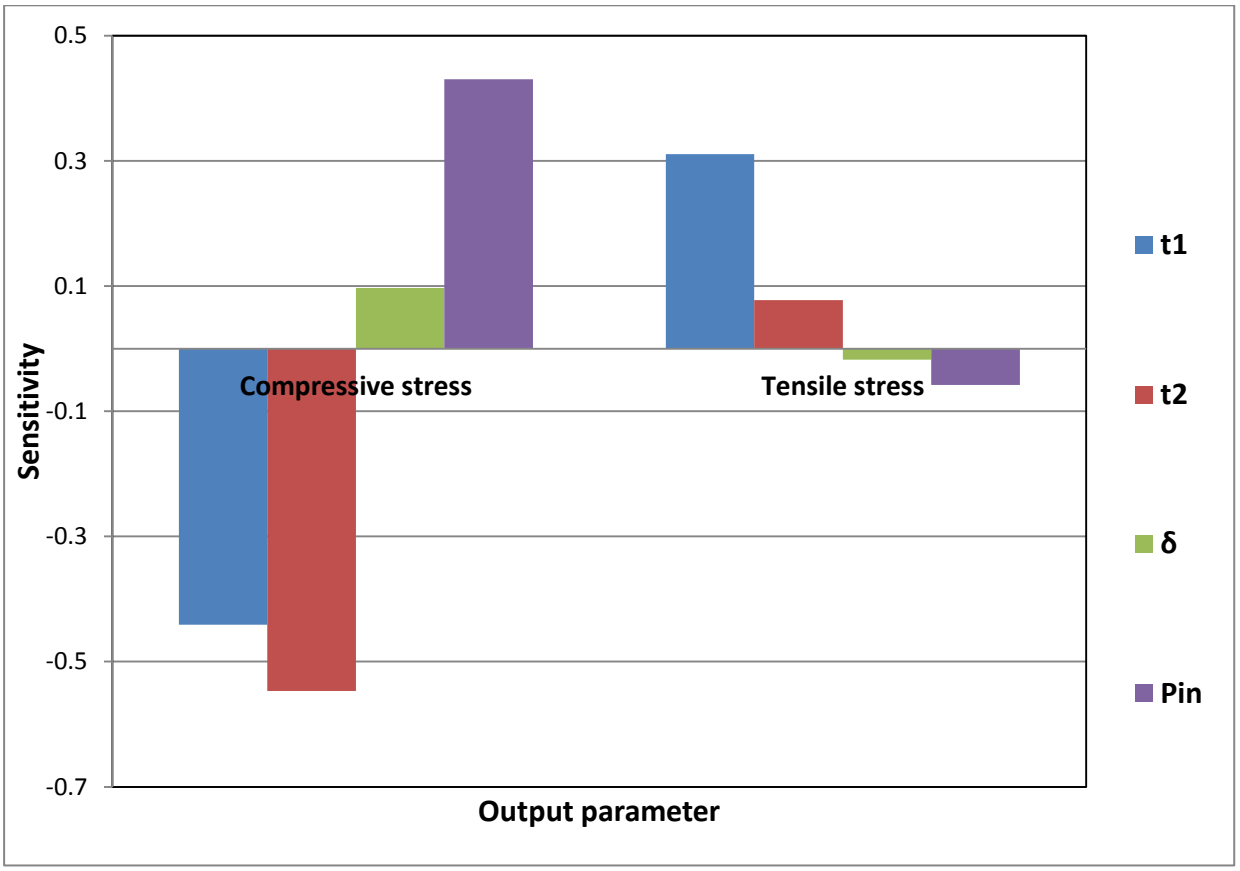

Figure 5.7: Local sensitivity of the objective functions for different design variables in the first combination.

Figure 5.7 reveals that maximum compressive and tensile residual stresses are very sensitive to local variation of thicknesses of layers while they are less sensitive to the radial interference.in the given range.

It should be again noted that, the previous steps regarding evaluation of the DOE matrix and generation of response surfaces have been repeated for six other combinations mentioned in Chapters 2 and 4.

5.1.3.2.1 Goodness of fitness of the response surfaces

To examine the accuracy of the derived response surfaces, Figures 5.8 and 5.9 compare the values of the compressive and tensile residual stresses, respectively, obtained from the finite element model (exact response) and the derived response surface functions at specified design points for the first combination. It is noted that for the first combination, 25 design points exist, as provided in Table 5.3.

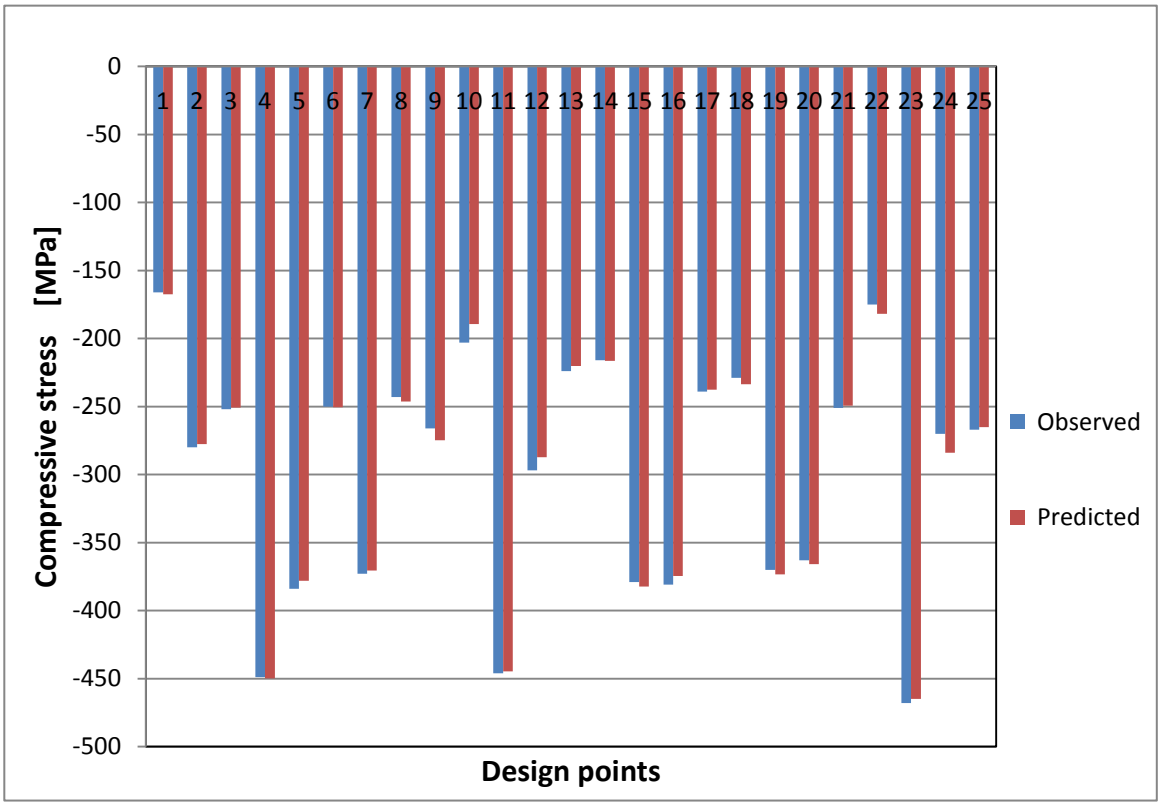

Figure 5.8: Comparison between the exact compressive residual stress and the predicted values from the response surface function at design points-Combination 1.

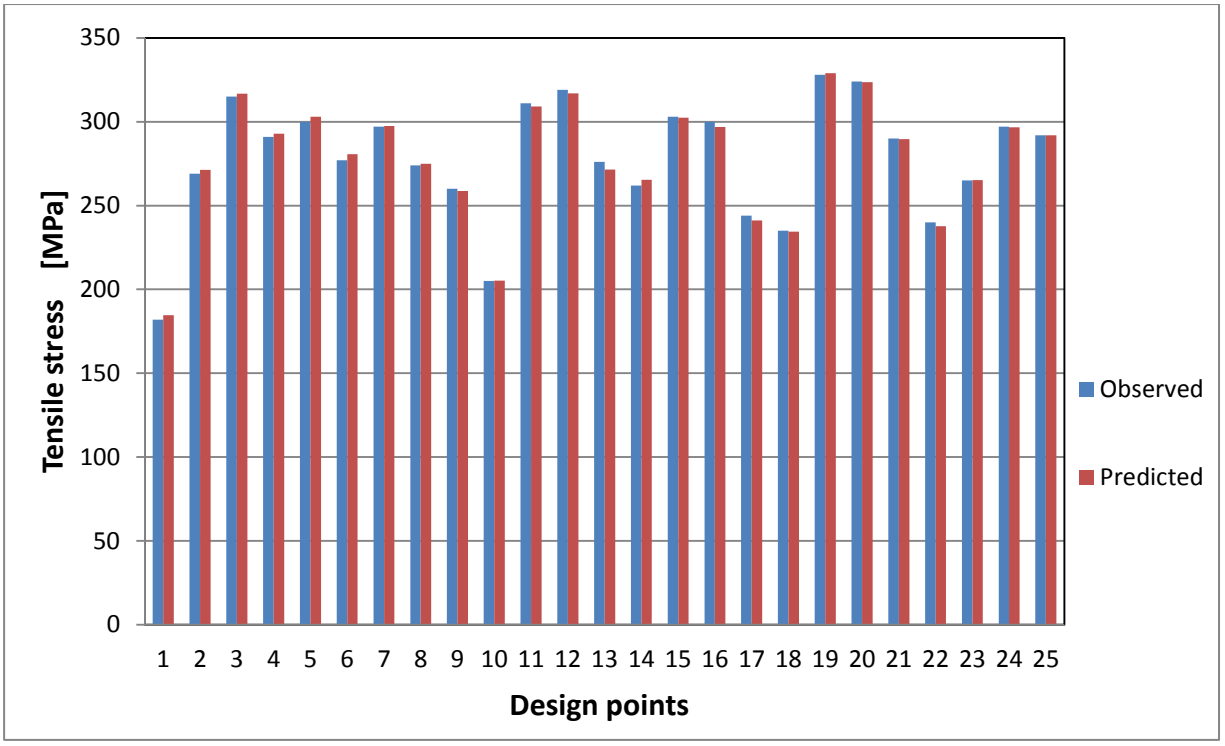

Figure 5.9: Comparison between the exact tensile stress and the predicted values from the response surface functions at design points-Combination 1.

Figures 5.9, 5.10 show very good agreement in all design points; however, the error and fitting accuracy along the whole surface still need to be determined.

It is important to verify the accuracy of the response function in given design space so that it can be used with confidence in the design optimization process. The following criteria are used to calculate the accuracy of fitting for the design points identified by DOE and 10% more random additional points between DOE design points [80]:

- Coefficient of Determination (R_2): The percent of the variation of the output parameter that can be explained by the response surface regression equation. If the response surface passes directly through each point, the coefficient of determination would be 1. This can be mathematically represented as:

$$R_2 = 1 - \frac{\sum_{i=1}^{n}(y_i - \hat{y}_i)^2}{\sum_{i=1}^{n}(y_i - \bar{y}_i)^2} \quad (5.6)$$

- Adjusted Coefficient of Determination (Adjusted R_2): The Adjusted Coefficient of Determination takes the sample size into consideration when computing the coefficient of determination. Usually, this is more reliable than the usual coefficient of determination when the number of samples is small (< 30). It can be mathematically represented as:

$$Adj\ R_2 = 1 - \frac{N-1}{N-P-1}\frac{\sum_{i=1}^{N}(y_i - \hat{y}_i)^2}{\sum_{i=1}^{N}(y_i - \bar{y}_i)^2} \quad (5.7)$$

where y_i is the exact output value at the i^{th} design point, $\hat{y}_i$ is the predicted output value at the i^{th} design point, $\bar{y}_i$ is the arithmetic mean of exact output values y_i, N is the number of design points, and p is the number of polynomial terms in the full quadratic equation of the response function.

Table 5.4 shows the goodness of fitness of the response surface of the first combination using above mentioned error criteria.

Table 5. 4: Error calculation for the response surface of the first shrink-fit and autofrettage combination

Name of criteria	Compressive stress	Tensile stress
R_2 (Best Value = 1)	0.995702012	0.996543517
$Adj\ R_2$ (Best Value = 1)	0.99426935	0.994074601

As it can be realized, the derived response surface functions can accurately predict the response (hoop stress). Thus, these functions can be effectively utilized as the objective

functions in the optimization problems. It should be noted that the same level of accuracy has also been observed for all other combinations.

5.2 Optimization Techniques

There are many features affecting the precision and successful closure of the optimization problem such as: optimization problem formulation, selection of the appropriate optimization techniques, and a full understanding of the system performance [81, 82]. Gradient-based and non-gradient based optimization algorithms have been used to address optimization problems. Among the gradient-based optimization algorithms, the Sequential Quadratic Programming (SQP) algorithm is a prevailing technique that can easily deal with nonlinear constrained optimization problems [83, 84]. The weaknesses of the gradient-based optimization algorithms are that they can be easily trapped in local optimum points without any mechanism to climb up. On the other hand, non-gradient random-based algorithms such as Genetic Algorithm (GA) [85] can approximately recognize the location of the global optimal point.

5.2.1 Optimization objectives

The developed approximate response surface functions can now be effectively used in the design optimization problems, which aim at finding optimum design variables to satisfy the following requirements:

(a): Maximizing the beneficial compressive residual hoop stress at the bore area (Max f_1 or Min $1/f_1$),

(b): Minimizing the maximum detrimental tensile residual hoop stress (Min f_2),

(c): Maximizing the compressive residual hoop stress at the bore and minimizing the maximum tensile residual hoop stress (max f_1 and min f_2).

It is noted that, for the Case (c), there are two conflicting objectives to be satisfied simultaneously. Considering equal weighting factors, here, both objectives have been combined to establish a single objective function in the form of f_3=0.5/ f_1+0.5 f_2. Thus, for case three above, one may write Min f_3.

In this work, both Genetic Algorithm (GA) and Sequential Quadratic Programming (SQP) optimization technique have been employed to accurately capture the optimal configurations for each combination of autofrettage and shrink-fit processes. The Genetic Algorithm is capable of capturing global optimal solutions approximately. The results from GA will be then used as initial values for the SQP optimization technique to accurately locate the true global optimal solutions. In the following brief discussions regarding the GA and SQP are presented.

5.2.2 Genetic Algorithm (GA)

GA is a stochastic optimization algorithm based on the mechanics of natural genetics and natural selection. In GA, design variables are coded into strings of binary bits. The length of binary string depends on the accuracy of the anticipated solution [86, 87]. An initial population is generated randomly in GA in which each element represents a typical design called chromosome [86, 87].

GA accomplishes a random search on the defined population by evaluating the fitness value of each string in the population and conduct three main operations to create a new population of design points as [87]:

Reproduction: This is a process of selecting members from the population of strings based on their fitness function value, *f*, and then carrying them into the next generation. In this process strings with higher fitness values would have higher probability to contribute one or more offspring in the next generation.

Crossover: In this operation, the reproduced springs are randomly mated by selecting a random fitness value along the length of the string and then swapping all the fitness values after that point.

Mutation: In this operation, a bit within a string will be flipped (0 becomes 1 and 1 becomes 0) using probability random operation. This is usually a very low value such as 0.001for binary encoded genes.

The new population is further evaluated and tested according to the termination criteria (if the member with the lowest cost remains the same for the past two consecutive generations). If the termination criterion is not met, the population is iteratively operated by the above three operators and evaluated. The process is continued until the termination criterion is met.

5.2.3 Sequential Quadratic Programming (SQP) technique

SQP is a powerful gradient based method to solve continuous nonlinear optimization problems. The basic idea of SQP is to solve nonlinearly constrained problems using a

sequence of quadratic programming (QP) sub-problems. The constraints of each QP sub-problem are linearization of the constraints in the original problem, and the objective function of the sub-problem is a quadratic approximation of the Lagrangian function [88].

SQP allows you to closely mimic Newton's method for constrained and unconstrained optimization problems. During each iteration process, an approximation is made by Jacobean and Hessian of the Lagrangian function using a quasi-Newton updating method. This is then used to generate a quadratic sub-problem (QP sub-problem) whose solution is used to form a search direction for a line search procedure [89].

The optimal results due to SQP may be local optimal points. Thus different initial points are randomly selected to conduct optimization in an attempt to catch the global optimum values.

Here, the Matlab optimization toolbox has been utilized to solve the optimization problem using SQP technique [90].

5.3 Optimization Results

Material of all layers is considered to be the same as that used for all previous case studies (NiCrMoV125 steel). As mentioned in Chapter 2, bilinear kinematic hardening model has been used to approximate the real material behavior of this steel. It should be mention that the inner diameter of the compound cylinder for all the combinations is kept constant and assumed to be a=100 mm. The limits on thickness dimensions, radial interference and autofrettage pressure values were discussed in Section 5.1.2 , Table 5.2.

As mentioned before in Section 5.2, the optimum values have been found by GA, starting with the initial values of the design variables. SQP has also been used using the optimum values obtained by GA as initial values in an attempt to locate accurate global optimal solutions.

Tables 5.5-5.11 show the optimum values for different autofrettage and shrink-fit combinations for three different requirements mentioned in Section 5.2.1 using GA and SQP algorithms. Also, the maximum compressive and tensile residual stresses and the fatigue life time (See section 3.5) have been calculated for these combinations for different requirements.

Table 5. 5: Optimum values and fatigue life for the first combination.

DVs		Initial values	Req. (a) (SQP +GA)	Req. (a) (GA)	Req. (b) (SQP +GA)	Req. (b) (GA)	Req. (c) (SQP +GA)	Req. (c) (GA)
t_1 [mm]		50	55	54.7	30	30.4	55	54.8
t_2 [mm]		50	55	53.8	30	30.3	55	54.5
δ [mm]		0.2	0.213	0.21	0.185	0.196	0.197	0.201
P_{1in} [MPa]		736	630	645	770	768	630	635
Objective function	MCRS [MPa]	-347	-470	-466	-72	-71	-460	-463
	MTRS [MPa]	314	257	253	100	106	239	241
Life time [Cycles]	Inner layer	6.4×10^4	2.7×10^5		400		2.66×10^5	
	Outer layer	2.3×10^4	3.8×10^3		4.7×10^3		4.1×10^3	

Table 5. 6: Optimum values and fatigue life for the second combination.

DVs		Initial values	Req. (a) (SQP +GA)	Req. (a) (GA)	Req. (b) (SQP+ GA)	Req. (b) (GA)	Req. (c) (SQP +GA)	Req. (c) (GA)
t_1 [mm]		50	30	31.5	44	48	30	33
t_2 [mm]		50	55	54.6	30	31	55	54.8
δ [mm]		0.2	0.183	0.187	0.206	0.206	0.18	0.18
P_{1in} [MPa]		520	570	541	572	516	484	509
$P_{2\,in}$ [MPa]		280	252	254	280	299	252	264
Objective function	MCRS [MPa]	-330	-512	-501	-138	-151	-460	-488
	MTRS [MPa]	228	264	260	112	125	248	230
Life time [cycles]	Inner layer	1.02×10^5	2.1×10^5		3.6×10^4		1.88×10^5	
	Outer layer	1.4×10^4	1.7×10^3		4.3×10^4		3.5×10^3	

Table 5. 7: Optimum values and fatigue life for the third combination.

DVs		Initial values	Req. (a) (SQP +GA)	Req. (a) (GA)	Req. (b) (SQP +GA)	Req. (b) (GA)	Req. (c) (SQP +GA)	Req. (c) (GA)
t_1 [mm]		50	30	30.1	55	54.5	40	32
t_2 [mm]		50	55	52.7	55	54.6	55	54.3
δ [mm]		0.2	0.193	0.18	0.197	0.196	0.19	0.18
$P_{1\,in}$ [MPa]		520	493.6	476	468	468	481	480
Objective function	MCRS [MPa]	-330	-362	-357	-266	-267	-313	-340
	MTRS [MPa]	156	155	158	132	131	100	122
Life time [Cycles]	Inner layer	2.6×10^4	2.0×10^4		4.6×10^4		3.7×10^4	
	Outer layer	7.7×10^3	2.1×10^3		2.0×10^3		4.2×10^3	

Table 5. 8: Optimum values and fatigue life for the fourth combination.

DVs		Initial values	Req. (a) (SQP +GA)	Req. (a) (GA)	Req. (b) (SQP GA+)	Req. (b) (GA)	Req. (c) (SQP +GA)	Req. (c) (GA)
t_1 [mm]		50	30	32	55	54	30	33
t_2 [mm]		50	55	54	30	31	55	54.8
δ [mm]		0.2	0.213	0.213	0.2	0.2	0.213	0.213
P_{1in} [MPa]		250	275	245	225	236	251	229
P_{1out} [MPa]		520	570	560.5	506	526	525	508
P_{2in} [MPa]		280	252	261	225	293	256	267
Objective function	MCRS [MPa]	-387	-574	-562	-36	-71	-534	-526
	MTRS [MPa]	172	215	211	117	120	193	201
Life time [cycles]	Inner layer	1.5×10^5	1.05×10^6		8.6×10^3		9.3×10^5	
	Outer layer	7.2×10^3	2.9×10^3		1.6×10^4		3.05×10^3	

Table 5. 9: Optimum values and fatigue life for the fifth combination.

DVs		Initial values	Req. (a) (SQP +GA)	Req. (a) (GA)	Req. (b) (SQP +GA)	Req. (b) (GA)	Req. (c) (SQP +GA)	Req. (c) (GA)
t_1 [mm]		50	30	31	55	54	30	30.9
t_2 [mm]		50	55	54.7	55	54.8	55	54.7
δ [mm]		0.2	0.22	0.22	0.18	0.18	0.22	0.22
P_{1in} [MPa]		250	275	261	225	228	275	225
P_{1out} [MPa]		520	468	471	572	561	468	470
Objective function	MCRS [MPa]	-387	-510	-509	-334	-330	-441	-443
	MTRS [MPa]	167	203	309	102	103	160	164
Life time [cycles]	Inner layer	1.3×10^5	2.06×10^5		8.2×10^4		1.9×10^5	
	Outer layer	2.4×10^3	1.4×10^3		5.9×10^3		1.7×10^3	

Table 5. 10: Optimum values and fatigue life for the sixth combination

DVs		Initial values	Req. (a) (SQP +GA)	Req. (a) (GA)	Req. (b) (SQP +GA)	Req. (b) (GA)	Req. (c) (SQP+ GA)	Req. (c) (GA)
t_1 [mm]		50	41.2	41.3	30	30	42.3	55
t_2 [mm]		50	55	54.7	30	30	55	55
δ [mm]		0.2	0.22	0.22	0.2	0.203	0.22	0.2
P_{1in} [MPa]		550	550	550.8	500	507	536	500
P_{2out} [MPa]		735	700	703	737	726	700	708
Objective function	MCRS [MPa]	-491	-502	-501	-322	-322	-470	-460
	MTRS [MPa]	326	311	311	257	257	250	255
Life time [cycles]	Inner layer	8.7×10^5	6.2×10^5		8×10^3		5.8×10^5	
	Outer layer	3.25×10^3	2.2×10^4		1.09×10^3		2.6×10^4	

Table 5. 11: Optimum values and fatigue life for the seventh combination

DVs		Initial values	Req. (a) (SQP +GA)	Req. (a) (GA)	Req. (b) (SQP +GA)	Req. (b) (GA)	Req. (c) (SQP +GA)	Req. (c) (GA)
t_1 [mm]		50	30	30.8	55	54.6	30	55
t_2 [mm]		50	55	52	30	31	55	50
δ [mm]		0.2	0.22	0.213	0.22	0.2	0.192	0.214
P_{1in} [MPa]		250	275	271	225	225	275	235
P_{2out} [MPa]		520	572	553	520	518	538	505
P_{2in} [MPa]		250	225	230	244	240	225	225
P_{1out} [MPa]		520	472	478	468	476	571	551
Objective function	MCRS [MPa]	-380	-507	-507	-144	-140	-493	-410
	MTRS [MPa]	203	272	269	76	74	231	210
Life time [cycles]	Inner layer	1.1×10^5	9.3×10^4		3.3×10^3		8.8×10^4	
	Outer layer	1.6×10^4	5.6×10^3		1×10^9		7.1×10^3	

It is noted that in above tables MCRS and MTRS stand for maximum compressive and tensile residual stresses, respectively. It should also be mentioned the evaluation of fatigue life in Tables 5.5-5.11, is based on accurate optimum values obtained by combined GA and SQP algorithms.

5.4 Comparisons

To better examine the results, the maximum compressive and tensile residual stresses for the optimal configuration in each combination of autofrettage and shrink-fit processes have been extracted from Tables 5.5-5.11 and compared in Figures 5.10-5.12.

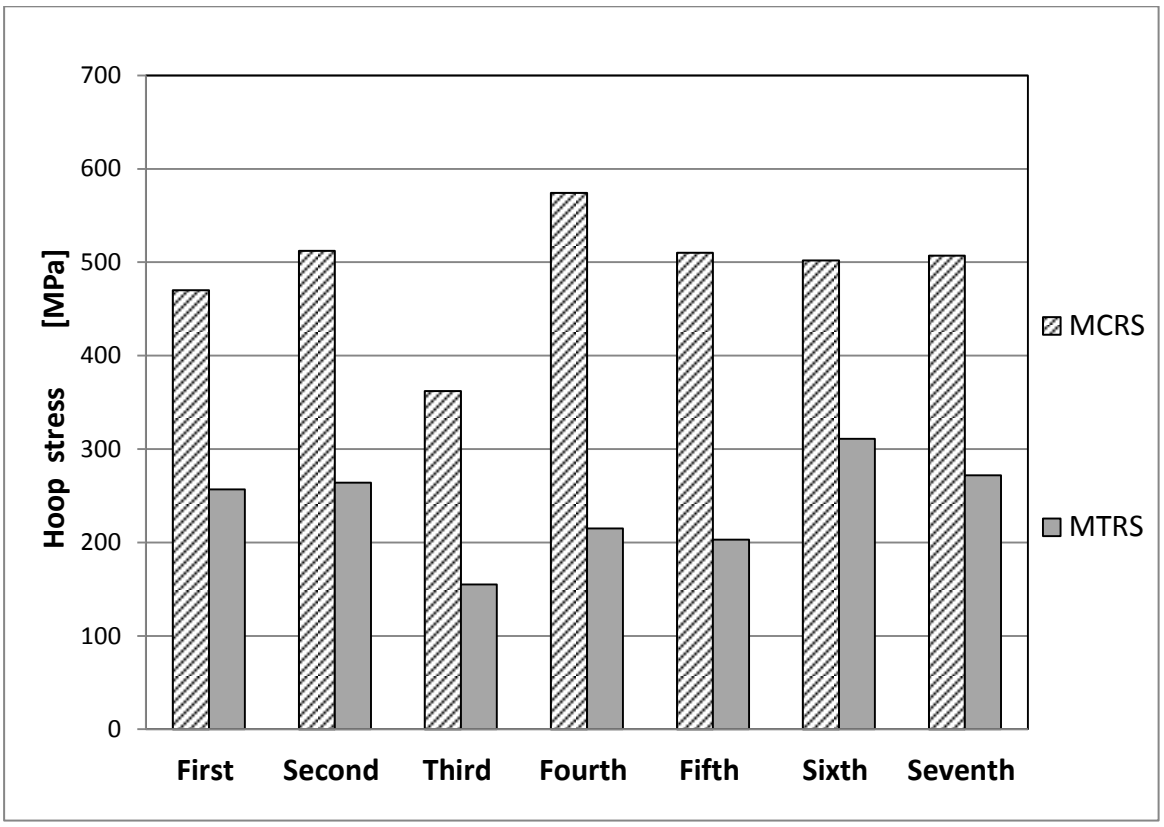

Figure 5.10: Maximum residual hoop stresses for different combinations- Req. (a).

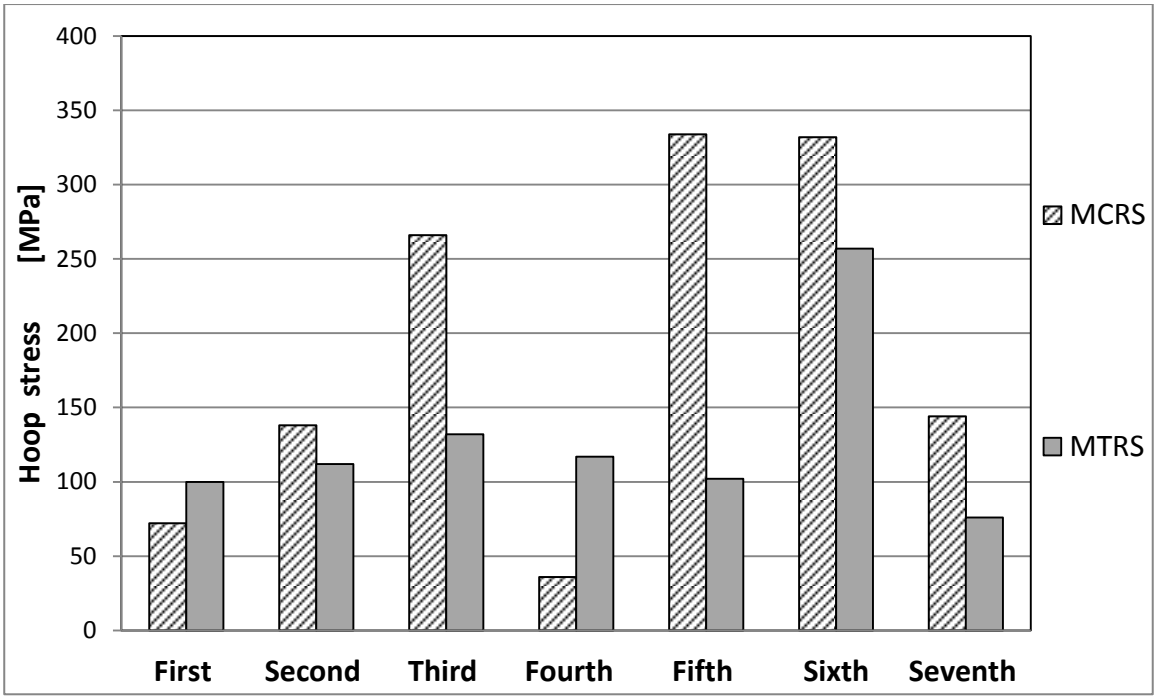

Figure 5.11: Maximum residual hoop stresses for different combinations-Req. (b).

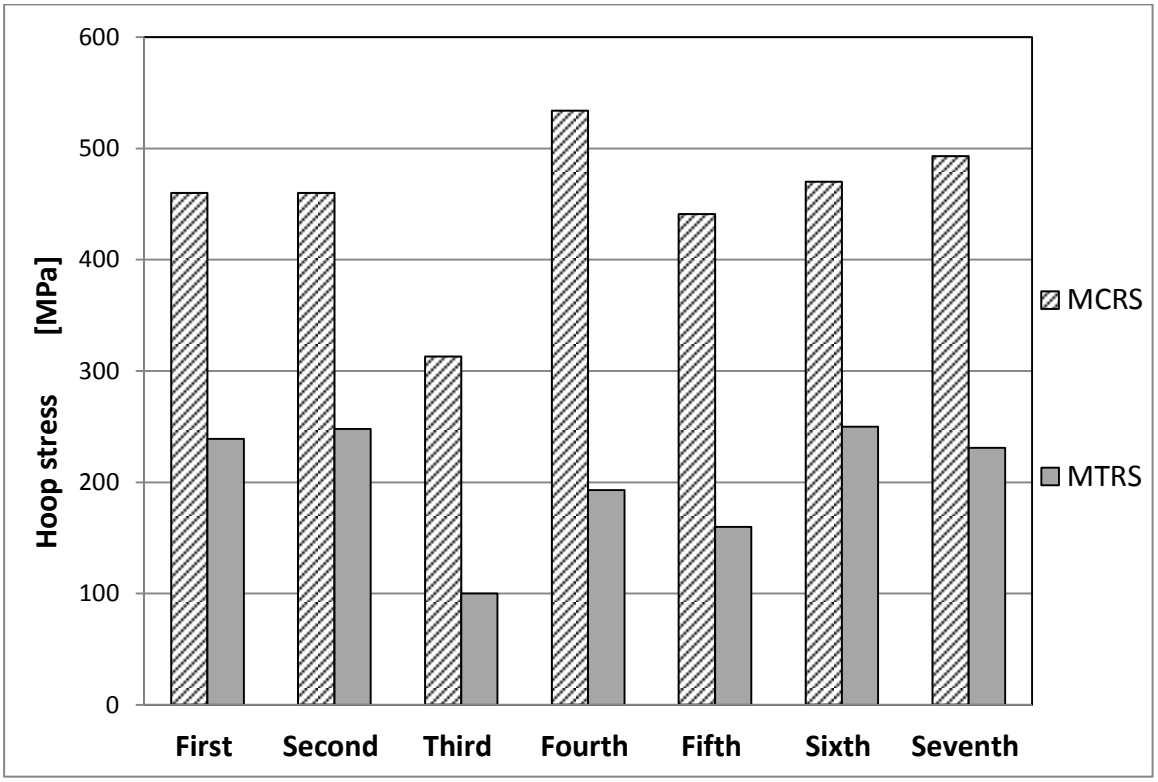

Figure 5.12: Maximum residual hoop stresses for different combinations- Req. (c).

As it can be realized, the fourth combination has the highest compressive residual stress in the case of requirement (a) and (c), while the seventh configuration has the least tensile residual stress, which takes place in case of requirement (b). Figures 5.10-5.12 show only the maximum values of either the compressive or tensile residual stresses, not the full distribution of the residual stresses through the whole thickness of the compound cylinder. These stress distributions are required to evaluate the fatigue life of the different layers of the cylinders. Figures 5.13-5.19 illustrate the distribution of the residual hoop stress through the whole thickness of the compound two-layer cylinder for the seven combinations discussed before. It should be noted that these distributions are calculated at both optimum configurations in case of each requirement, and initial configurations.

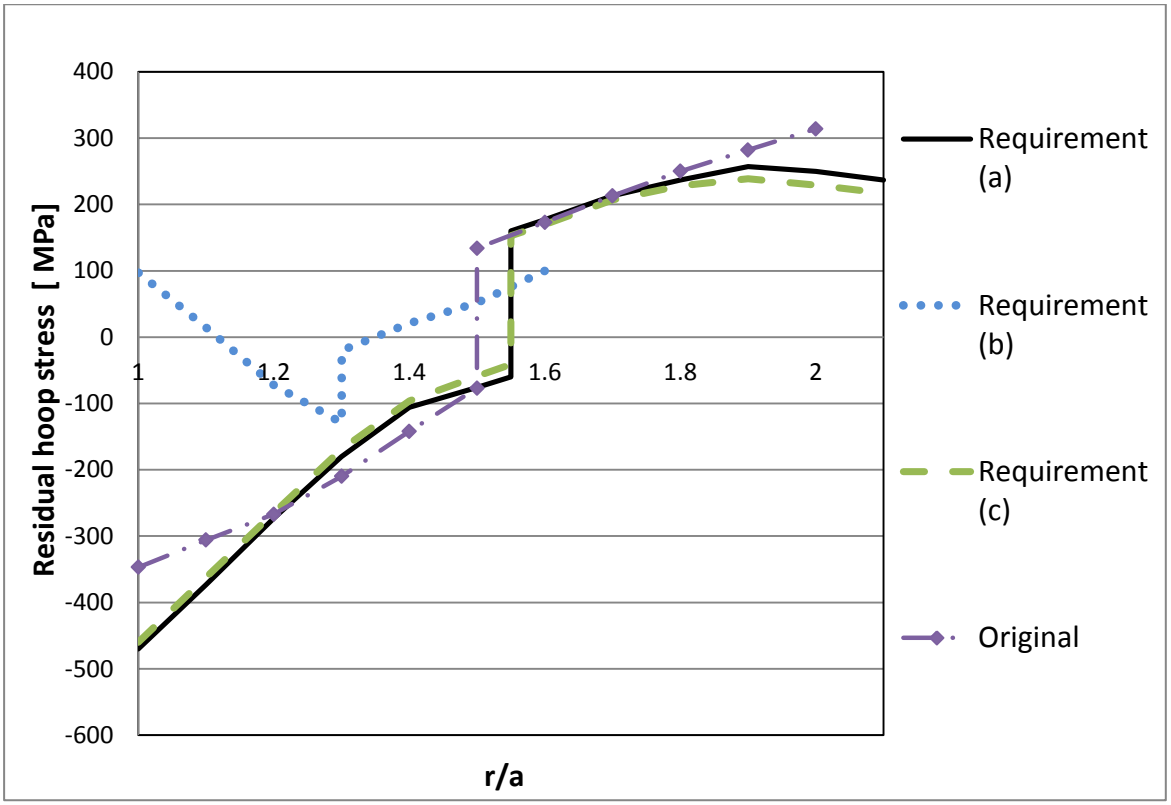

Figure 5.13: Residual hoop stress distribution through the cylinder thickness for the first combination.

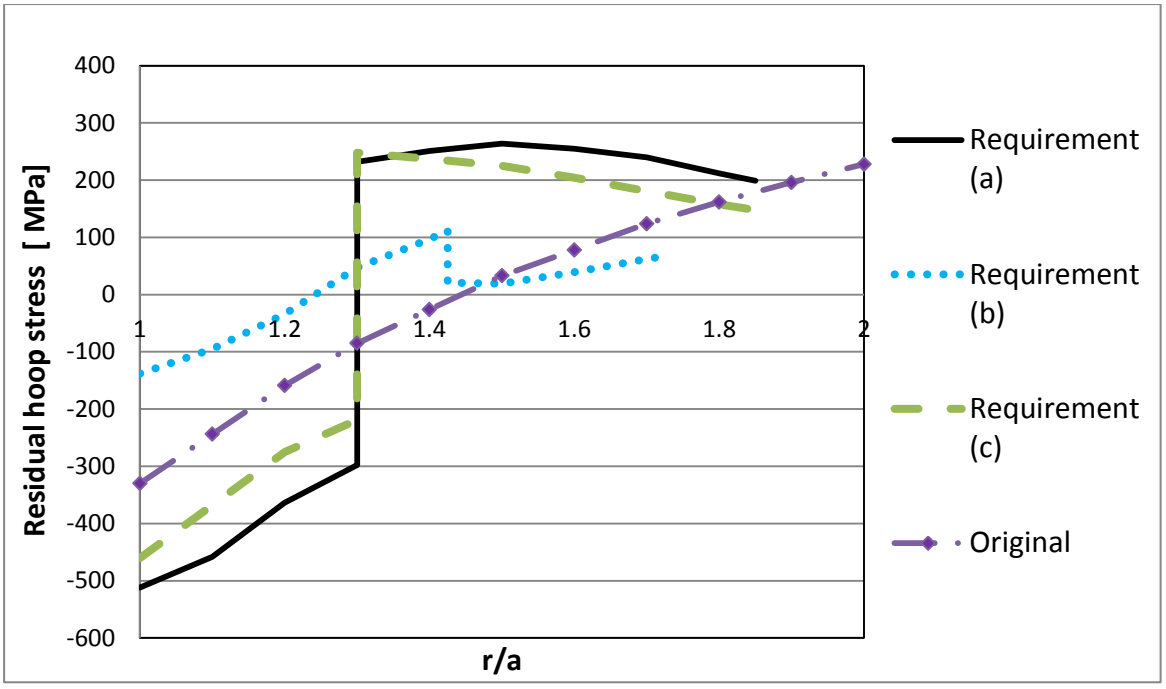

Figure 5.14: Residual hoop stress distribution through the cylinder thickness for the second combination.

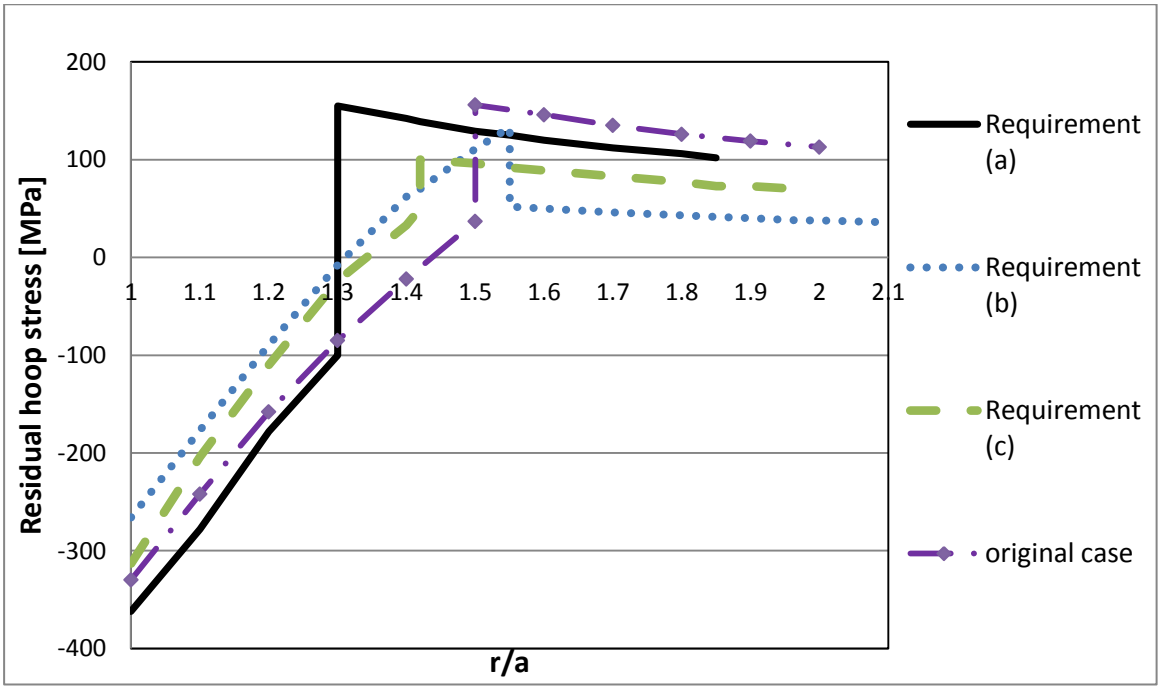

Figure 5.15: Residual hoop stress distribution through the cylinder thickness for the third combination.

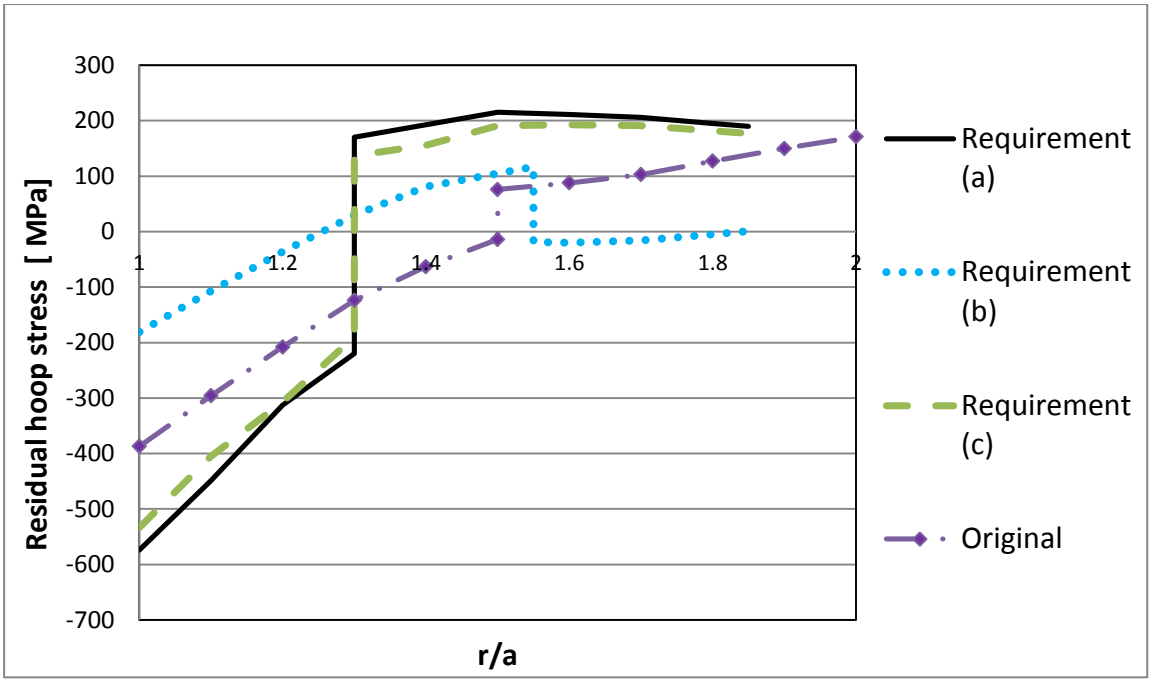

Figure 5.16: Residual hoop stress distribution through the cylinder thickness for the fourth combination.

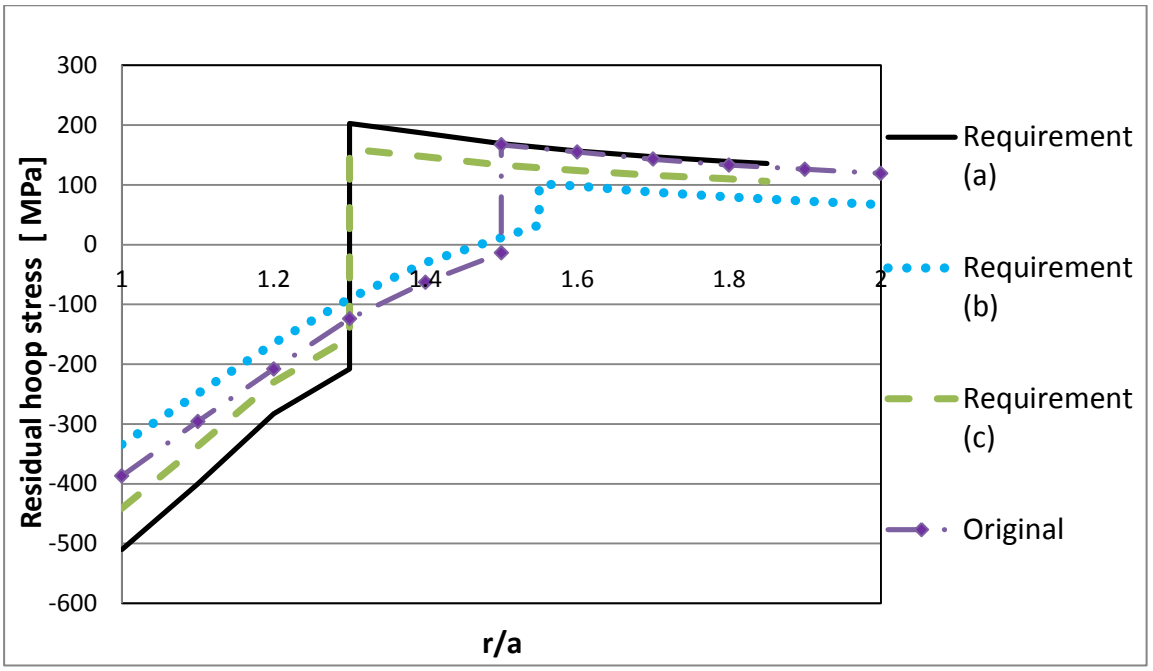

Figure 5.17: Residual hoop stress distribution through the cylinder thickness for the fifth combination.

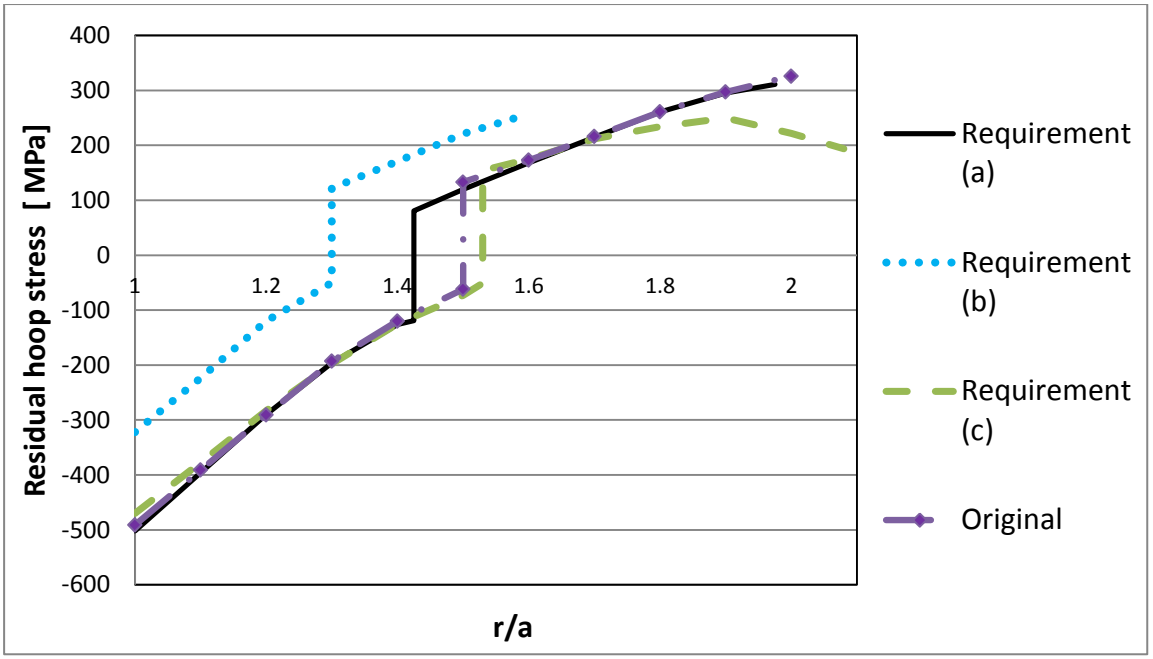

Figure 5.18: Residual hoop stress distribution through the cylinder thickness for the sixth combination.

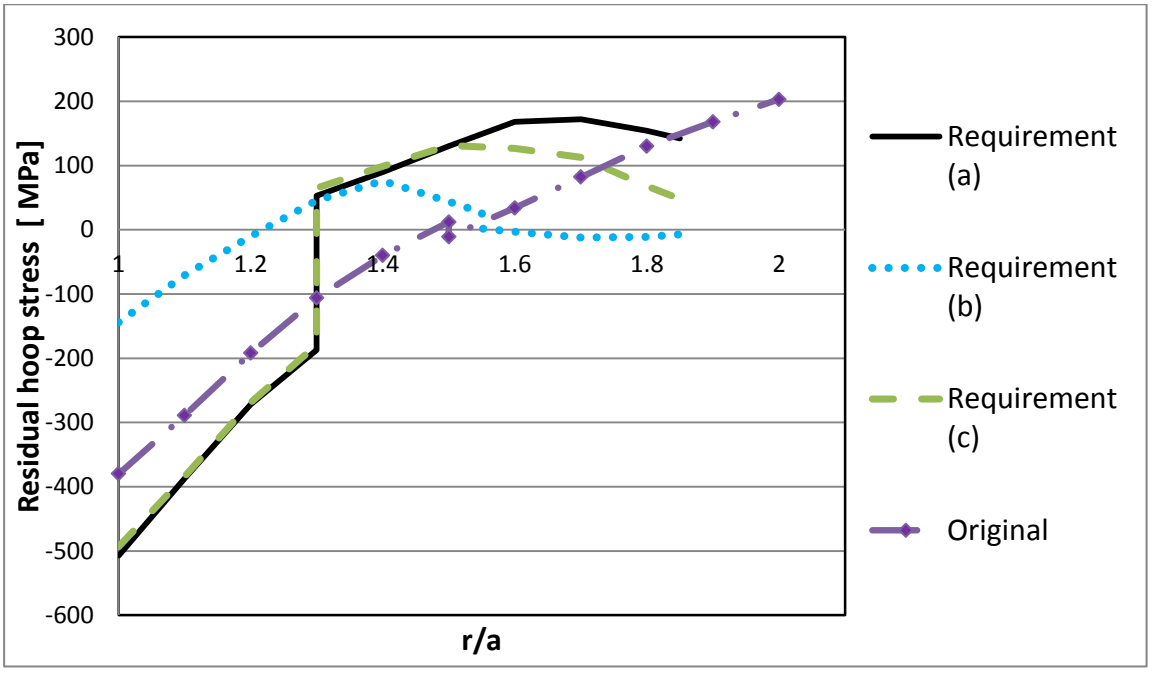

Figure 5.19: Residual hoop stress distribution through the cylinder thickness for the seventh combination.

One can observe that the hoop stress distributions differ for different requirements. In the case of requirement (a), the beneficial compressive residual hoop stress has been substantially improved compared with the original configuration, especially at the near bore area; while in the case of requirement (b), the detrimental tensile residual stresses have been decreased. Finally, in the case of requirement (c), a trial of increasing the compressive residual stresses while decreasing the tensile residual stresses has been achieved.

For a fair comparison, the mechanical fatigue lives (Section 3.5.1) at optimal configurations have also been compared for all seven combinations of autofrettage and shrink-fit processes considering the three different requirements, as shown in Figures 5.20- 5.22.

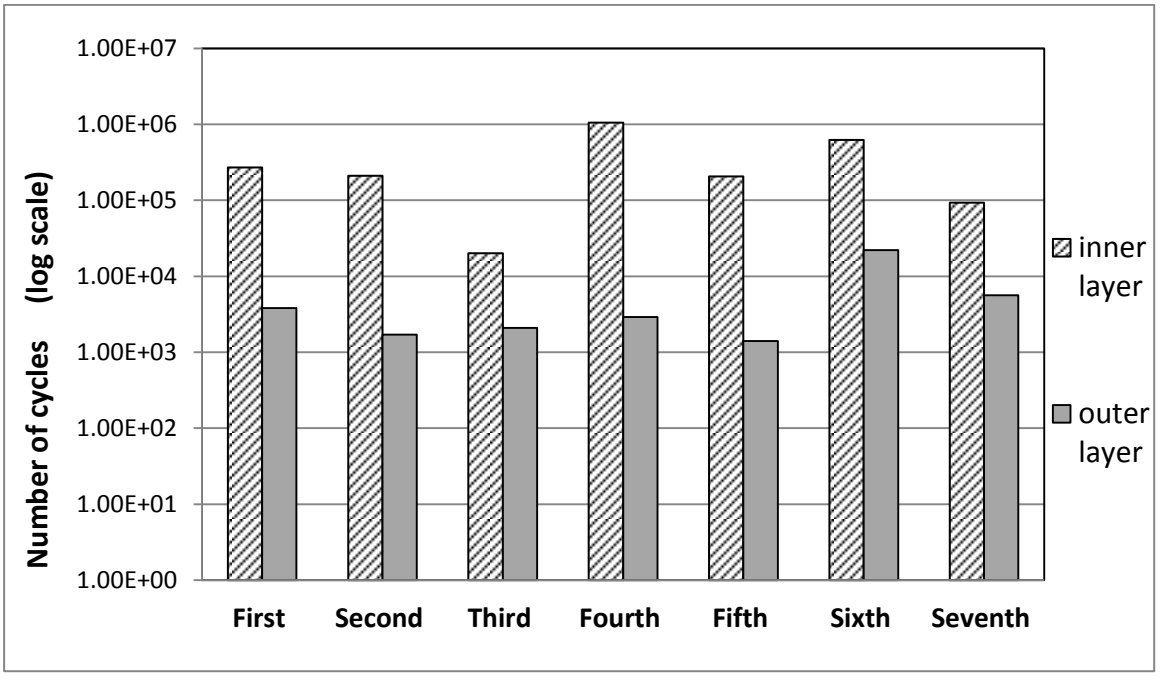

Figure 5.20: Fatigue life for different combinations in the case of requirement (a) for the inner and outer layers of the compound cylinder.

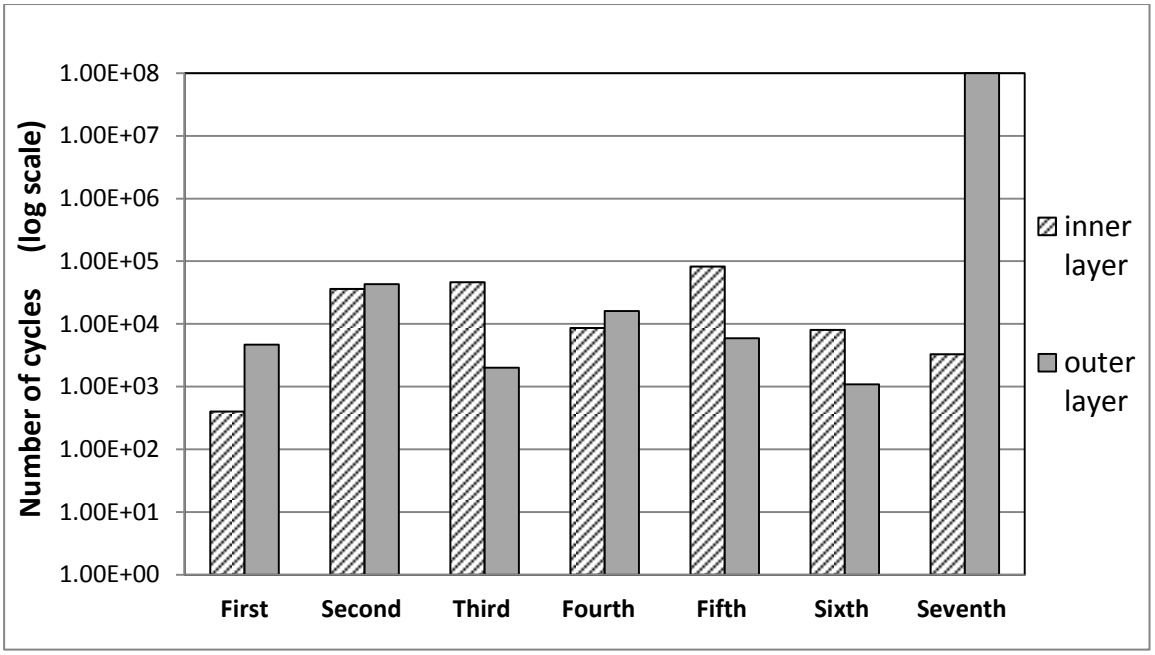

Figure 5.21: Fatigue life for the different combinations in the case of requirement (b) for the inner and outer layers of the compound cylinder.

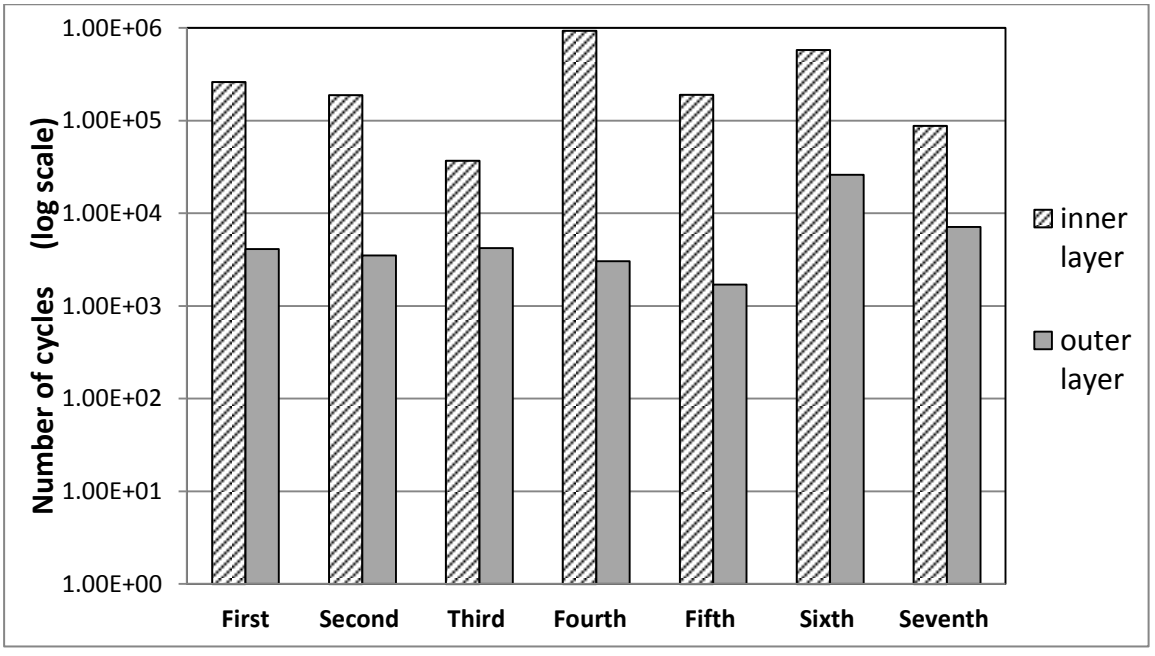

Figure 5.22: Fatigue life for the different combinations in the case of requirement (c) for the inner and outer layers of the compound cylinder.

Examination of Figures 5.20-5.22 reveal that the highest fatigue life time for the inner layer occurs for the fourth combination either in cases of requirement (a) or (c); while the highest fatigue life time for the outer layer occurs for the seventh combination in the case of requirement (b). Moreover, the sixth combination provides a high life time in both layers at the same time compared with the other combinations especially in the case of requirements (a) and (c).

5.5 Summary

In this chapter, the developed finite element model mentioned in Chapters 2 and 3 has been combined with design of experiment and response surface techniques to derive explicit relations to describe the defined objective functions (maximum compressive and minimum tensile residual stresses) with respect to design variables over the complete design regions in each combination of autofrettage and shrink-fit processes accurately. The derived response functions have then been effectively utilized to conduct design optimization in order to maximize the beneficial compressive residual stress and to minimize the detrimental tensile residual stress. Optimization has been first conducted using GA to obtain the near global optimal solutions for each combination. The optimal results from GA have then been forwarded as initial values to the powerful gradient based SQP optimization technique to capture accurate global optimal solutions.

The following observations have been made:

1- The hoop stress distribution through the cylinder thickness can be improved using the optimum design variables.

2- The values of maximum compressive and tensile residual hoop stresses are a good indication of the load bearing capacity of the cylinder; however, they are not major indicators of the enhancement of the fatigue life.

3- The fatigue life time of the fourth combination is the highest among the other combinations regarding the inner layer; while the highest life time is at the seventh combination regarding the outer layer.

4- The sixth combination is highly recommended because it can provide a high fatigue life time for both the inner and outer layers of the cylinder.

CHAPTER 6

CONCLUSIONS, CONTRIBUTIONS, AND FUTURE RECOMMENDATIONS

6.1 Highlights and Conclusions of Dissertation Research

The complicated and severe environment in which the thick-walled compound cylinder operates makes the analysis, fatigue life calculation and optimization of these compound cylinders very challenging. In this dissertation research, an accurate 3D finite element simulation of different arrangements of shrink-fitted and autofrettaged compound cylinders has been conducted. The residual stresses for different combinations have been evaluated. Also, using the developed finite element model, the stresses due to different cyclic thermo-mechanical loads have been calculated for the different combinations of compound cylinder considering thermal accumulation. An experimental set up has also been designed to find the temperature distribution through the thickness of shrink-fitted cylinder under cyclic thermal load in order to validate the developed fully coupled finite element model.

For a greater understanding of the behavior of the compound cylinders under different thermo-mechanical loads, the fatigue life due to cyclic inner pressure, cyclic inner

thermal pulses and cyclic combined thermo-mechanical pulses has been calculated using ASME codes for high pressure vessel.

After detail examination of different proposed arrangement of the two layer compound cylinders subjected to shrink-fit and conventional single autofrettage process, a new procedure named double autofrettage process has been introduced to further enhance the residual stresses distribution along the wall thickness of the cylinder. In this process, an outer autofrettage cycle is performed prior to a conventional inner autofrettage cycle. It has been observed that using the proposed double autofrettage process, one can provide not only an increase in the beneficial compressive residual stresses at the near bore area of the cylinder, but also a decrease in the detrimental tensile residual stress at the outer part of the compound cylinder. Subsequently, using the proposed double autofrettage process, new combinations of autofrettage, shrink-fit and double autofrettage have been constructed and the residual stress for these new combinations has been evaluated and then compared together with the old combinations.

Finally a design optimization methodology has been developed to identify the optimal configuration of each combination for different objective requirements such as increasing the maximum value of compressive residual stress at the near bore area, decreasing the maximum value of tensile residual stress along the whole thickness of the cylinder or considering both simultaneously. As optimization problems based on full finite element model is computationally very expensive and may not render accurate optimum results, DOE and RSM techniques have been used to develop smooth response surface functions which can accurately describe the behavior of the tensile and compressive hoop stresses (responses) with the change of design variables. A road map to identify the design

variables associated with each combination has been defined. The complete set of design variables are considered to be the thickness of the inner and outer layers, the autofrettage pressures at the inner and outer surfaces of the inner layer, the autofrettage pressures at the inner and outer surfaces of the outer layer and the diametral interference for shrink-fitting δ. The developed response surface functions have been utilized effectively in design optimization formulation. Genetic algorithm optimization technique has been initially used to approximately find the global optimum point. Then the optimum results from GA have been forwarded to SQP as initial values to find accurately the global optimum solutions.

The optimum values for each combination have been used to evaluate the hoop stress distribution using the finite element model. Then, the fatigue lives of these optimum configurations have been calculated and then compared together.

The conclusion's highlights of the dissertation research are summarized below as:

- Combining autofrettage with shrink-fit can provide more compressive residual stress at the near bore area of the cylinder; also, it may reduce the detrimental tensile residual stress along the cylinder wall.
- The fully coupled thermo-elastic model is much more accurate than the partially coupled one, especially when the component is subjected to cyclic thermal shocks. In addition, the thermal accumulation has a significant effect on the thermal stresses.
- The different combinations of the compound cylinder can reduce the hoop stress at the near bore area up to 75% compared with an equivalent single layer virgin cylinder.

- The values of maximum compressive and tensile residual hoop stresses are a good indication of the load bearing capacity of the cylinder; however, they are not major indicators of the enhancement of the fatigue life.
- For the case of internal cyclic pressure, the shrink-fitting of two autofrettaged layers is found to be the best combination and it could enhance the life time significantly compared with the equivalent shrink-fitted cylinder. It is clearly shown that the outer layer is the critical layer in this case.
- For the case of internal cyclic thermal loads, the shrink-fitting of two layers then autofrettage of the assembly is found to be the best combination and can enhance the life time by 14% compared with an equivalent single layer mono-block cylinder.
- For the case of combined pressure and thermal loads, the shrink-fitting of two layers and then autofrettage of the assembly is also found to be the best combination and can enhance the life time by 29.4% compared with an equivalent single layer mono-block cylinder.
- The proposed double autofrettage process, in which autofrettage process has been performed on the outer surface before its application on inner surface, can improve not only the compressive residual hoop stress at the near bore area of the cylinder, but also decrease the detrimental residual tensile stress at the outer part of the cylinder.
- The double autofrettage process combined with the standard autofrettage and shrink-fit processes can provide new promising combinations of the compound autofrettage and shrink-fit cylinders. It is found that these new combinations

could enhance the residual hoop stress over the whole thickness of the cylinder wall.

- The results of mechanical fatigue life indicate that the combination of shrink-fitting two virgin layers then performing double autofrettage for the whole assembly has the highest fatigue life only at the inner layer of the cylinder, while the combination of performing double autofrettage for each layer individually then shrink-fitting them together can provide high fatigue life in both layers.
- DOE and RSM techniques combined with the finite element model can generate accurate response surface functions which can be effectively used as objective functions in the design optimization formulation.
- GA and SQP can be effectively used together to eliminate the disadvantages of each other and capture global optimum solutions accurately.
- Optimization results show considerable improvement in the hoop stress distribution through the cylinder thickness.
- With respect to inner layer, the fatigue life time for optimum configuration of the compound cylinder subjected to double autofrettage for the inner layer, conventional single autofrettage for the outer layer, and finally shrink-fit of autofrettaged layers has the highest value compared with other configurations. However with respect to outer layer, the fatigue life time for optimum configuration of the compound cylinder subjected to double autofrettage for each layer individually and shrink-fit of double autofrettaged layers has the highest value.

- The optimum configuration of shrink-fit of two layers then performing double autofrettage for the whole assembly combination is highly recommended because it can provide relatively high fatigue life time for both the inner and outer layers of the compound cylinder.

6.2 Contributions

The major contributions of this dissertation research can be summarized as follows:

A. Developed an efficient and accurate design optimization algorithm to improve residual stress profile through the thickness of the compound cylinder under different combinations of autofrettage and shrink-fit processes.
B. Developed an accurate, fully coupled thermo-mechanical formulation for compound cylinders considering thermal accumulation.
C. Designed an experimental set up to validate the finite element model.
D. Investigated the performance of the different combinations of compound multilayer cylinders under different thermo-mechanical loads.
E. Investigated the fatigue life of the combined autofrettage and shrink fit multilayer cylinder considering both the thermal and mechanical cyclic loads.
F. Developed a new design philosophy of using autofrettage named as double autofrettage in order to reduce the Bauschinger effect near to the bore and also to reduce detrimental tensile residual stress at the outer surface.
G. Investigated the new combinations of compound cylinders when considering the double autofrettage process and their residual hoop stress distribution along the

whole thickness of the cylinder wall as well as their effect on the fatigue life time of compound cylinders.

H. Utilized the developed finite element model combined with the design of experiment and response surface techniques to derive explicit relations to describe the defined hoop stress response functions with respect to different design variables at different autofrettage and shrink-fit combinations.

I. Combining Genetic Algorithm (GA) and Sequential Quadratic Programming (SQP) optimization techniques to accurately capture the optimal configurations for each combination of autofrettage and shrink-fit.

6.3 Recommendations for Future Works

This dissertation research includes a fundamental and systematic study of the analysis and design optimization of combined autofrettaged and shrink-fitted multilayer cylindrical shells under thermo-mechanical loads. However several interesting topics, which can be considered as the natural extension of the present research work, have been realized for future work as:

1. **Analysis of three or more layer compound cylinders**

   In this thesis, the finite element model has been used for analysis of the two-layer compound cylinders. The model can be used for a compound cylinder consisting of three or more layers.

2. **Analysis for non-axisymmetric loads**

   In this thesis, the finite element model has been used for analysis of the performance of two-layer compound cylinders under different thermo-mechanical axisymmetric loads. The developed finite element model is a 3D model which can be used for non-axisymmetric loads.

3. **Extension of experimental work**

   In this thesis, experimental work has been done to validate the finite element model for two-layer shrink-fitted cylinders subjected to cyclic inner thermal pulses by comparing the results of the temperature distribution as well as the stain at the outer surface. The experimental work can be developed to measure the strain history at different locations through the wall thickness of the cylinder when subjected to combined thermal and pressure pulses. Moreover, the fatigue life due to these combined loads can be measured experimentally.

4. **Re-autofrettage technique combined with standard and double autofrettage processes**

   In this thesis, combinations of shrink-fit, autofrettage and double autofrettage have been discussed. New combinations may be developed by employing re-autofrettage technique combined with the above-mentioned processes to investigate if fatigue life can be increased.

5. **Considering number of layers and autofrettage cycles as design variables in the design optimization formulation**

In this thesis, the design variables for optimization process have been considered to be the thickness of each layer, the autofrettage pressures at the inner surfaces, the autofrettage pressures at the outer surfaces (if any), and the diametral interference for shrink-fitting. Additional design variables such as number of layers and number of autofrettage cycles may be included in the design optimization formulation.

REFERENCES

[1] Timoshenko, S. and Goodmr, J. N., *Theory of Elasticity*, 3rd Edn. McGraw-Hill, New York (1970).

[2] Gamer, U. and Lance, R., "Residual Stresses in Shrink Fits", International journal of Mechanical Science, vol. 25, No. 7, pp.465-470, 1983.

[3] Gamer, U., "The Shrink Fit with Nonlinearity Hardening Elastic Plastic Hub", journal of applied mechanics vol. 45, pp.474-479, 1987.

[4] Guven, U., "Stress Distribution in Shrink Fit with Elastic-Plastic Hub Exhibiting Variable Thickness", International journal of Mechanical Science, vol. 35, No. 1, pp.39-46, 1993.

[5] Pedersen, P., "On Shrink-Fit Analysis and Design", Journal of Compute Mech. vol. 37, No. 2, pp.121-130, 2006.

[6] Franklin, G. J. and Morrison, J. L. M., "Autofrettage of Cylinders: Prediction of Pressure, External Expansion Curves and Calculation of Residual Stresses" Proceeding of Institute of Mechanical Engineers, vol. 174 PP. 947–74, 1960.

[7] Chen, P. C. T., "Stress and Deformation Analysis of Autofrettaged High Pressure Vessels", ASME special publication 110, PVP. New York: ASME United Engineering Center; PP. 61–7, 1986.

[8] Chen, P. C. T., "Generalized Plane-Strain Problems in an Elastic‑Plastic Thick-Walled Cylinder", In Transcripts of 26th Conference of Army Mathematicians, pp. 265–275, 1980.

[9] Stacey, A. and Webster, G. A., "Determination of Residual Stress Distributions in Autofrettaged Tubing", Int. J. Pressure Vessels and Piping, 1988, 31, 205–220.

[10] Chen P. C. T., "The Bauschinger and Hardening Effects on Residual Stresses in an Autofrettaged Thick-Walled Cylinder", Trans. ASME, J. Pressure Vessel Technology vol.108, pp.108–112, 1986.

[11] Lazzarin, P. and Livieri, P., "Different Solution for Stress and Strain Fields in Autofrettaged Thick-Walled Cylinders", Int. J. Pressure Vessels and Piping, vol. 31, pp. 231–238, 1997.

[12] Parker, A. P. and Underwood, J. H., "Influence of the Bauschinger Effect on Residual Stress and Fatigue Lifetimes in Autofrettaged Thick-Walled Cylinders", Fatigue and Fracture Mechanics: 29th Volume, ASTM STP 1321,T. L. Panontin and S. D. Sheppard, eds,1998.

[13] Parker, A. P. Underwood, J. H., and Kendall, D. P., "Bauschinger Effect Design Procedure for Autofrettaged Tubes Including Material Removal and Sachs' Method", ASME J. Pressure Vessel Technol., Vol. 121, pp. 430–437, 1999.

[14] Parker, A. P., "Autofrettage of Open-End Tubes—Pressures, Stresses, Strains, and Code Comparisons", ASME, Journal of Pressure Vessel Technology, vol. 123, pp. 271–281, 2001.

[15] Livieri, P. and Lazzarin, P., "Autofrettaged Cylindrical Vessels and Bauschinger Effect: an Analytical Frame for Evaluating Residual Stress Distributions", Trans. ASME, J. Pressure Vessel Technology, vol. 124, pp. 38–45, 2002.

[16] Jahed, H., and Ghanbari, G., "Actual Unloading Behavior and Its Significance on Residual Stress in Machined Autofrettaged Tube", ASME J. Pressure Vessel Technol., vol. 125, pp. 321–235, 2003.

[17] Huang, X P., "A General Autofrettage Model of A Thick-Walled Cylinder Based on Tensile–Compressive Stress–Strain Curve of a Material", Journal of Strain Analysis for Engineering Design, vol. 40, No. 6, pp.599-607, 2005.

[18] Huang, X. and Moan, T.," Residual Stress in an Autofrettaged Tube Taking Bauschinger Effect as a Function of the Prior Plastic Strain", ASME ,Journal of Pressure Vessel Technology Vol. 131, pp. 021207-1-7, APRIL 2009.

[19] Parker, A. P., "A Re-Autofrettage Procedure for Mitigation of Bauschinger Effect in Thick Cylinders", ASME, Journal of Pressure Vessel Technology, vol. 126, pp. 451–454, 2004.

[20] Jahed, H. Ahmadi, B. and Shambooli, M., "Re-Autofrettage", ASME, Journal of Pressure Vessel Technology, vol. 128, pp. 223–226, 2006.

[21] Kapp, J. A. Brown, B. LaBombard, E. J. and Lorenz, H. A., "On the Design of High Durability High Pressure Vessels" Proceeding of PVP Conference in San Diego, L. Picquer and M. Kawahara, eds., PVP _Am. Soc. Mech. Eng., vol. 371, pp.85–91, 1998.

[22] Parker, A. P., "Bauschinger Effect Design Procedures for Compound Tubes Containing an Autofrettaged Layer", ASME, Journal of Pressure Vessel Technology, vol. 123, pp. 203–206, 2001.

[23] Parker, A. P. and Kendall, D. P., "Residual Stresses and Lifetimes of Tubes Subjected to Shrink Fit Prior to Autofrettage", ASME, Journal of Pressure Vessel Technology, vol. 125, pp. 282–286, 2003.

[24] Majzoobi, G. H. Farrah, G.H. Pipelzadeh, M. K. and Akbari, A., "Experimental and Finite Element Prediction of Bursting Pressure in Compound Cylinder", International Journal of Pressure Vessels and Piping, vol. 81, pp.889–896, 2004.

[25] Jahed, H. Farshi, B. and Karimi, M., " Optimum Autofrettage and Shrink-Fit Combination in Multi-Layer Cylinders", ASME, Journal of Pressure Vessel Technology, vol. 128, pp. 196–200, 2006.

[26] Lee, E_Y. Lee, Y-S. Yang, Q-M. Kim, J-H. Cha, K-U. and Hong S-K., "Autofrettage Process Analysis of a Compound Cylinder Based on the Elastic-Perfectly Plastic and Strain Hardening Stress-Strain Curve", Journal of Mechanical Science and Technology, vol. 23, pp. 3153–3160, 2009.

[27] Chen, H. Kuang, C. Lee, Z. and Lee, C., "Thermo-elastic Transient Response of Multilayered Hollow Cylinder with Initial Interface Pressure", Journal of Thermal Stresses, vol. 24, pp. 987-1006, 2001.

[28] Lee, Z. Kuang, C. and Hung, C. "Hybrid Numerical Method Applied to Multilayered Hollow Cylinder with Time-Dependent Boundary Conditions", Journal of Thermal Stresses, vol. 28, pp. 839–860, 2005.

[29] Lee, Z., "Hybrid Numerical Method Applied To 3-D Multilayered Hollow Cylinder with Periodic Loading Conditions", Journal of Applied Mathematics and Computation, vol. 166, pp. 95‑117, 2005.

[30] Lee, Z., "Generalized Coupled Transient Response Of 3-D Multilayered Hollow Cylinder", Journal of International Communications in Heat and Mass Transfer, vol. 33, pp.1002‑1012, 2006.

[31] Ahmed, El-K. and Ezzat, M., "Thermal Shock Problem In Generalized Thermo-Viscoelasticty Under Four Theories", Journal of Engineering Science Vol. 42, PP. 649–671, 2004.

[32] Lord, H.W. and Shulman, y., "A Generalized Dynamical Theory of Thermoelasticity", Journal of Elasticity, vol. 2, pp.1-7, 1972.

[33] Green, A.E. and Lindsay, K.E., "Thermoelasticity", Journal of Elasticity, vol. 2, pp.1-7, 1972.

[34] Touz, D.Y., "A Unified Approach for Heat Conduction from Macro to Micro Scale", Journal of heat transfer, vol. 117, pp.8-16, 1995.

[35] Chandrasekharaiah, D.S., "One-dimensional Wave Propagation in the Linear Theory of Thermoelastisity without Energy Dissipation", Journal of thermal stress, vol.19, pp.695-710, 1996.

[36] Tian, X. Shen, Y. Chen, C. and He, T., "A Direct Finite Element Method Study of Generalized Thermo-Elastic Problems" ,International Journal of Solids and Structures, vol.43, pp. 2050–2063, 2006.

[37] Birsan, M., "Thermal Stresses in Cylindrical Cosserat Elastic Shells", European Journal of Mechanics A/Solids, vol. 28, pp. 94–101, 2009.

[38] Ying, J. and Wang, H.M., "Axisymmetric Thermoelastic Analysis in a Finite Hollow Cylinder Due to Nonuniform Thermal Shock", International Journal of Pressure Vessels and Piping, vol. 87, pp. 714-720, 2010.

[39] Brischetto, S. and Carrera, E., "Coupled Thermo-Mechanical Analysis of One-layered and Multilayered Plates", Journal of Composite Structures, vol. 92, pp. 1793-1812, 2010.

[40] Carrera, E., "Temperature Profile Influence on Layered Plates Response Considering Classical and Advanced Theories", AIAA Journal, vol.40, No.9, pp.1885–1896, 2002.

[41] Feldhacker, J L. and Hu, Z., "The Dynamic Response of a Cannon Barrel to a Ballistic Event Using Thermo-Structural Coupled Finite Element Analysis", M.Sc. Thesis, University of South Dakota State University, USA, 2008.

[42] ASME Boiler and Pressure Vessel Code, 2001, Section VIII, Division 3, AppendixD.

[43] Jahed, H. Farshi, B. and Hosseini, M., "The Actual Unloading Behavior Effect on Thermo-Mechanical Stress Intensity Factor and Life of Autofrettage Tubes", International Journal of Fatigue vol. 29, pp.360–369, 2007.

[44] Alegre, J. M. Cuestal, I. I. and Bravol P. M., "Comparative Study of Different Fatigue Crack Growth Methods for the Design of Wire-Wound Vessels", http://www.gef.es/Congresos/27/PDF/2.pdf, 2010.

[45] Nabavi, S. M. and Shahani, A. R., "Thermal Stress Intensity Factors for a Cracked Cylinder under Transient Thermal Loading", International Journal of Pressure Vessels and Piping vol.86, pp.153–163,2009.

[46] Nabavi, S. M. and Ghajar, R., "Analysis of Thermal Stress Intensity Factors for Cracked Cylinders Using Weight Function Method", International Journal of Engineering Science vol.48, pp.1811-1823, 2010.

[47] Ghajar, R. and Nabavi, S. M., "Closed Form of Thermal Stress Intensity Factors for an Internal Circumferential Cracked in a Thick-Walled Cylinder", Journal of Fatigue and Fracture of Engineering Materials and Structure, vol. 33, pp.504-512,2010.

[48] Lee, Y. S. Park, J. H. Kim, J. H., Yang, Q. M. Cha, K-U. and Hong, S-K., "Fatigue Life of Compound Cylinder Combining Autofrettage and Shrink-fit Due

to Firing", The 2nd International Conference on Advanced Nondestructive Testing, Pusan, Korea, II:394-399, 2007.

[49] Amran, A. and Kabashi, E. M., "Optimum Autofrettage Pressure in Thick Cylinders", Jurnal MeKaniKal, vol.24, PP. 1-14, 2007.

[50] Kumar, N. Mandal, D. K. Mondal, S. C. and Acharyya, S. K., " Optimization of Shell Thickness in Multilayer Pressure Vessel and Study on Effect of Number of Shells on Maximum Hoop Stress", International Journal of Engineering Science and Technology (IJEST), Vol. 3 No. 4, pp. 2693- 2700, 2011.

[51] Kumar, N. Mandal, D. K. Mondal, S. C. and Acharyya S. K., "Optimum Autofrettage Pressure and Shrink-Fit Combination for Minimum Stress in Multilayer Pressure Vessel", International Journal of Engineering Science and Technology (IJEST), Vol. 3 No. 5, pp. 4020- 4030, 2011.

[52] Maximator test, LLC, White paper Autofrettage, http://www.maximator-test.com.

[53] Bauschinger J., "Über die Veranderung der Elasticitatagrenze und dea Elasticitatamoduls verschiadener Metalle", Zivilingenieur, vo.l 27, columns 289-348, 1881.

[54] Bate, P. S. and Wilson, D.V., "Analysis of the Bauschinger Effect", Acta Metallurgica, vol. 34, No. 6, pp.1097-1105, 1986.

[55] Youtsos, A.G., *Residual Stress and Its Effect on Fatigue and Fracture*, Springer, 2006.

[56] ANSYS Theory Manual, Release 12.1 Documentation, ANSYS Inc, 2009.

[57] Totten, G. Howes, M. and Inoue, T., *Handbook of residual stress and deformation of steel*, ASM International, 2002

[58] Hu, Z., "Design and Modeling of Internally Pressurized Thick-Walled Cylinder", Presentation at 2010 NDIA Conference, Dallas, Texas, May 17-20, 2010

[59] Norton, R. L., *Machine Design, fourth edition*, Prentice Hall, 2011.

[60] Parker, A. P., "Compound and Monobloc Cylinders Incorporating Reverse-Autofrettage to Reduce External Hoop Stresses", Paper PVP2012-78298, Proceedings of ASME PVP2012 Pressure Vessels and Piping Division Conference July 15-19, Toronto, Ontario, Canada, 2012.

[61] Vilganlte, G. Troiano, E. and Mossey, C., " Liquid Metal Embrittlement of ASTM A723 Gun Steel by Indium and Gallium", Benét Laboratories Technical Report ARCCB-TR-99011, US ARMY Armament Research and Development Center, Watervliet Arsenal, NY, 12189-4050, USA, June 1999.

[62] Allan, F. B., *Applied mechanics of solids*, CRC press, 2009.

[63] Jabbari, M. Dehbani, H. and Eslami, M.R., "An Exact Solution for Classic Coupled Thermoelasticity in Cylindrical Coordinate", ASME, Journal of Pressure Vessel Technology, vol. 133, pp. 051204-1-10, 2011.

[64] Rao, D. M. and Sinha, P. K., "Finite Element Coupled Thermostructural Analysis of Composite Beams", Journal of Computer and Structure, vol. 63, pp.539-549, 1997.

[65] Holman, J.P., *Heat transfer*, McGraw-Hill International. (U.k), 1992.

[66] Abdelsalam, O. R. Sherif, H. and Abo-elkhair, M., "Instability of Barrel Due to Mechanical and Thermal Excitations" M.Sc. Thesis, MTC, Cairo, 2003.

[67] ASME (2004), *Alternative Rules for Construction of High Pressure Vessels in Boiler and Pressure Vessel Code*, Section VIII, Division 3. American Society of Mechanical Engineers.

[68] Sacks, J. Welch, W.J. Mitchell, T.J. and Wynn, H.P., "Design and Analysis of Computer Experiments," Statistical Science Vol. 4, PP. 409-435, 1989.

[69] Welch, W.J. Yu, T. Kang, S. and Sacks J., "Computer Experiments for Quality Control by Parameter Design," Journal of Quality Technology, Vol. 22, No.1, PP. 15-22, 1990.

[70] Fisher, R.A., *The Design of Experiments*, Macmillan Pub Co., 1971.

[71] Antony, J., *The Design of Experiments for Engineers and Scientists*, Buterworth-Heniemann, 2003.

[72] Montgomery, D. C., *Design and Analysis of Experiments*, Wiley, 2008.

[73] Myers, R. H. and Montgomery D. C., *Response Surface Methodology – Process and Product Optimization Using Designed Experiments*, Wiley Series in Probability and Statistics, New York, 1995.

[74] Box G. and Behnken D., "Some New Three Level Designs for the Study of Quantitative Variables", Technometrics, Vol. 2, pp. 455–475, 1960.

[75] Nuran, B. and Yi, C. "The Response Surface Methodology ", M.Sc. Thesis, University of South Bend, USA, 2007.

[76] Khuri, A.I. and Cornell, J.A., *Response surface: Designs and Analysis*, CRC press, 1996.

[77] Myers, R. H. Montgomery, D. C. Vining, G.G. and Kowalski, S.M.," Response Surface Methodology: A retrospective and Literature survey" Journal of quality technology", Vol.36, NO. 1, pp. 35-77, 2004.

[78] Conn, A.R. Scheinberg, K. and Vicente, L.N., *Introduction to Derivation-Free Optimization*, Society for Industrial and Applied Mathematics and the Mathematical Programming Society, 2009.

[79] Kaymaz, I. and McMahon, C. A.,"A Response Surface Method Based on Weighted Regression for Structural Reliability Analysis" Journal of Probabilistic Engineering Mechanics Vol. 20, pp. 11–17, 2005.

[80] Huber-Carol, C. Balakrishnan, N. Nikulin, M. and Mesbah, M., *Goodness-of-Fit Tests and Model Validity*, Series: Statistics for Industry and Technology, Birkhäuser Boston, 2002.

[81] Holnicki-Szulc, J. and Pawłowski, P., "The Concept Of Multifolding and its Experimental Validation", 21st International Congress of Theoretical and Applied Mechanics (ICTAM), August 2004, Warsaw, Poland.

[82] Tan, K. C. Lee, T. H. and Khor, E. F., "Evolutionary Algorithms for Multi-Objective Optimization: Performance Assessments and Comparisons", proceedings of the 2001 IEEE Congress on Evolutionary Computation, May 2001, Soul, Korea.

[83] Agarwal, H. and Renaud, J. E., "Reliability Based Design Optimization For Multidisciplinary Systems Using Response Surfaces", Journal of Engineering Optimization, Vol. 36, No. 3, pp. 291–311, June 2004.

[84] Liao, X. Li, Q. Yang, X. Zhang, W. and Li, W., "Multiobjective Optimization for Crash Safety Design of Vehicles using Stepwise Regression Model", Journal of. Structural Multidisciplinary Optimization, Vol. 35, No. 6, pp: 561–569, 2008.

[85] Ibrahim, H. K., "Design Optimization of Vehicle Structures for Crashworthiness Improvement", PhD dissertation, Concordia University, 2009, Canada.

[86] Jasbir, S. A., *Introduction to Optimum Design*, Elsevier Academic Press, second edition, 2004.

[87] Ashlock, D., *Evolutionary Computation for modeling and optimization*, Springer, 2005.

[88] Philip, E. Walter, M. and Michael, S., "An SQP Algorithm for Large Scale Constrained Optimization", SIAM review, Vol. 47, No.1, pp. 99-131, 2005.

[89] Kim, C.H. Mijar, A.R. and Arora, J. S., "Development of Simplified Models for Design and Optimization of Automotive Structures for Crashworthiness", Structural and Multidisciplinary Optimization, Vol. 22, No. 4, pp. 307–321, 2001.

[90] Matlab online help, Optimization Toolbox Documentation-R2009a, http://www.mathworks.com/help/toolbox/optim/.

APPENDIX A

von-Mises distribution through the thickness of compound cylinders subjected to different combinations of shrink-fit, conventional autofrettage and doubled autofrettage processes.

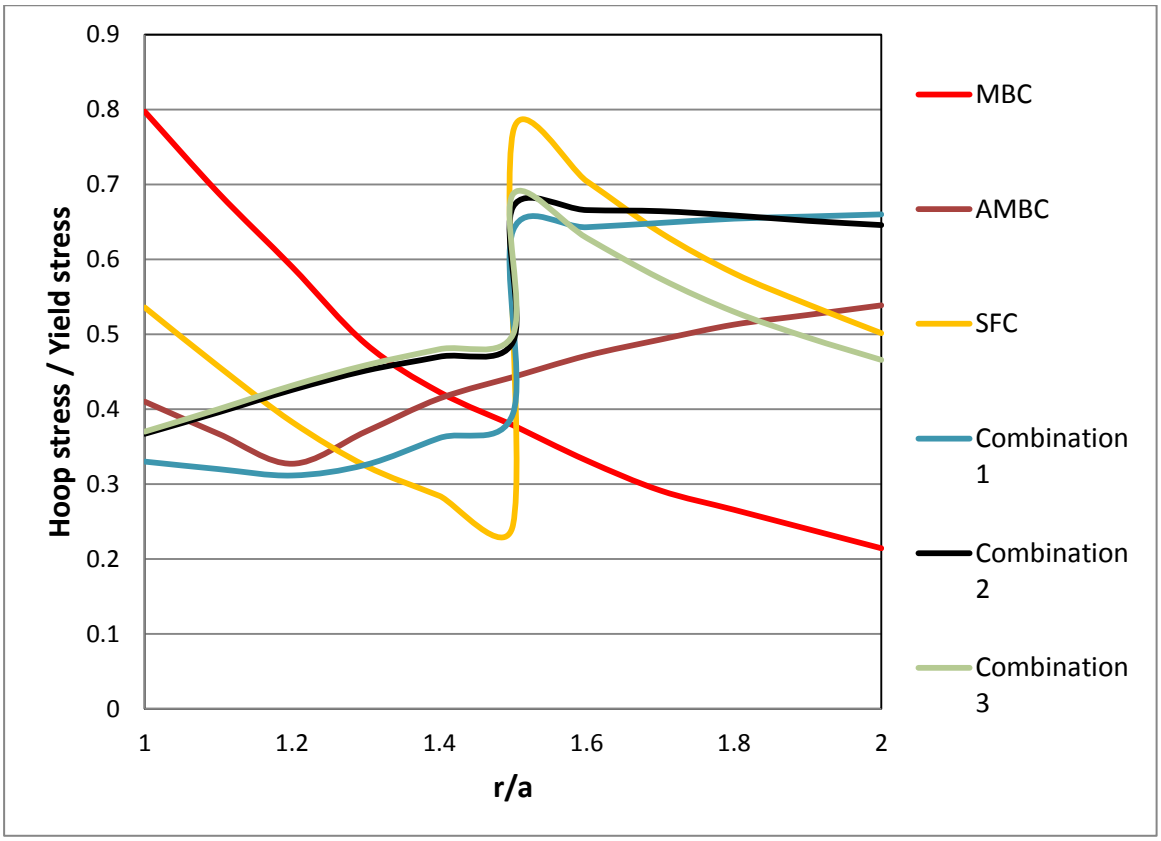

Figure A-1: von-Mises stress distribution in compound cylinders subjected to combinations 1-3 under static inner pressure of 250 MPa.

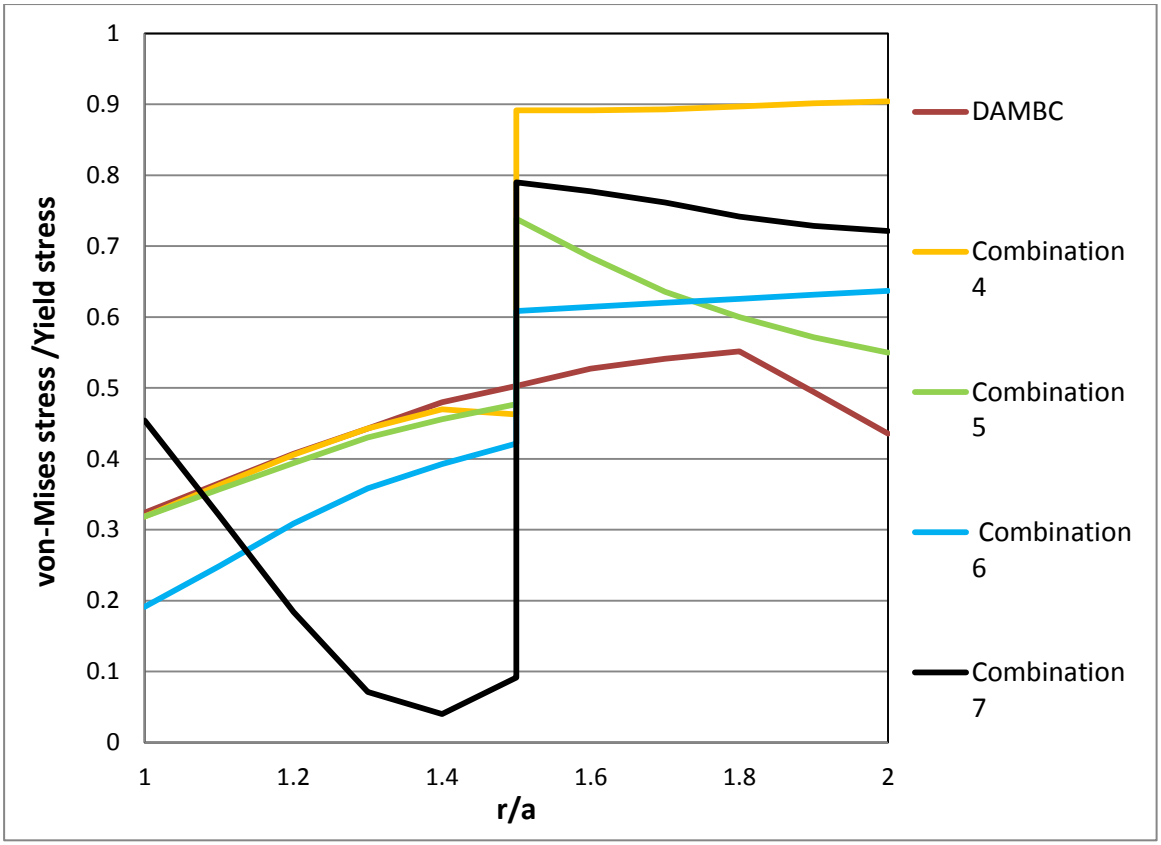

Figure A-2: von-Mises stress distribution in compound cylinders subjected to combinations 4-7 under static pressure of 250 MPa.

APPENDIX B

DOE matrices for Combinations 2-7 are presented in Tables B.1 to B.6

Table B. 1: DOE Matrix for the second combination

Number of experiments	t_1	t_2	δ	P_{1in}	P_{2in}	Max. residual compressive stress MPa	Max. residual tensile stress MPa
1	30	30	0.2	520	280	-65	78
2	30	55	0.2	520	280	-501	256
3	55	30	0.2	520	280	-177	133
4	55	55	0.2	520	280	-370	205
5	42.5	42.5	0.22	468	280	-215	118
6	42.5	42.5	0.22	572	280	-223	207
7	42.5	42.5	0.18	468	280	-194	140
8	42.5	42.5	0.18	572	280	-214	191
9	42.5	30	0.2	520	252	-354	249
10	42.5	30	0.2	520	308	-159	147
11	42.5	55	0.2	520	252	-508	251
12	42.5	55	0.2	520	308	-383	230
13	30	42.5	0.22	520	280	-335	277
14	30	42.5	0.18	520	280	-313	260
15	55	42.5	0.22	520	280	-226	170
16	55	42.5	0.18	520	280	-221	165
17	42.5	42.5	0.2	468	252	-308	199
18	42.5	42.5	0.2	468	308	-177	143
19	42.5	42.5	0.2	572	252	-319	279
20	42.5	42.5	0.2	572	308	-117	119
21	42.5	30	0.22	520	280	-24	99
22	42.5	30	0.18	520	280	-24	102
23	42.5	55	0.22	520	280	-475	283
24	42.5	55	0.18	520	280	-450	266
25	30	42.5	0.2	468	280	-338	234
26	30	42.5	0.2	572	280	-345	294
27	55	42.5	0.2	468	280	-224	166
28	55	42.5	0.2	572	280	-181	169
29	42.5	42.5	0.22	520	252	-359	248
30	42.5	42.5	0.22	520	308	-139	142
31	42.5	42.5	0.18	520	252	-346	226
32	42.5	42.5	0.18	520	308	-146	138
33	30	42.5	0.2	520	252	-415	318
34	30	42.5	0.2	520	308	-222	216
35	55	42.5	0.2	520	252	-253	150
36	55	42.5	0.2	520	308	-183	168
37	42.5	30	0.2	468	280	-74	118

38	42.5	30	0.2	572	280	-50	76
39	42.5	55	0.2	468	280	-400	237
40	42.5	55	0.2	572	280	-450	299
41	42.5	42.5	0.2	520	280	-249	163

Table B. 2: DOE Matrix for the third combination

Number of experiments	t_1	t_2	$\boldsymbol{\delta}$	P_{1in}	Max. residual compressive stress MPa	Max. residual tensile stress MPa
1	30	30	0.2	520	-215	270
2	30	55	0.2	520	-346	136
3	55	30	0.2	520	-319	160
4	55	55	0.2	520	-322	91
5	42.5	42.5	0.22	572	-312	231
6	42.5	42.5	0.22	468	-321	130
7	42.5	42.5	0.18	572	-305	206
8	42.5	42.5	0.18	468	-288	100
9	30	42.5	0.2	572	-246	230
10	30	42.5	0.2	468	-348	166
11	55	42.5	0.2	572	-332	171
12	55	42.5	0.2	468	-267	134
13	42.5	30	0.22	520	-308	244
14	42.5	30	0.18	520	-303	215
15	42.5	55	0.22	520	-348	148
16	42.5	55	0.18	520	-316	123
17	30	42.5	0.22	520	-317	190
18	30	42.5	0.18	520	-305	178
19	55	42.5	0.22	520	-317	134
20	55	42.5	0.18	520	-295	106
21	42.5	30	0.2	572	-261	266
22	42.5	30	0.2	468	-289	163
23	42.5	55	0.2	572	-344	176
24	42.5	55	0.2	468	-281	90
25	42.5	42.5	0.2	520	-339	172

Table B. 3: DOE Matrix for the fourth combination

Number of experiments	t_1	t_2	δ	P_{1in}	P_{1out}	P_{2in}	Max. residual compressive stress MPa	Max. residual tensile stress MPa
1	30	30	0.2	225	520	280	-156	82
2	30	30	0.2	275	520	280	-278	155
3	30	55	0.2	225	520	280	-640	271
4	30	55	0.2	275	520	280	-700	300
5	55	30	0.2	225	520	280	-187	132
6	55	30	0.2	275	520	280	-208	146
7	55	55	0.2	225	520	280	-402	176
8	55	55	0.2	275	520	280	-492	238
9	42.5	30	0.18	250	468	280	-162	141
10	42.5	30	0.18	250	572	280	-165	150
11	42.5	30	0.22	250	468	280	-160	142
12	42.5	30	0.22	250	572	280	-162	149
13	42.5	55	0.18	250	468	280	-516	295
14	42.5	55	0.18	250	572	280	-532	296
15	42.5	55	0.22	250	468	280	-635	337
16	42.5	55	0.22	250	572	280	-637	339
17	42.5	42.5	0.18	225	520	252	-312	181
18	42.5	42.5	0.18	225	520	308	-162	141
19	42.5	42.5	0.18	275	520	252	-413	271
20	42.5	42.5	0.18	275	520	308	-208	115
21	42.5	42.5	0.22	225	520	252	-416	247
22	42.5	42.5	0.22	225	520	308	-233	86
23	42.5	42.5	0.22	275	520	252	-514	340
24	42.5	42.5	0.22	275	520	308	-314	138
25	30	42.5	0.2	225	468	280	-453	273
26	30	42.5	0.2	225	572	280	-449	271
27	30	42.5	0.2	275	468	280	-509	311
28	30	42.5	0.2	275	572	280	-509	307
29	55	42.5	0.2	225	468	280	-167	79
30	55	42.5	0.2	225	572	280	-207	137
31	55	42.5	0.2	275	468	280	-236	115
32	55	42.5	0.2	275	572	280	-255	126
33	42.5	30	0.2	250	468	252	-165	137
34	42.5	30	0.2	250	468	308	-184	139
35	42.5	30	0.2	250	572	252	-197	140
36	42.5	30	0.2	250	572	308	-166	150
37	42.5	55	0.2	250	468	252	-618	311
38	42.5	55	0.2	250	468	308	-501	257
39	42.5	55	0.2	250	572	252	-608	304
40	42.5	55	0.2	250	572	308	-497	257
41	30	42.5	0.18	250	520	252	-500	312
42	30	42.5	0.18	250	520	308	-360	211
43	30	42.5	0.22	250	520	252	-606	363
44	30	42.5	0.22	250	520	308	-480	271

45	55	42.5	0.18	250	520	252	-241	105
46	55	42.5	0.18	250	520	308	-190	137
47	55	42.5	0.22	250	520	252	-339	140
48	55	42.5	0.22	250	520	308	-200	142
49	42.5	42.5	0.2	250	520	280	-312	135

Table B. 4: DOE Matrix for the fifth combination

Number of experiments	t_1	t_2	$\boldsymbol{\delta}$	P_{1in}	P_{1out}	Max. residual compressive stress MPa	Max. residual tensile stress MPa
1	30	30	0.2	250	520	-380	262
2	30	55	0.2	250	520	-437	162
3	55	30	0.2	250	520	-327	212
4	55	55	0.2	250	520	-393	167
5	42.5	42.5	0.22	225	520	-381	195
6	42.5	42.5	0.22	275	520	-432	252
7	42.5	42.5	0.18	225	520	-331	141
8	42.5	42.5	0.18	275	520	-383	197
9	42.5	30	0.2	250	468	-354	238
10	42.5	30	0.2	250	572	-339	241
11	42.5	55	0.2	250	468	-405	165
12	42.5	55	0.2	250	572	-276	164
13	30	42.5	0.22	250	520	-450	222
14	30	42.5	0.18	250	520	-385	179
15	55	42.5	0.22	250	520	-392	213
16	55	42.5	0.18	250	520	-341	155
17	42.5	42.5	0.2	225	468	-354	168
18	42.5	42.5	0.2	225	572	-354	168
19	42.5	42.5	0.2	275	468	-409	219
20	42.5	42.5	0.2	275	572	-413	223
21	42.5	30	0.22	250	520	-377	269
22	42.5	30	0.18	250	520	-308	209
23	42.5	55	0.22	250	520	-430	185
24	42.5	55	0.18	250	520	-367	140
25	30	42.5	0.2	225	520	-385	176
26	30	42.5	0.2	275	520	-446	227
27	55	42.5	0.2	225	520	-333	158
28	55	42.5	0.2	275	520	-390	211
29	42.5	42.5	0.22	250	468	-411	223
30	42.5	42.5	0.22	250	572	-414	226
31	42.5	42.5	0.18	250	468	-348	169

32	42.5	42.5	0.18	250	572	-350	171
33	30	42.5	0.2	250	468	-421	202
34	30	42.5	0.2	250	572	-404	203
35	55	42.5	0.2	250	468	-343	210
36	55	42.5	0.2	250	572	-364	179
37	42.5	30	0.2	225	520	-319	203
38	42.5	30	0.2	275	520	-373	276
39	42.5	55	0.2	225	520	-380	141
40	42.5	55	0.2	275	520	-441	186
41	42.5	42.5	0.2	250	520	-384	198

Table B. 5: DOE Matrix for the sixth combination

Number of experiments	t_1	t_2	$\boldsymbol{\delta}$	P_{1in}	P_{2out}	Max. residual compressive stress MPa	Max. residual tensile stress MPa
1	30	30	0.2	550	735	-237	257
2	30	55	0.2	550	735	-470	283
3	55	30	0.2	550	735	-401	328
4	55	55	0.2	550	735	-499	267
5	42.5	42.5	0.22	500	735	-431	307
6	42.5	42.5	0.22	600	735	-423	313
7	42.5	42.5	0.18	500	735	-426	300
8	42.5	42.5	0.18	600	735	-412	299
9	42.5	30	0.2	550	700	-361	308
10	42.5	30	0.2	550	770	-360	305
11	42.5	55	0.2	550	700	-494	302
12	42.5	55	0.2	550	770	-497	311
13	30	42.5	0.22	550	735	-397	278
14	30	42.5	0.18	550	735	-388	272
15	55	42.5	0.22	550	735	-466	336
16	55	42.5	0.18	550	735	-458	329
17	42.5	42.5	0.2	500	700	-438	297
18	42.5	42.5	0.2	500	770	-430	301
19	42.5	42.5	0.2	600	700	-417	314
20	42.5	42.5	0.2	600	770	-419	308
21	42.5	30	0.22	550	735	-366	307
22	42.5	30	0.18	550	735	-353	299
23	42.5	55	0.22	550	735	-504	308
24	42.5	55	0.18	550	735	-485	303

25	30	42.5	0.2	500	735	-394	268
26	30	42.5	0.2	600	735	-296	259
27	55	42.5	0.2	500	735	-390	262
28	55	42.5	0.2	600	735	-296	265
29	42.5	42.5	0.22	550	700	-436	313
30	42.5	42.5	0.22	550	770	-433	310
31	42.5	42.5	0.18	550	700	-424	305
32	42.5	42.5	0.18	550	770	-421	303
33	30	42.5	0.2	550	700	-389	275
34	30	42.5	0.2	550	770	-389	274
35	55	42.5	0.2	550	700	-462	332
36	55	42.5	0.2	550	770	-465	333
37	42.5	30	0.2	500	735	-359	297
38	42.5	30	0.2	600	735	-282	299
39	42.5	55	0.2	500	735	-487	299
40	42.5	55	0.2	600	735	-495	311
41	42.5	42.5	0.2	550	735	-425	304

Table B. 6: DOE Matrix for the seventh combination

Number of experim-ents	t_1	t_2	$\boldsymbol{\delta}$	P_{1in}	P_{1out}	P_{2in}	P_{2out}	Max. residual compressive stress MPa	Max. residual tensile stress MPa
1	42.5	42.5	0.2	225	572	225	520	-351	214
2	42.5	42.5	0.2	225	572	275	520	-161	138
3	42.5	42.5	0.2	225	468	225	520	-357	225
4	42.5	42.5	0.2	225	468	275	520	-163	140
5	42.5	42.5	0.2	275	572	225	520	-416	268
6	42.5	42.5	0.2	275	572	275	520	-207	122
7	42.5	42.5	0.2	275	468	225	520	-422	270
8	42.5	42.5	0.2	275	468	275	520	-218	117
9	30	42.5	0.2	250	520	225	572	-480	291
10	30	42.5	0.2	250	520	225	468	-481	293
11	30	42.5	0.2	250	520	275	572	-314	207
12	30	42.5	0.2	250	520	275	468	-311	206
13	55	42.5	0.2	250	520	225	572	-262	99
14	55	42.5	0.2	250	520	225	468	-243	93
15	55	42.5	0.2	250	520	275	572	-207	145
16	55	42.5	0.2	250	520	275	468	-163	84
17	42.5	30	0.2	250	572	250	572	-162	148
18	42.5	30	0.2	250	572	250	468	-164	141
19	42.5	30	0.2	250	468	250	572	-156	150

20	42.5	30	0.2	250	468	250	468	-153	137
21	42.5	55	0.2	250	572	250	572	-479	218
22	42.5	55	0.2	250	572	250	468	-471	217
23	42.5	55	0.2	250	468	250	572	-477	213
24	42.5	55	0.2	250	468	250	468	-470	213
25	30	30	0.2	225	520	250	520	-115	109
26	30	30	0.2	275	520	250	520	-182	99
27	30	55	0.2	225	520	250	520	-504	202
28	30	55	0.2	275	520	250	520	-577	234
29	55	30	0.2	225	520	250	520	-183	127
30	55	30	0.2	275	520	250	520	-204	135
31	55	55	0.2	225	520	250	520	-356	162
32	55	55	0.2	275	520	250	520	-455	231
33	42.5	42.5	0.22	225	520	250	572	-243	115
34	42.5	42.5	0.22	225	520	250	468	-249	117
35	42.5	42.5	0.22	275	520	250	572	-358	221
36	42.5	42.5	0.22	275	520	250	468	-358	209
37	42.5	42.5	0.18	225	520	250	572	-170	144
38	42.5	42.5	0.18	225	520	250	468	-175	136
39	42.5	42.5	0.18	275	520	250	572	-294	171
40	42.5	42.5	0.18	275	520	250	468	-294	167
41	30	42.5	0.22	250	572	250	520	-435	271
42	30	42.5	0.22	250	468	250	520	-435	273
43	30	42.5	0.18	250	572	250	520	-394	217
44	30	42.5	0.18	250	468	250	520	-361	227
45	55	42.5	0.22	250	572	250	520	-207	141
46	55	42.5	0.22	250	468	250	520	-218	141
47	55	42.5	0.18	250	572	250	520	-198	140
48	55	42.5	0.18	250	468	250	520	-200	141
49	42.5	30	0.22	250	520	225	520	-166	134
50	42.5	30	0.22	250	520	275	520	-166	138
51	42.5	30	0.18	250	520	225	520	-172	142
52	42.5	30	0.18	250	520	275	520	-171	139
53	42.5	55	0.22	250	520	225	520	-529	236
54	42.5	55	0.22	250	520	275	520	-470	259
55	42.5	55	0.18	250	520	225	520	-456	179
56	42.5	55	0.18	250	520	275	520	-392	207
57	42.5	42.5	0.2	250	520	250	520	-261	148